THE EFFECT OF TRANSMISSION DESIGN ON FORCE-CONTROLLED MANIPULATOR PERFORMANCE

by

William T. Townsend

B.S.M.E., Northeastern University
(1982)

M.S.M.E., Massachusetts Institute of Technology
(1984)

SUBMITTED IN PARTIAL FULFILLMENT
OF THE REQUIREMENTS FOR THE
DEGREE OF

DOCTOR OF PHILOSOPHY

at the

MASSACHUSETTS INSTITUTE OF TECHNOLOGY

April 1988

Signature of Author _____
Department of Mechanical Engineering
April 1988

Certified by _____
Dr. J. Kenneth Salisbury, Jr.
Thesis Supervisor

Accepted by _____
Professor A.A. Sonin
Chairman, Department Graduate Committee

THE EFFECT OF TRANSMISSION DESIGN ON FORCE-CONTROLLED MANIPULATOR PERFORMANCE

by

William T. Townsend

Submitted to the Department of Mechanical Engineering
on 8 April 1988 in Partial Fulfillment of the Requirements for the Degree of
Doctor of Philosophy.

Abstract

The concept of manipulator force control and a corresponding emphasis on the choice of appropriate servo implementation have been developing for many years. However, the selection of appropriate mechanical hardware may ultimately be the limiting performance factor in force control. Mechanism properties, such as contact compliance, actuator-to-joint compliance, torque ripple, and highly nonlinear dry friction, affect, and often degrade, manipulator performance in force-controlled systems.

This thesis describes a set of requisites for good performance, analyzes the effects of transmission-mechanism properties on force-controlled manipulators, and recommends mechanical-design strategies to improve performance. While much of the analysis applies to a broad class of transmissions, a special control-volume analysis quantifies a limit on the power efficiency of tension-element drives.

A single-degree-of-freedom transmission testbed was constructed and used to confirm the predicted effect of Coulomb friction on robustness; design of a cable-driven, four-degree-of-freedom, "whole-arm" manipulator illustrates the recommended mechanical-design strategies.

Thesis Supervisor:

J. Kenneth Salisbury, Jr.
Research Scientist
MIT AI Laboratory

ACKNOWLEDGEMENTS

Ken Salisbury has been advisor, mentor, and close friend. He is one of the brightest people on Earth. Nearly every clever concept in this thesis was born from lively meetings with Ken.

My sweet heart, Julie, devoted tremendous, endless love. Julie also spent countless hours as my personal chauffeur and chef as well as assisting with the thesis drawings.

My family gave me more than the right genes. My mom and dad always believed in me; and my younger, handicapped brother, Steve, was a big source of inspiration as a person who, against all odds, is happy and successful. My mom's parents extended important support during my study at MIT. My 91-year-old grandmother (dad's mom) proofread this thesis. If there are any mistakes in this thesis, it's because I made too many changes after she proofed it.

Special thanks go to my thesis committee professors Woodie Flowers, who encouraged me at just the right times, and David Gossard, whose advice and perspective on entrepreneurial ventures were inspirational. Two professors who had a particularly big impact on my love of design and professional development were Warren Seering and Joseph Smith, Jr.

David DiPietro, Ken Pasch, Neil Singer, and Eric Vaaler suggested essential improvements which I implemented in the design of the MIT/WAM manipulator. My intelligent, progressive machinist and president of Ramco, Randy Jezowski, made one-up CNC jobs economically desirable — a rarity.

Important student associations at the Artificial Intelligence Laboratory were David Brock, Mike Caine, Steve Gordon, Brian Eberman, Steve Eppinger, Ben Paul, and Karl Ulrich.

The advice of my good friends Maury Cosman, Alan Crunkleton, Bedana Sabin, and Lou Terricone is dearly appreciated.

I would also like to thank professors Ernesto Blanco, Karl Hedrick, Neville Hogan, Tomas Lozano-Perez, Jean-Jacques Slotine, and Gerald Wilson for assistance along the way.

I have had countless more associations at and outside MIT who are not named here but whose contributions to my thesis and my happiness at MIT will never be forgotten. Thank you.

Support for this thesis was provided in part by the ONR University Research Initiative Program under ONR contract N00014-86-K-0180 and in part by DARPA under ONR contract N00014-85-K-0124.

TABLE OF CONTENTS

LIST OF SYMBOLS

A	Sinusoidal amplitude fed to an SIDF nonlinear block.
A	Cross-sectional stress area of a transmission element.
b	Linear-viscous damping coefficient.
C	Distance between a speed reducer and the actuator that drives it.
C	Contour of integration.
D_{cyl}	Diameter of a grasped cylindrical object.
E	Modulus of elasticity of the transmission element.
F_c, $\dot{F}_c$	Contact force (or torque) and its first time derivative.
$F_{c_{impact}}$	The maximum contact force generated during an impact.
F_c', F_c''	The amplitudes of two successive cycles of an oscillatory contact force.
F_{dcs}	A desired (commanded) force.
$F_{dynamic}$	Dynamic, sliding friction.
F_{error}	The force error computed in explicit-force feedback control.
$F_{friction}$	Level of Coulomb friction.
F_m	Actuator force or torque.
F_{static}	Static, breakaway friction.
ΔF	Difference between the static and dynamic friction levels in stiction.
G(s)	The feedforward transfer function used in an SIDF analysis.
G_I	Integral gain.
G_P	Proportional gain.
g	Acceleration of gravity.
J_l	Link inertia.
J_m	Actuator (or motor) inertia.
j	Square root of -1.
K	Combined transmission and contact stiffness.
k_c	Contact stiffness between the manipulator and the environment.
k_{eff}	Effective transmission stiffness measured at the joint.
k_{tr}	Transmission stiffness between the actuator and link.
k_{tr_a}, k_{tr_b}	Stiffnesses of the low- and high-speed parts of a 2-stage transmission.
L	Link length.
L'	Useful grasping length of a link.
L	Transmission length (actuator-to-joint span).
N	Transmission ratio (ratio of actuator speed to joint speed).
N_m	Transmission ratio which matches the reflected actuator and link inertias.
N(A)	Describing function for Coulomb friction.
n	Number of transmission stages.
P_{L_a}, P_{L_b}	Power losses at the drive and driven pulleys.
P_{in}, P_{out}	Input and output power of a tension-element transmission.
$\mathcal{P}$	Average power dissipated per half cycle in an actuator-only limit cycle.

r_a, r_b	Drive and driven pulley radii in a tension-element transmission.
r_I, r_{II}	The minimum and maximum radii in a sprocket/chain drive.
s	The differential operator, $\frac{d}{dt}()$.
T	Transmission-element tension.
T_1, T_2	Low and high transmission-element tensions .
t	time
V_1, V_2	Low and high tension-element velocities.
v_l	Link velocity immediately before impacting the environment.
W	Link width.
$\mathcal{W}$	Work dissipated per half cycle of an actuator-only limit cycle.
x	Position of a contact force from the nearest joint toward the base.
x_l, $\dot{x}_l$, $\ddot{x}_l$	Link position, velocity, and acceleration.
x_m, $\dot{x}_m$	Actuator (or motor) position and velocity.
Δx_l	Link position change during slip mode in a system with stiction.
Δx_m	Actuator position change during slip mode in a system with stiction.
z	Height in a gravity field.
β	Arc angle of tension-element slip around a pulley.
ϵ_1, ϵ_2	Mechanical strain of low- and high-tension transmission elements.
ζ	Linear-viscous damping ratio.
η	Transmission power efficiency.
θ	Friction-cone angle.
θ_a, $\dot{\theta}_a$	Position and velocity of a drive pulley.
θ_b, $\dot{\theta}_b$	Position and velocity of a driven pulley.
$\theta_{b_{error}}$	Error in estimated joint position caused by slip in a tension-element drive.
μ	Static coefficient of friction.
ρ	Tension-element material density.
σ	Mechanical stress.
τ	Time constant in a simple force-feedback model without friction.
τ_{delay}	Delay caused by Coulomb friction in a simple force-feedback model.
τ_{linear}	Slip-mode duration in a system with stiction.
τ_{spinup}	Stick-mode duration in a system with stiction.
τ_1, τ_2	Joint torques.
τ_a, τ_b	Drive- and driven-pulley shaft torques.
Ψ	The ratio of two successive cycles of an oscillatory contact force.
Ω	Correction coefficient for the effect of damping on the size of limit cycles.
ω	Breakpoint frequency in chapter 4; SIDF limit-cycle frequency in chapter 5.

LIST OF FIGURES

Chapter 1
Introduction

This chapter is divided into two sections. The first section gives a brief background, defines transmission, and states the problems addressed in this thesis. The second section is a guide to the thesis contents.

1.1 Introduction

1.1.1 Definition of "Transmission"

We define the word transmission, in the context of a manipulator system, to make clear the distinction between servo implementation and mechanical design. In general, a mechanical transmission has two purposes:

- to transmit power over some distance and
- to boost torque or speed from the input to the output.

Similarly, "transmission" is defined here to mean the mechanical hardware which transforms an actuator torque into a contact force against the environment. With the exception of the design of multiple transmissions described in chapter 7 to drive a four-degree-of-freedom manipulator, the analysis focuses on individual single-input-single-output transmissions. Figure 1.1 depicts a number of possible types of transmissions driving a revolute joint.

A two-mass, lumped-parameter model of a manipulator transmission is shown in figure 1.2. To simplify the illustration, all of the components are shown translating, rather than rotating as many actuators do; this simplification has no effect on the generality of results derived from this model. J_m and J_l are the motor and link inertias, and x_m and x_l are their positions. k_{tr} is the stiffness between the motor and joint, which is assumed to be compliant compared to the link. k_c is the contact stiffness, which is the inverse of the sum of link, soft link covering (if any), and environment compliances. The actuator or motor force is F_m and the contact force is F_c.

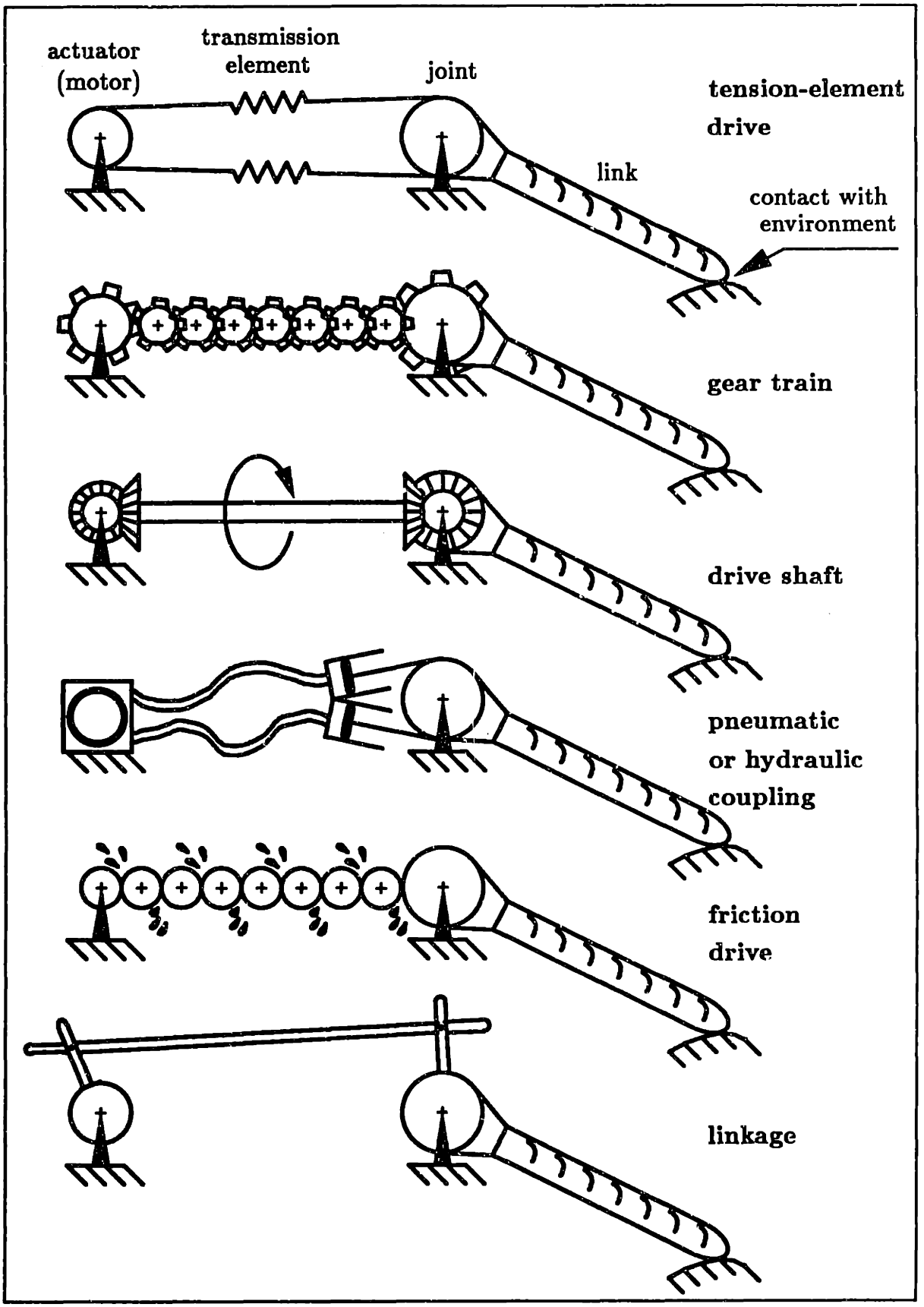

Figure 1.1. *Various types of transmissions.*

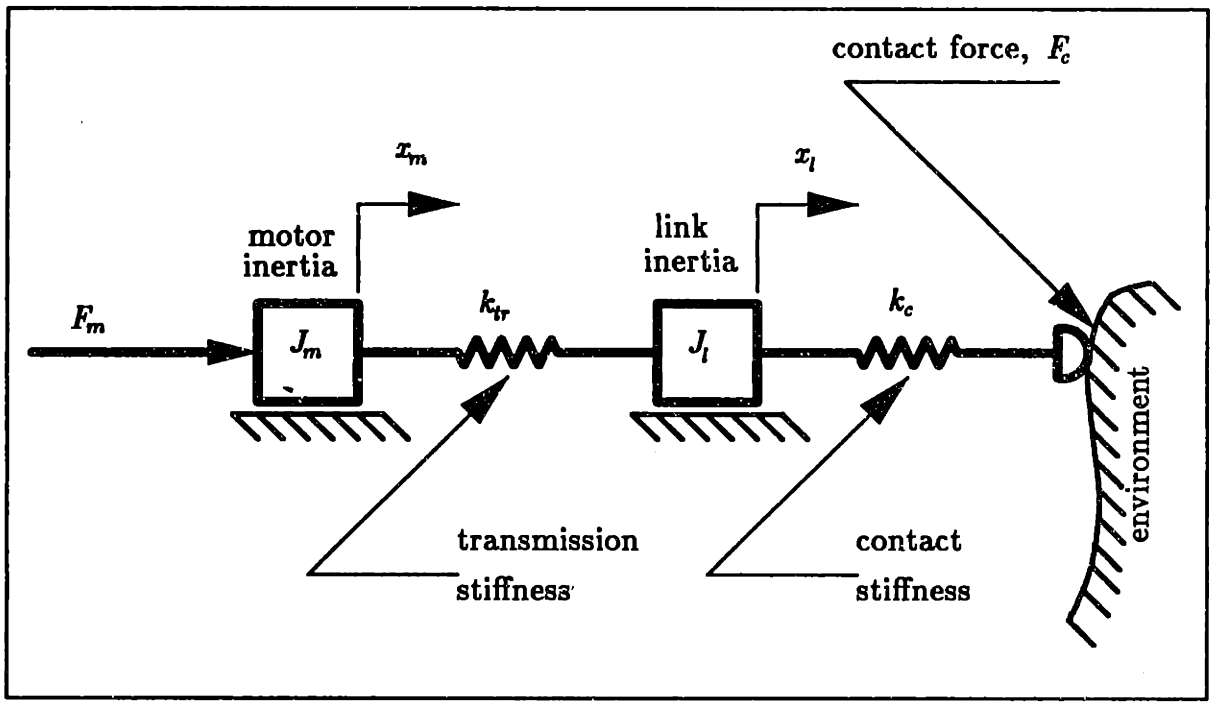

Figure 1.2. *Transmission model.*

Although the model includes link inertia and contact stiffness, some of the results derived in this thesis do not apply to direct-drive joints, where the stiffness between the actuator and joint is essentially infinite. By implementing true direct drive, where the rotor, stator, and supporting bearings *are* the joint, many of the problems of transmissions vanish. However, in most multi-degree-of-freedom, serial-link manipulator designs, it is necessary to include one or more transmissions to remove the actuator bulk from distal joints towards the base and/or to boost output torque through a speed reduction while reducing actuator size and power consumption.

1.1.2 Problem Statement

The problems addressed in this thesis are threefold:

- to identify a set of mechanical design requirements for force-controlled manipulators;
- to analyze the effect of transmission properties such as stiffness, transmission reduction ratio, and nonlinear friction disturbances on manipulator performance; and
- to propose transmission-design strategies for improving performance.

1.2 A Guide to this Thesis

Chapters 1 through 3 lay the groundwork for the analysis in the remainder of the thesis. Chapter 1 provides the problem statement and a guide to the thesis. Chapter 2 cites and classifies current servo strategies for controlling existing manipulators, reviews problems researchers have had in implementing these servo strategies on real hardware, and gives examples of good hardware for force control.

Chapter 3 describes three requirements the author believes are important for good manipulator performance in general and three additional requirements which address the special needs of whole-arm manipulation, a class of force-controlled manipulators built to explore in and interact well with unfamiliar environments. The requirements for good performance described in chapter 3 are:

- large dynamic range of force controllability (ratio of force capacity to force accuracy),
- robustness,
- high bandwidth,
- high-aspect-ratio links (i.e., long and slender),
- high efficiency,
- good backdrivability.

The analytical content is contained in chapters 4 through 6. Chapters 4 and 5 study force-controlled manipulators in general while chapter 6 is specific to tension-element drives.

Chapter 4 looks at the force-in-force-out and position-in-position-out transfer functions of our transmission model to see how the open-loop bandwidth of the transmission may be improved by varying linear parameters in the design. We find that position and force bandwidth are improved by placing a speed reducer at the joint instead of at the motor shaft. Next, we examine the relationship between transmission stiffness and contact stiffness and their combined effect on force bandwidth. A strategy is suggested for allocating stiffness between the transmission and the point of contact with the environment.

Chapter 5 studies the effects of nonlinear dry friction on performance. We focus most strongly on force-feedback schemes with an inner position or velocity servo loop

and an outer force-feedback loop because these schemes are commonly used by designers to improve performance in the face of dry friction. We find a paradox for stability: while dry friction extends the region of stability beyond that for the stable linear system, the extended region of stability is command and disturbance dependent. This dependence means that the system with dry friction has poor robustness. Furthermore, we find conditions under which Coulomb friction causes the actuator to enter a limit cycle and other conditions under which stiction causes the contact force to enter a limit cycle of predictable amplitude and period. Several controller and mechanical-design strategies are suggested to eliminate or reduce these limit cycles and to improve robustness, such as allocating high stiffness between the motor and joint and allowing the environment contact to be compliant.

Chapter 6 examines the efficiency and sources of friction and torque ripple in tension-element drives. We choose to study tension-element drives over the many other types of mechanical and fluid drives such as pneumatic, hydraulic, gear, friction, torsion, and linkage because tension-element drives are particularly well suited to high-performance transmissions. When properly designed, these drives have high material strength, low weight, low velocity and torque ripple, no backlash, and low friction. Furthermore, they do not leak, do not require surface lubrication, and can be guided over long distances (several meters) around pulleys through complex geometries. Tension-element drives do not transfer power though compression or shear, and so avoid added compliance and strength limitations from bending moments or buckling.

A control-volume analysis of these drives reveals a quantitative efficiency limit*. This limit is maximized by:

- using a *stiff* tension-element material such as steel cable or tape in place of more-compliant materials such as nylon, rubber, etc.,
- minimizing the number of separate tension-element stages when idler pulleys can be used instead, and
- maximizing the cable speed to reduce the tension difference between the high- and low-tension cables.

---

* The author believes that the quantification of this limit is a new result in mechanism theory.

Chapter 7 reviews important points of the thesis and illustrates some of the design strategies via the MIT/WAM manipulator designed and built by the author. This chapter concludes with an outlook to important future issues for designing force-controlled hardware and how future research can benefit from high-performance, force-controlled manipulators.

Appendix A contains information on coordinate frames and transformations needed to control the MIT/WAM manipulator introduced in chapter 7.

Chapter 2
Literature Background

This chapter is divided into three sections. The first section reviews and classifies different servo schemes for controlling manipulator force. The second section then looks at some of the problems that researchers have had in trying to implement these strategies on real hardware. The last section reviews examples of teleoperators and manipulators which were designed for good force control.

2.1 Classification of Control Schemes

The quality of the transmission design is partly dependent on the manipulator's control strategy. However, so many schemes exist for generating actuator commands in force-controlled manipulators that it would be impossible to develop a transmission design strategy for each case. Our approach is to categorize control schemes into broad classifications and only study the cases which hold the highest promise for good force control when implemented on mechanical hardware.

2.1.1 No Force Feedback

Even without measuring joint torque or contact force directly we may infer the contact force. If the actuator is a DC motor, the most common actuator for force-controlled manipulators, we can drive a current through the windings, and with knowledge of the torque constant and transmission ratio, estimate the joint torque without reference to direct mechanical-strain measurements. If more than one joint torque is driven to contribute to the contact force, then both the position of contact, x, and the magnitude of contact force, F_c, can be calculated by summing the torque about each joint to zero [Salisbury 86]. Referring to figure 2.1,

$$F_c = \frac{\tau_1 - \tau_2}{\mathrm{L}} \tag{2.1}$$

and

$$x = \frac{\tau_2 \mathrm{L}}{\tau_1 - \tau_2} \tag{2.2}$$

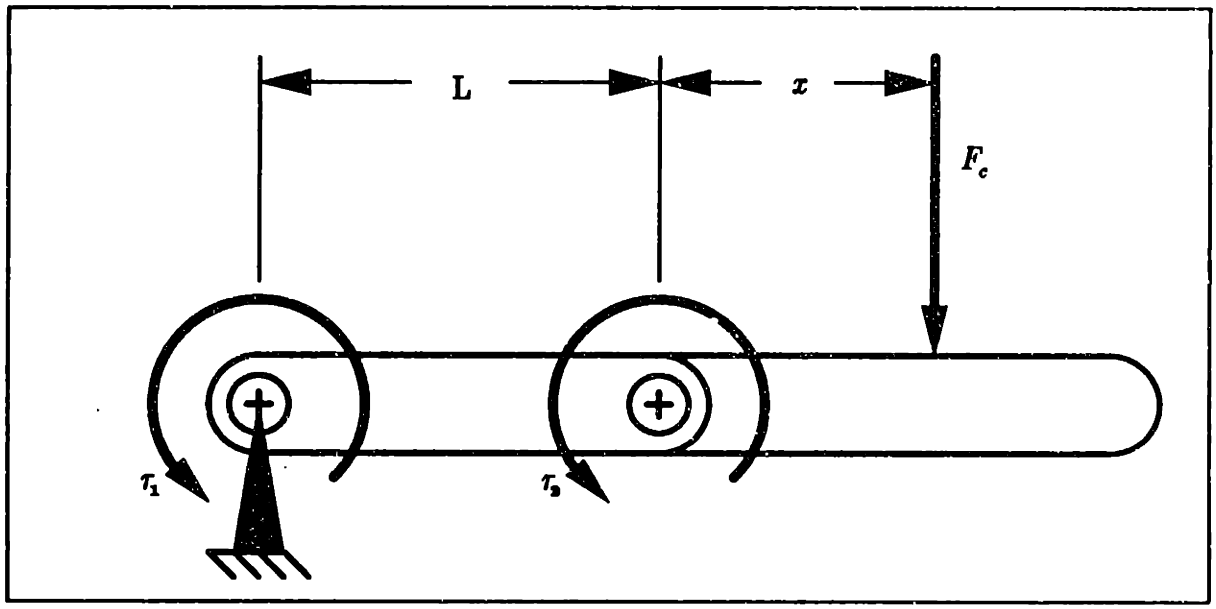

Figure 2.1. *Force applied to the outer link of a two-link planar manipulator.*

where L is the length of the inner link and τ_1 and τ_2 are the joint torques. More sophisticated sensing of this kind is discussed in [Salisbury 84b]. In fact, the kinematics of the manipulator design presented at the conclusion of this thesis facilitate force and position measurements all along the outer link in virtually all configurations.

We call this type of force control, where explicit force measurement is absent, "open-loop" control, although the motor current itself may be controlled in a closed loop and the controller may use motor-position or motor-velocity feedback. Uncertainties about the parameters of the motor and transmission, along with disturbances such as torque ripple, dynamic forces, and especially dry friction, degrade accuracy. Although this type of force control is relatively simple and robust, few researchers use it to control contact forces because of these actuator and transmission shortcomings.

Recently, there has been effort to improve the actuator and transmission qualities in order to increase the accuracy of open-loop force control. Paul [Paul 87] developed current-feedforward techniques in a 300-series Moog DC brushless motor which reduced motor-induced torque ripple to $\pm 2\%$ of commanded motor torque. The friction and controller deadband in this motor are already below 1.5% of the maximum steady-state torque. A motor of this quality driving a high-performance transmission should yield correspondingly accurate and robust force control. The recent improvements in actuator capability renew the focus on the design of high-quality transmissions for force

control without explicit force feedback.

2.1.2 Force Feedback

Many force-control implementations rely on force feedback to defeat the transmission and actuator shortcomings of open-loop control. Such manipulators measure forces by measuring the strain of some mechanical element in the system or in the environment. Force inferred from the strain measurement is fed back to the controller. We call this type of control "closed-loop" control. With appropriate compensation the accuracy can be improved over the open-loop system.

Maples and Becker [Maples 86] further classify closed-loop force-controlled systems by whether the inner-most servo loop is based on torque [Salisbury 80; Khatib 86; Raibert 81; An 86], velocity [Whitney 77], or position [Salisbury 84a; Maples 86]. Since motor velocity and position can be measured directly at the motor shaft with no intervening dynamics (i.e., colocated), an inner velocity or position loop can be very stiff and stable. This stiff inner loop attenuates the negative effects of dry friction and torque ripple disturbances located dynamically near the actuator by transforming a friction-sensitive force-control problem into a less-friction-sensitive position- or velocity-control problem.

If the inner-most loop is torque based, with non-colocated force sensing, then the intervening dynamics between the compliant sensor and the source of motor torques limit the stable gain of the inner loop and therefore its bandwidth. Thus, force disturbances cannot be well attenuated. In general, if closed-loop control is needed to overcome force disturbances, it is better to base the inner servo loop on position or velocity. When dealing with the complex case of closed-loop control with highly nonlinear Coulomb friction and stiction in chapter 5 of this thesis, we analyze only systems with position and velocity inner loops since these are the logical servo systems to use when dry-friction disturbances are significant.

2.2 Problems with Implementing Force Control

The previous section points out that force disturbances can reduce the accuracy of force control. Actually, there are many problems encountered by researchers trying to implement force control. Why isn't it as simple as it should be?

Force errors are common even when the inner loop is based on position or velocity because it is often impractical to measure force in the outer servo loop at the point of environment contact. Examples are the Salisbury hand and the Utah/MIT hand, both of which infer contact forces from tensions measured in the tendons. Disturbances between the sensor and the environment are not attenuated. Even when good force measurement can be made, sensor noise and calibration errors reduce accuracy. Since the outer-loop gain must be limited to maintain stability, the response to force errors may be sluggish [Whitney 85, An 86, Eppinger 86].

Often stability is difficult to maintain. In a linear system in which the parameters are constant, linear control theory guarantees that, if the system is stable for a particular set of gains, it will remain stable for all time regardless of initial conditions and disturbances. However, real transmissions are not linear. In fact, selecting a stable, even sluggish, gain empirically does not guarantee robust stability because the stability may be dependent on the magnitude of force errors fed to the controller [Townsend 87]. Instabilities may be caused by the changing kinematics [An 86] and dynamics. Time delays due to computational and transmission delays are often the source of instability [Whitney 77, Whitney 85], especially when the manipulator contacts stiff environments. Generally, the instability caused by stiff contact manifests itself as a bouncing contact [Eppinger 86].

In addition to causing steady-state force errors in open-loop systems, dry friction, which is a hard nonlinearity that cannot be eliminated in transmissions and actuators, is a commonly suspected source of poor performance. Armstrong showed that dry friction in the PUMA-560 transmission dominates the dynamic forces during position trajectory control [Armstrong 88]. Raibert and Craig [Raibert 81] observed sustained oscillations which they believed to be caused by the interaction of integral gain and Coulomb friction. Jacobsen [Jacobsen 86] abandoned the idea of using tendon sheaths in favor of pulleys in order to reduce dry friction. Hollars and Cannon [Hollars 85] attempted to feed forward compensation torques to counter Coulomb friction in the

transmission of a two-link manipulator with limited success.

Other less-severe problems also hamper attempts at implementing high-performance force control. Backlash in a harmonic drive, used as a speed reducer at the motor output of the Stanford arm, caused a stable limit cycle in a force-feedback implementation by Luh, Fisher, and Paul [Luh 81]. The high-frequency limit cycles (477 Hz and 334 Hz in the first two joints) were eliminated through proper compensation in the controller. Mechanical backlash is avoidable through proper mechanical design although the elimination of backlash by preloading generally leads to higher friction. This type of nonlinearity is well understood [Graham 61] and is to be minimized in manipulators designed for good position control.

Torque ripple is not a hard nonlinearity like dry friction, but makes accurate control difficult. This disturbance has many origins such as the geometry of the motor poles in DC motors and machining imprecision in gears and pulleys.

This literature survey cites several problems with implementing force control in real hardware. Two problems — dry friction, and robustness — are particularly important. To address these problems, dry friction and its relationship to robustness are explored in chapter 5 of this thesis.

2.3 Teleoperators and Manipulators Designed for Good Force Control

Some teleoperator mechanisms are capable of good-quality, force-controlled manipulation such as the French MA-22 and MA-23 [Vertut 86] and the JPL universal force-reflecting hand controller [Bejczy 80]. These teleoperators use light-weight, low-inertia, steel tapes and cables to locate the motors away from the joints.

Borrowing from teleoperator rather than position-controlled, automated-equipment technology, Takase et al [Takase 74] designed a cabled manipulator with joint-torque control. They considered it essential to use the actuators as torque rather than position or velocity sources. This arm used magnetic-clutch drives whose current-input-to-torque-output was much more linear than servo motors available at that time.

An example of a manipulator designed for good force control is the Asada Direct-Drive Arm [Asada 83]. This arm was built to improve the force-control performance by placing motors directly at the links and eliminating the actuator-to-joint mechanical transmission. In fact, the compliance, friction, backlash, inertia, and mechanism

complexity normally associated with the transmission are eliminated. Moreover, feed-forward control strategies can attenuate the effects of Coulomb friction (though not stiction) at the joints.

The use of direct-drive motors imposes two restrictions. First, there is no speed reducer (or increaser) between the motor and joint; so the joint torques are limited by the output torque of the motor. A speed reducer increases the effective actuator torque (and motor constant) by the transmission reduction ratio so that a small but high-speed motor can meet the joint-torque requirements. Second, the mass and bulk of direct-drive motors must be placed at the joints they drive. The heavy outermost joint motor must be supported and accelerated by a stronger and heavier supporting link. The next motor down the chain must then be yet larger to support and accelerate the outermost heavy motor and links and so on to the base where motors and joints are very large. The result is a heavy, power-inefficient robot with wide links which interfere with much of the manipulator's own workspace making it less capable of reaching between and around objects in its environment.

Chapter 3
Requisites for Good Performance

The first section introduces a set of performance requirements which address a broad spectrum of tasks including fixed assembly and whole-arm manipulation. The second section describes each of these requirements in detail.

3.1 Introduction

Our work has focused on the following six performance characteristics which the author believes are important for good performance of a wide variety of tasks:

- Large dynamic range of force controllability (the ratio of strength to accuracy)
- Robustness (system stability and mechanical durability)
- High bandwidth
- High-aspect-ratio links (long, slender links)
- High efficiency
- Good backdrivability

3.1.1 Spectrum of Tasks Based on Certainty

There is a spectrum of force-controlled tasks which can be categorized by the degree of advanced knowledge about the environment. At one (certain) extreme of the spectrum are hard-automation devices with parts feeders and fixtures which limit the amount of uncertainty in the environment. Most parameters such as payload mass, environment stiffness, disturbances, maximum force errors, and possible sets of joint positions are known in advance. At the other (uncertain) extreme of the spectrum are manipulators designed to explore completely unfamiliar environments without the availability of vision, such as a manipulator investigating a murky underwater environment. Whole-arm manipulation, described in the following subsection is particularly applicable to this type of force control. Most manipulators in use today perform tasks at the certain

end of the task spectrum, but it is likely that manipulators of the future will be asked to perform tasks more evenly distributed over this spectrum.

3.1.2 Whole-Arm Manipulation (WAM)

Salisbury [Salisbury 87, Salisbury 88] introduced the concept of whole-arm manipulation (WAM) to address a broad range of tasks. The WAM manipulator is designed to contact and interact with the environment using any of its surfaces, unlike any manipulator available today which contacts the environment with only the endtip of its last link. Often it is useful, if not inevitable, to contact the environment with other parts of the arm.

There are numerous examples where whole-arm manipulation is important. Obstacles that today's robots try to avoid can be used for leverage [West 87] or to guide a robot toward its goal. Furthermore, a human may use his shoulder for mechanical advantage to budge a heavy box, or he may carry firewood between his upper and fore arms by using these limbs as force-controlled grippers. It's hard, for example, to imagine an Olympic-style wrestler winning his match using only his finger tips! He must control, with tremendous strength, speed, and agility, positions and forces along many parts of his body simultaneously.

High-performance force control is very important to WAM since the system is intended to control contact forces between objects in the environment and any part of its mechanism. This is accomplished by controlling joint torques directly and inferring contact forces rather than measuring them explicitly through a wrist sensor.

There are distinct differences between a WAM-style manipulator and a conventional manipulator. For example, the contact impedance that the joint of a single link experiences varies as the square of the distance of contact from the joint. In a closed-loop system, this variable impedance continually changes the stability margin, thereby making robustness more difficult to guarantee.

The kinematics and geometry of the links must be considered carefully in a WAM design. The links should be slender to enhance the length of each link available for manipulation. The surfaces must be smooth and free of wires and protrusions which would snag on the environment. Compliant coverings are used to aid manipulation and reduce impact forces. Questions still remain about the best kinematics to maximize

force information and controllability and are topics of ongoing research at MIT.

3.2 Descriptions of Six Requirements for High-Performance Force Control

The first three requirements are derived from our perception of the current needs of force-controlled tasks, independent of the degree of certainty in the task. The remaining three requirements, while still valuable to all manipulators in the spectrum of certainty, are included primarily as a guide to designing WAM manipulators. The example design described in chapter 7 fulfills all of these requirements and is considered a WAM-style manipulator.

3.2.1 Large Dynamic Range of Force Controllability

The dynamic range of force controllability is the maximum controllable force (strength) divided by the minimum controllable force (accuracy) of the manipulator at a single point of contact. This ratio is useful in maximizing the range of tasks a particular manipulator can perform. One can increase without bound the maximum controllable force of a manipulator by giving it higher-torque actuators and bigger, stronger links. Similarly, one can achieve very small controllable forces by building a small, light manipulator with lightly preloaded bearings and sensitive force sensors. However, intricate tasks often demand the application and sensing of a broad range of forces.

Dynamic range of force control is selected in place of either strength or accuracy in order to address task performance more directly. This measure is dimensionless and independent of scale.

Since dynamic range is limited by the maximum and minimum controllable forces, we examine each of these separately. The maximum controllable force is limited by the motor-torque saturation limit times the transmission ratio, the strength of the transmission, and the strength of the links. In a system without explicit force feedback, the minimum controllable force is limited by torque ripple, dry friction, and deadband in the motor controller. In a system with force feedback, limit cycles arising from the combination of highly nonlinear elements and feedback control often limit the minimum controllable force.

3.2.2 Robustness

The manipulator must be robust. We attach a broader definition to the word "robust" than do researchers of systems and controls. By robust we mean that the manipulator be able to perform its tasks reliably and without suffering damage. A robust manipulator then must be

- dynamically stable and
- mechanically durable

under all conditions. This is true no matter what task must be achieved, even though section 3.1 states that robustness (dynamic stability) is more difficult to guarantee in uncertain environments.

Dynamic Stability:
Maintaining dynamic stability is the type of robustness most commonly referred to in systems and controls. This sense of robustness requires that a dynamically stable manipulator remains dynamically stable in the face of changing inputs, disturbances, payload, contact stiffness, and arm configuration. Advanced techniques such as sliding-mode control have been developed which deal directly with parameter uncertainty [Slotine 84]. In chapter 5 we explore an important source of dynamic instability which is input and disturbance dependent.

Mechanical Durability:
To maximize mechanical durability, on the other hand, we want to minimize any impact-induced force and to minimize fragility so that the manipulator can bash around, exploring an uncertain environment without damaging itself. We can improve the survivability of the manipulator by using tough materials, tucking fragile transmissions and sensing mechanisms inside the load-carrying structure, adding protective coverings around the links and joints, and minimizing the forces of impact.

By equating kinetic energy before collision to potential energy during collision, we find that the maximum impact force, $F_{c_{impact}}$, is

$$F_{c_{impact}} = v_l \sqrt{J_l k_c} \tag{3.1}$$

where
J_l is the inertia of the link measured at the point of contact,

k_c is the contact stiffness, and

v_l is the contact velocity.

In order to minimize impact forces, the designer must minimize the backdriven mass, increase the contact compliance (perhaps with a soft covering), and limit velocity of the moving mass.

3.2.3 High Bandwidth

High bandwidth of force and position control is important in manipulators used for assembly, where the cycle time of tasks is critical. Bandwidth is also important for controlling forces against shaking and undulating environments. For position-controlled manipulator designs, maintaining high bandwidth may be an unconscious decision; but, since some designers believe that force-controlled manipulators should be naturally compliant [Nevins 73, Andeen 88], the danger exists for their resulting designs to exhibit significantly lower mechanical bandwidth. Chapter 4 studies the effects of transmission design (especially stiffness distribution) on the mechanical, open-loop bandwidth of force and position control. Chapter 5 then shows how to allocate stiffness in the transmission to aid the rejection of dry-friction and torque-ripple disturbances.

3.2.4 High Aspect Ratio

We define aspect ratio of the link as its length, L, divided by its width, W. When the aspect ratios are high, the links are long and slender. In all manipulators, increasing the aspect ratio increases the unobstructed workspace and allows the manipulator links to reach in and around obstacles in the environment more easily.

High-aspect-ratio links are better at grasping and manipulating as shown in figure 3.1. This figure illustrates a serial-link manipulator trying to grasp a cylindrical object of diameter, D_{cyl}, between consecutive links of length, L. In each case the link width, W, and the coefficient of friction, μ, between the object and the cylinder, are the same and determine the friction-cone angle and the maximum permissible joint angle, each equal to θ, which allows a secure grasp. The useful grasping length, L′, normalized by the link length, L, is

$$\frac{L'}{L} = 1 - 1/2 \frac{W}{L} \frac{1}{\tan\frac{\theta}{2}}, \tag{3.2}$$

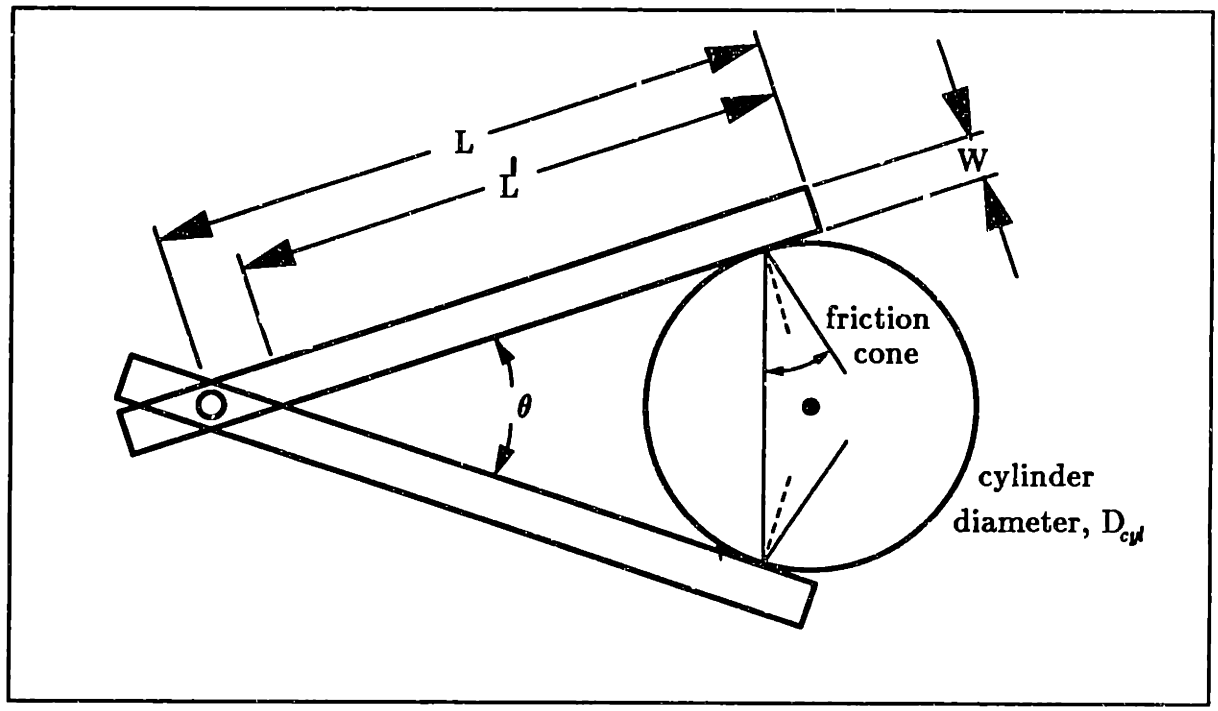

Figure 3.1. *Effect of aspect ratio on available contact length.*

and the largest cylinder that the pair of links can grasp is

$$\frac{D_{cyl}}{L} = 2\mu - \frac{W}{L}. \tag{3.3}$$

Therefore, the grasp length, L′, and the largest diameter cylinder that can be grasped are dependent directly on the aspect ratio, $\frac{L}{W}$, and are both maximized when the aspect ratio is made as large as possible.

Many design considerations affect aspect ratio. For example, the decision to use a compact transmission in order to remove actuator bulk from the joint to the base or just back a few links improves aspect ratio. When a not-so-compact, single-stage reduction is used, the diameter of the final drive pulley or gear at the joint or the length of the output link of a four-bar linkage, if made large to increase the effective transmission stiffness, transmission ratio, and/or joint strength, decreases aspect ratio. When a more-compact multiple-stage reduction increases torque at the joint, aspect ratio is improved over the single-stage reduction at the cost of lower power efficiency (chapter 6) and higher complexity.

3.2.5 High Efficiency

High efficiency is most important in mobile robots and underwater and space environments where power is limited. It is in these unstructured and changing environments that WAM is most essential; so we associate the need for high efficiency with WAM.

The efficiency of the transmission is defined as the output power at the joint divided by the input power at the motor shaft and is the primary focus of the analysis in chapter 6 where we analyze the efficiency of tension-element drives. Power loss in the transmission is always realized as friction dissipation, which when large, degrades velocity-dependent backdrivability.

3.2.6 Good Backdrivability

There are two types of backdrivability:

- acceleration-dependent and
- velocity-dependent.

Backdrivability is measured in Cartesian coordinates at a fixed point on the manipulator, usually the endtip. A mechanism which has good acceleration-dependent backdrivability generates small inertia-induced forces when accelerated. The backdrivability of a single link is improved by minimizing the link-structure inertia and then keeping the transmission ratio smaller than the matched-inertia transmission ratio so that the reflected motor inertia remains relatively small.

Similarly, a mechanism which has good velocity-dependent backdrivability generates small friction-induced forces in response to imposed endtip velocities. It is commonly known that a transmission mechanism which uses worm gears and has dry friction will not be backdrivable at all if the pitch angle of the worm gear is less than the friction-cone angle.

The concept of designing manipulators for good backdrivability is borrowed from high-quality teleoperator design where high backdriven inertia and friction in the master/slave system would mask the transmission of forces in bilateral force reflection. Also, isotropy in the backdriven inertia and friction improves teleoperator performance by reducing the disparity between the desired and achieved motions. Some manipulator designers as well have begun to design for good backdrivability. For example, in order

to simplify the dynamic equations for calculating the actuator torques in the trajectory control of a direct-drive arm, Asada [Asada 84] redesigned a manipulator so that the inertia properties at its endtip would be nearly isotropic over a large portion of its workspace.

Good backdrivability causes the manipulator to behave desirably without dependence on closed-loop control. If closed-loop control is used, system accuracy can be improved. If open-loop force control is used and the manipulator is backdrivable over a practical bandwidth, then forces which are applied to the manipulator are "sensed" at the actuator without the need for endtip sensors. In effect, the distinction between actuator and sensor vanish. Furthermore, the good backdrivability means that the impulse force generated upon impacts will be smaller and a manipulator will be naturally robust to collisions and impacts by lowering the effective mass, J_l in equation (3.1).

Chapter 4
The Effect of Transmission Design on Bandwidth

This chapter is divided onto four sections. The first section describes the importance of open-loop bandwidth and clarifies the definition of a speed reduction. The second section shows the effect of transmission stiffness and speed-reduction location on open-loop bandwidth of a position-controlled manipulator. The third section studies the open-loop bandwidth of a force-controlled manipulator. The fourth section suggests a strategy for allocating transmission and contact stiffness to maximize open-loop bandwidth.

4.1 Introduction

A high-performance manipulator must respond quickly to both commands and disturbances, and so its bandwidth must be large. Factors such as the distribution and level of transmission compliance and the location of a speed reduction affect bandwidth. It is commonly known [Nevins 73, Whitney 77, Andeen 88] that compliance can aid the stability and quality of force control. But manipulator compliance can also reduce position and force bandwidth. Moreover, it is often most convenient for the designer to attach any speed reducer directly to the motor shaft. This decision produces a design with lower stiffness, and therefore lower bandwidth, than if the same reducer were placed at the joint.

4.1.1 The Relationship Between Open- and Closed-Loop Bandwidth

Open-loop bandwidth of the transmission is a measure of the quickness with which the transmission mechanism communicates position and force from the actuators to the output. Explicit force feedback may be used to close a control loop around the open-loop mechanism in order to boost the resulting (closed-loop) bandwidth, in effect attempting to alter the impedance actively [Colgate 87, Hogan 87] — but with associated costs. These costs are:

- much larger actuator torques than would be needed to supply a given level of output torque within the open-loop bandwidth (i.e., the controller must *fight* the relatively sluggish dynamics of the mechanism), and
- lower robustness because the stability of these systems often depends on accurate knowledge of mechanical parameters and the assumption that unmodeled dynamics are insignificant.

A simple solution for achieving high bandwidth while minimizing the closed-loop control costs is to boost the open-loop bandwidth. Open-loop bandwidth is determined independently of the control algorithm used and depends only on the physical parameters of the transmission mechanism. This independence simplifies the mechanical designer's task because improving the open-loop bandwidth in position- and force-controlled tasks is relatively straightforward as the following sections of this chapter demonstrate.

Beginning in section 4.2 we define simple models of the transmission for position-in-position-out and force-in-force-out and examine the corresponding transfer functions. The bandwidth of each of our simple models (which neglect damping) is approximately equal to the frequency of the first breakpoint* in the magnitude of the frequency response which, in turn, is equal to its lowest resonant frequency. We want the open-loop bandwidth to be as high as possible to increase the quickness of the manipulator's response to commands and disturbances.

---

* The first breakpoint frequency in these cases is the smallest root of the characteristic equation of the transfer function.

4.1.2 The Speed Reducer

We must introduce one additional mechanical attribute, the speed reducer, to the transmission model of figure 1.2 before proceeding with the analysis. Commonly a speed-reducer mechanism is included in the transmission to boost the actuator torque capacity and the effective motor constant of a small-but-fast actuator by the magnitude of the speed reduction. This magnitude, N, (also called transmission ratio) is the ratio of motor speed to joint speed. In a practical force-controlled manipulator, $unity \leq N \leq N_m$, where *unity* includes direct drive and N_m is the transmission ratio which matches the link inertia to the reflected motor inertia for maximum link acceleration; so that $N_m = \sqrt{J_l/J_m}$ where J_m is the motor inertia. If N were greater than N_m, the reflected motor inertia would dominate the total inertia measured at the joint and thus degrade the acceleration-dependent backdrivability.

The reducer may be a part of the mechanism which communicates power over a distance or distinct from it as we illustrate with the following descriptions of tension-element drives. In the single-stage, tension-element speed reduction of figure 4.1, the reduction is the ratio of the output-pulley diameter to the input-pinion diameter. The speed reducer is integral with the mechanism which communicates power over some distance between the actuator and the joint. Figure 4.2 represents a tension-element transmission in which the speed reducer is distinct from the mechanism (tension element) which communicates power over some distance. There is also a mixed mode shown in figure 4.3 in which part of the reduction is distinct and part is integral.

This classification extends beyond tension-element drives to other transmission types. For example, equal-diameter input and output pinion/gear sets connect an electric motor to a joint via a long rotating shaft in figure 4.4.a. A separate gear box may be included as a distinct speed reducer at the motor shaft to boost output torque leading to the shaft and joint as shown in figure 4.4.b.

When these two functions of the transmission are distinct, the designer is free to select the position of the speed reduction as well as its magnitude. This design freedom exists to some degree in the mixed mode of figure 4.3 as well. We can modify the lumped-parameter model presented in figure 1.2 to include the distinct speed reducer, as shown in figure 4.5, where the reducer is located at some distance, C, from the motor, thus dividing the transmission stiffness into two parts, k_{tr_a} and k_{tr_b}, where subscript

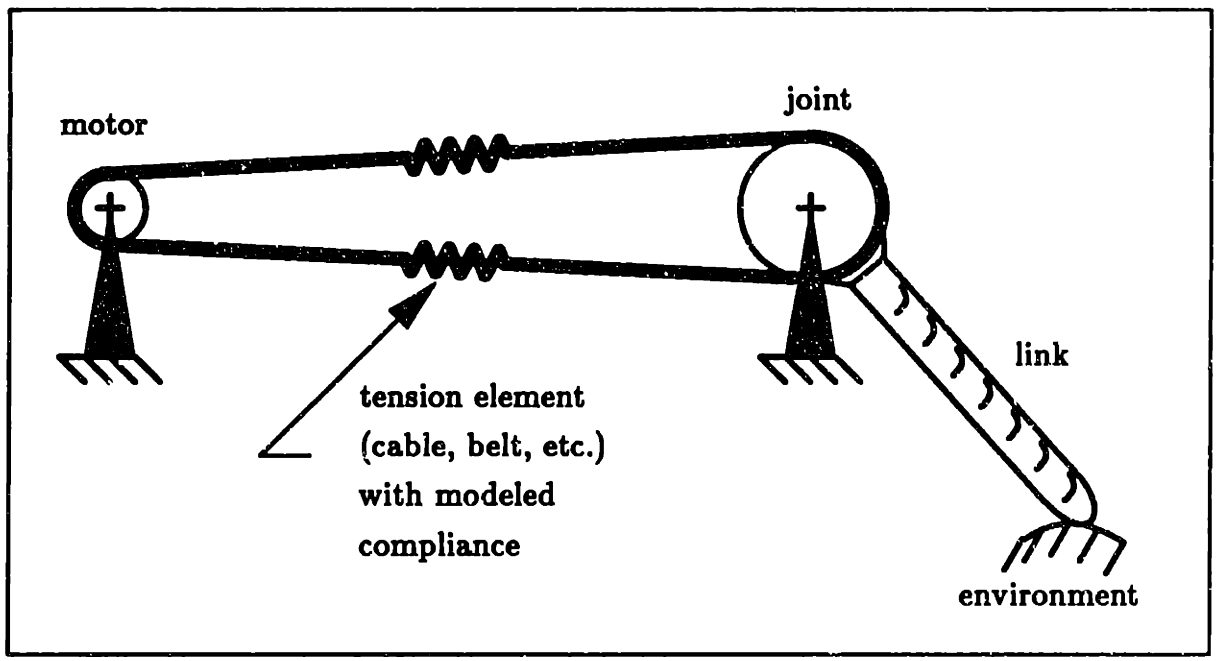

Figure 4.1. *Single-stage tension-element transmission.*

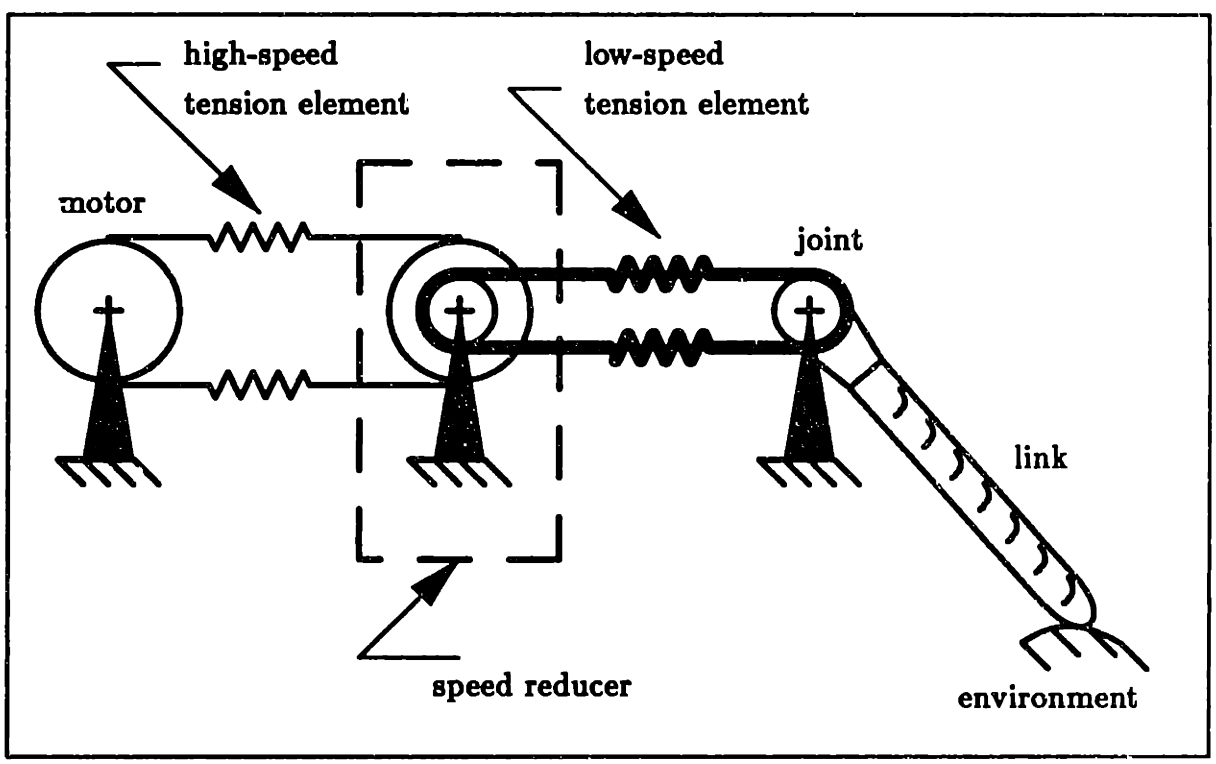

Figure 4.2. *Transmission with a speed reducer.*

a refers to the high-speed, low-tension part of the transmission, and subscript b refers to the low-speed, high-tension part of the transmission.

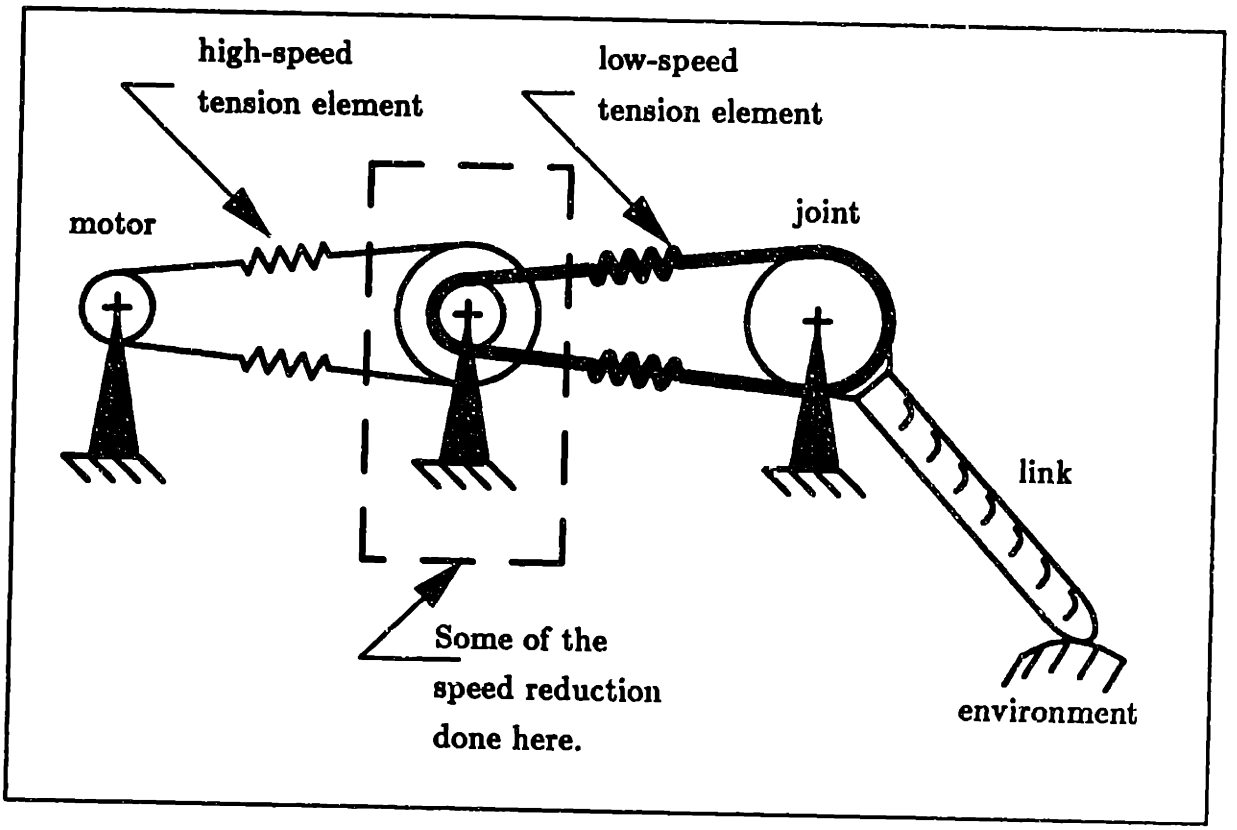

Figure 4.3. *Transmission with both integral and distinct reduction.*

In many types of transmissions, such as tension-element drives, both stiffness and strength are proportional to the shear, tension, or compression cross-sectional area. Suppose the cross-sectional areas for the high- and low-speed parts of the transmission are selected so that the stress is constant along the transmission. We find that, although the element in part a of the transmission is lighter than that in part b by N, the effective stiffness of part a for a given transmission length is greater by N. Furthermore, the effective transmission stiffness, k_{eff}, for the transmission model of figure 4.5, measured at the joint, is

$$k_{eff} = \frac{\mathrm{N}^2 EA}{\mathrm{N}L + C(1-\mathrm{N})}, \tag{4.1}$$

where L is the transmission length, E is the modulus of elasticity of the transmission-element material, and A is the cross-sectional area of the high-speed part of the transmission. The effective transmission stiffness of equation (4.1) is maximized by letting $C = L$, i.e., by placing the reduction mechanism at the joint, so that the high-speed part of the transmission spans most of the distance between the actuator and joint.

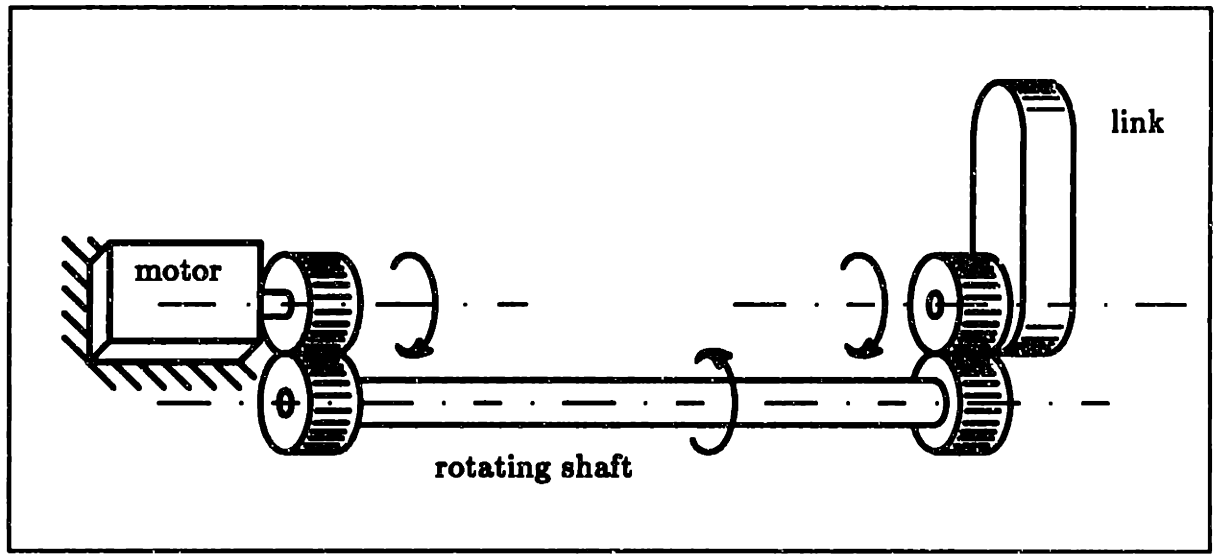

a) Power communicated over a distance through a rotating shaft.

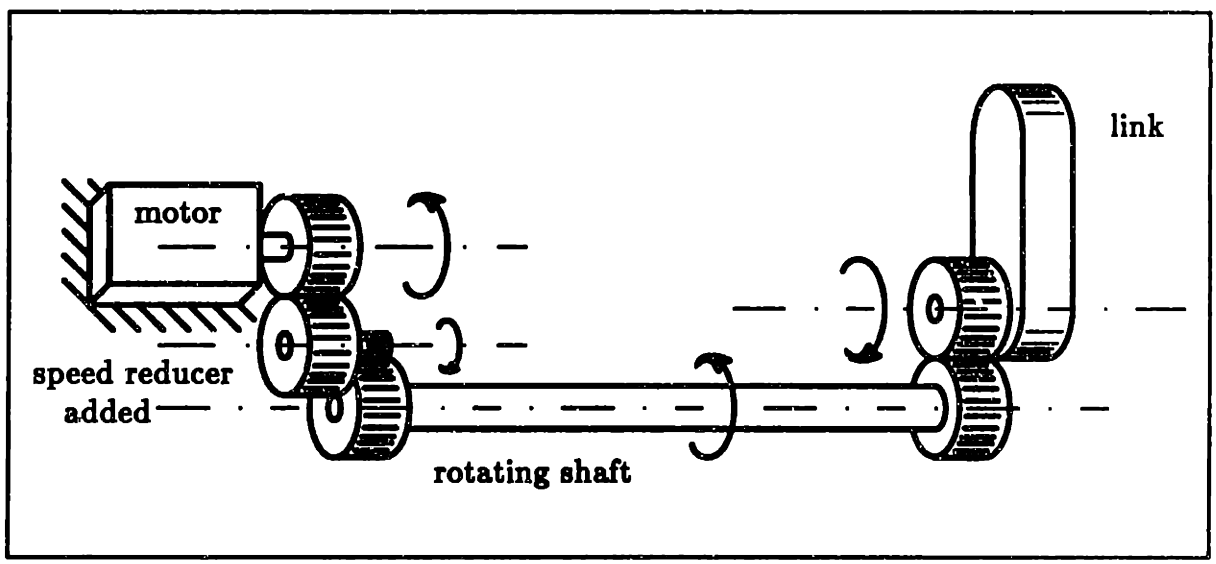

b) A speed reducer increases torque to the joint.

Figure 4.4. *Rotating shaft and pinion/gear transmission.*

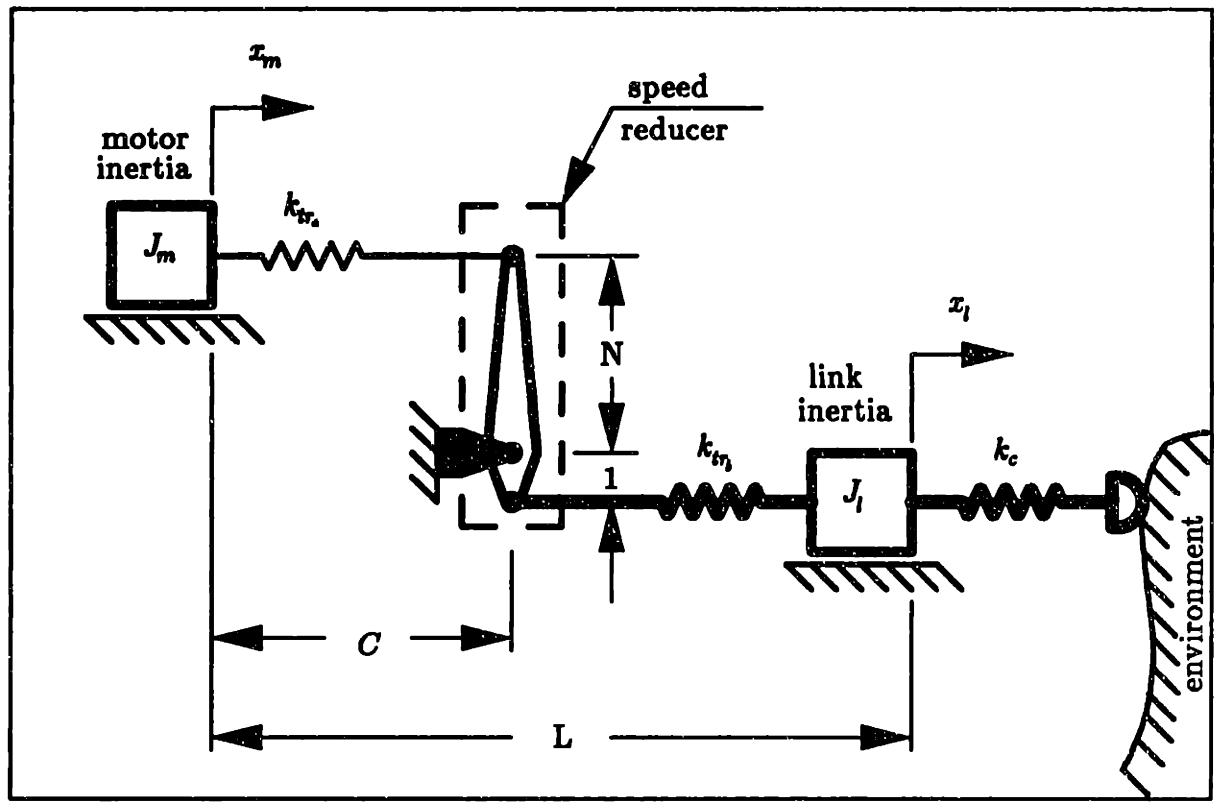

Figure 4.5. *Transmission model similar to figure 1.2, modified to include a distinct speed reduction.*

4.2 Open-Loop Position Bandwidth

Figure 4.6 illustrates a simple transmission model, without speed reducer, for controlling joint position. k_{tr} is the transmission stiffness and J_l is the link inertia. For stiff position control, we may model the actuator as a position source, x_m; the response is the joint position, x_l. If s is the differentiation operator, then

$$\frac{x_l}{x_m}(s) = \frac{k_{tr}}{J_l s^2 + k_{tr}}, \tag{4.1}$$

and the bandwidth (i.e., the lowest resonant frequency) is simply $\sqrt{\frac{k_{tr}}{J_l}}$.

Nearly always when a speed reduction is used in a manipulator transmission, the reducer, generally multi-stage and included to boost torque, is placed at the motor rather than the joint. How does this decision affect position bandwidth? Figure 4.7 illustrates the same simple transmission, but with a transmission reduction. Again we assume stiff position control at the actuator. We consider two cases, depending on the actuator location — at the motor (figure 4.7.a) and at the joint (figure 4.7.b). The

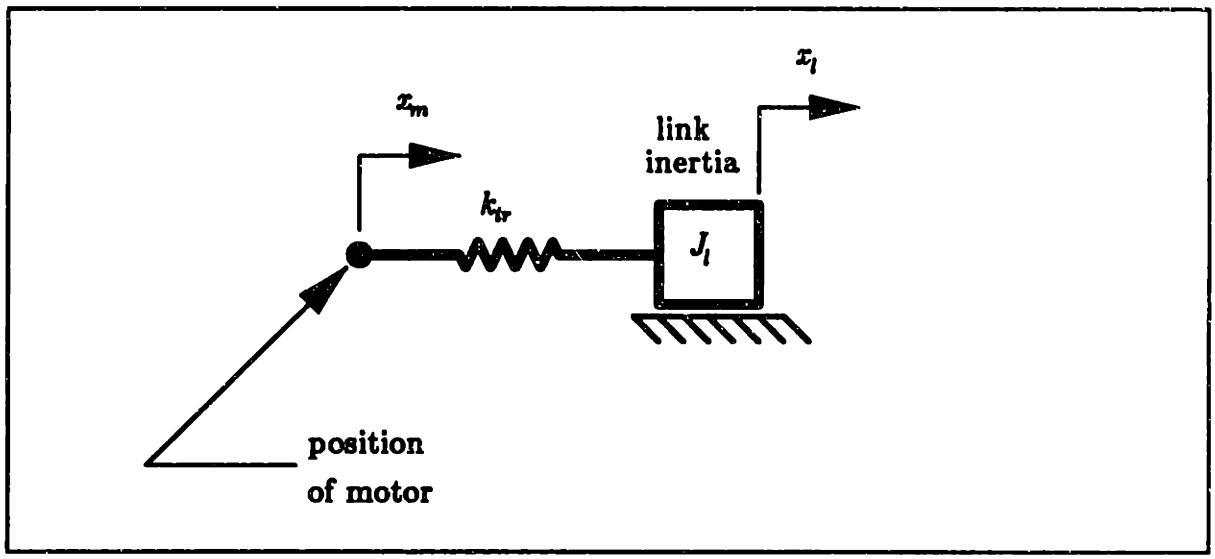

Figure 4.6. *Simple model of a position-controlled manipulator without reducer.*

transfer function for figure 4.7.a is identical to equation (4.1), with the same bandwidth. However, the transfer function for figure 4.7.b is

$$\frac{x_l}{x_m}(s) = \frac{\mathrm{N}^2 k_{tr}}{J_l s^2 + \mathrm{N}^2 k_{tr}}, \tag{4.2}$$

and the bandwidth is $\mathrm{N}\sqrt{\frac{k_{tr}}{J_l}}$. The bandwidth is made N times higher simply by locating the reducer at the joint.

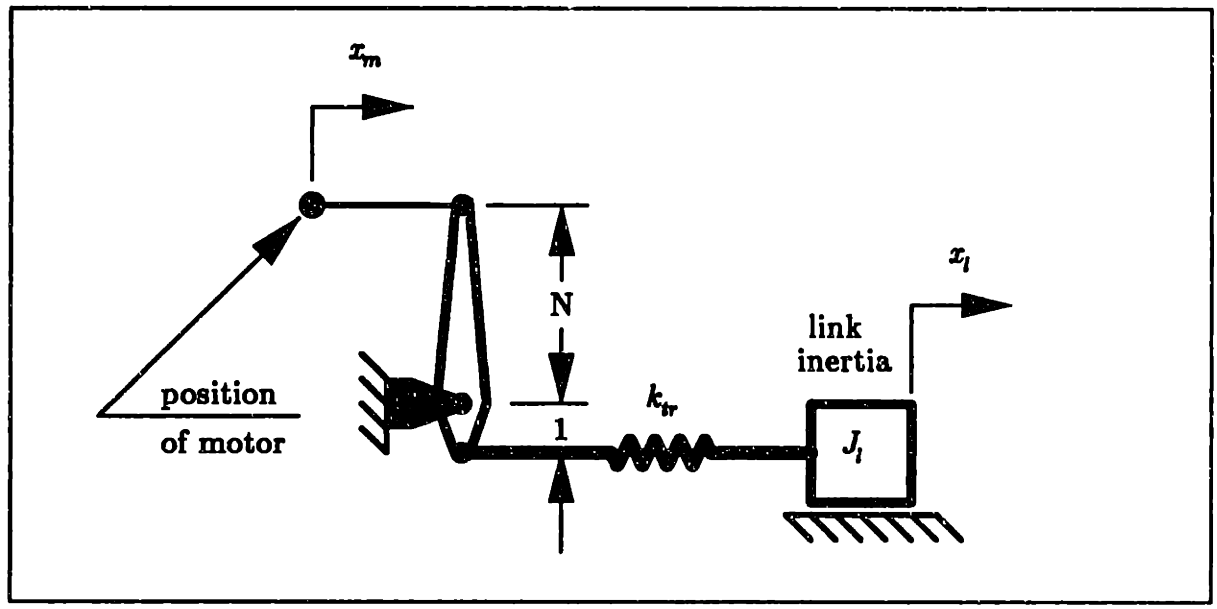

a) Reducer located at motor.

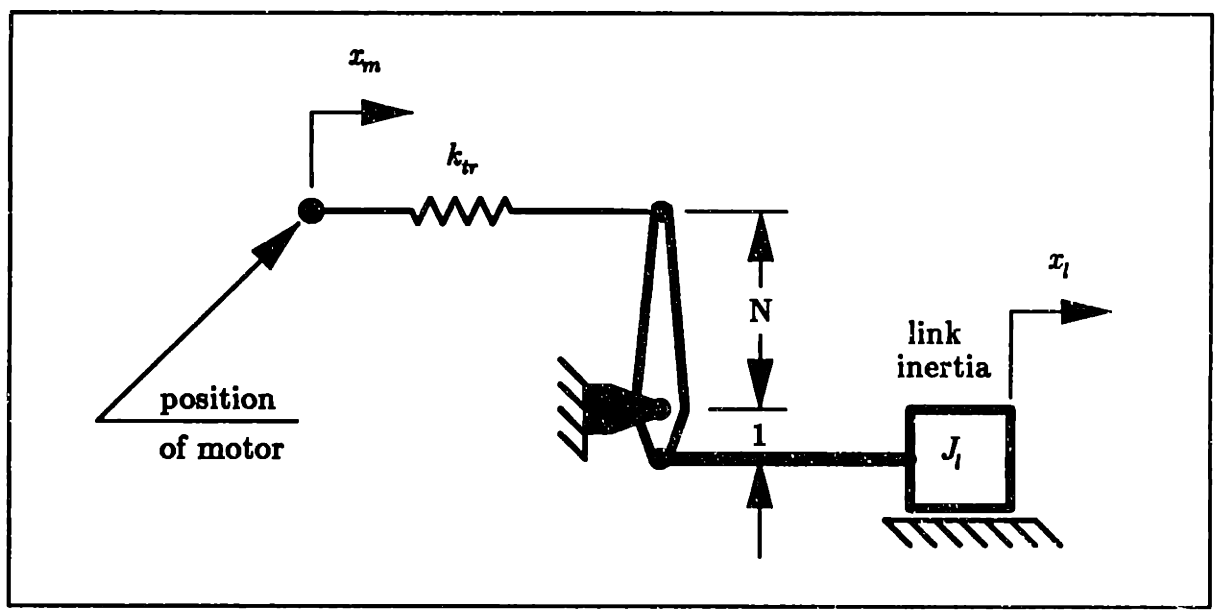

b) Reducer located at joint

Figure 4.7. *Two simple models of position-controlled manipulators with reducers.*

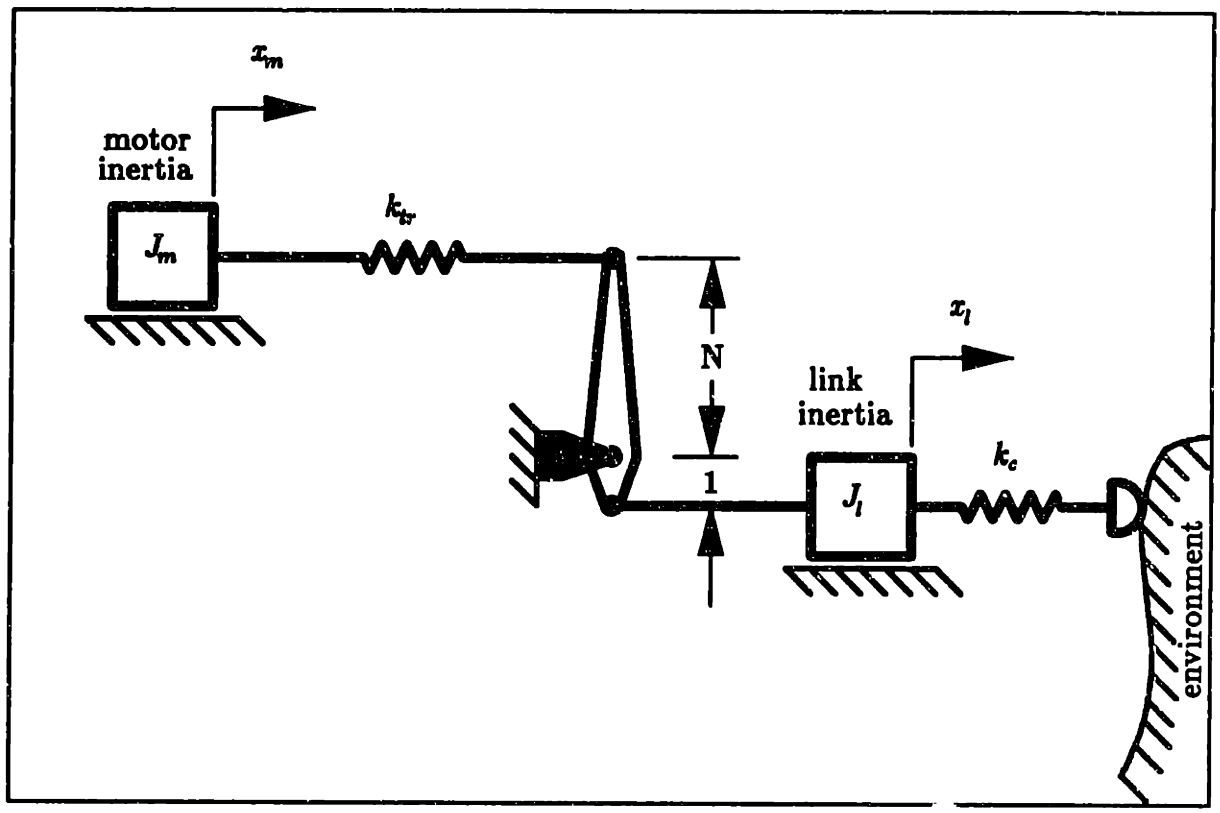

Figure 4.8. *Transmission model for force control.*

4.3 Open-Loop Force Bandwidth

4.3.1 General Form

Figure 4.8 illustrates a transmission model, with reducer at the joint, for controlling joint force. Force, F_m, is applied to the motor inertia, J_m. Contact with the environment is made through stiffness, k_c, generating contact force, F_c. The transfer function is

$$\frac{F_c}{F_m}(s) = \frac{k_{tr}k_c}{J_m J_l s^4 + (J_m k_c + J_l k_{tr} + \mathrm{N}^2 J_m k_{tr})s^2 + k_{tr}k_c}. \tag{4.3}$$

The characteristic equation has two breakpoint frequencies; the lower one limits the bandwidth. By substituting $j\omega$ for s in equation (4.3), where $j = \sqrt{-1}$, and solving for the two real roots of the denominator, we find the values of both breakpoints. The solutions for ω are

$$\omega_{1,2}^2 = \frac{1}{2}\left[\frac{k_c}{J_l} + \frac{k_{tr}}{J_m} + \frac{N^2 k_{tr}}{J_l} \mp \sqrt{\left(\frac{k_c}{J_l}\right)^2 + \left(\frac{k_{tr}}{J_m}\right)^2 + \left(\frac{N^2 k_{tr}}{J_l}\right)^2 + 2\left(\frac{N^2 k_{tr} k_c}{J_l^2} + \frac{N^2 k_{tr}^2}{J_m J_l} - \frac{k_{tr} k_c}{J_m J_l}\right)}\right] \quad (4.4)$$

Let ω_2 be the larger frequency, and let ω_1 be the smaller solution that limits bandwidth. If we explore the behavior of ω_1 as a function of k_c, we find two asymptotes.

$$\lim_{k_c \to 0} \omega_1 = 0, \quad (4.5)$$

and

$$\lim_{k_c \to \infty} \omega_1 = \sqrt{\frac{k_{tr}}{J_m}}. \quad (4.6)$$

Also, between these extremes of contact stiffness, we explore the effect of large and small transmission ratios.

$$\lim_{N \to 0} \omega_1 = \begin{cases} \frac{k_c}{J_l}, & \text{if } k_c \leq k_{tr}\frac{J_l}{J_m}; \\ \frac{k_{tr}}{J_m}, & \text{if } k_c \geq k_{tr}\frac{J_l}{J_m}. \end{cases} \quad (4.7)$$

And

$$\lim_{N \to \infty} \omega_1 = 0 \quad (4.8)$$

4.3.2 Practical Example

In order to visualize the character of the frequency solutions of equation (4.4), we plotted them versus contact stiffness in figure 4.9.a for a practical manipulator transmission*. This cabled transmission is driven by a Moog 303-003 DC brushless motor with an inertia of 0.0057 oz-in-sec^2 and a pinion diameter of 0.75 in. The 0.044-in diameter stainless-steel cable circuit spans 36 in, and each half of the circuit has a stiffness of 262 lb/in. The transmission ratio, N, is 14 ($N_m = 104$); and the reducer is located at the joint, which drives a relatively rigid, 36-in-long link with an inertia of 64 oz-in-sec^2.

If the hard link surface contacts a hard environment, then the contact stiffness is effectively that of the link. If the link contacts a soft environment and/or it is given a soft covering, then the effective contact compliance will equal the sum of these compliances. In whole-arm manipulation, the contact stiffness measured at the joint can assume a broad range of effective values because it varies with the square of the distance between the contact point and the joint.

Referring to figure 4.9.a, we notice that there is a contact stiffness above which bandwidth is no longer improved if we increase contact stiffness. This is an important result because researchers [Whitney 85] have shown that decreasing the contact stiffness may improve stability, but it is unclear how far the stiffness should be reduced. To optimize stability margin and bandwidth together we suggest reducing contact stiffness until just before the bandwidth begins to decrease appreciably, which occurs at about $k_c = 9\text{x}10^5$ in-lb — the equivalent of gluing a foam covering to the 36-in-long link that would give a contact stiffness near its tip of 650 lb/in.

In fact, for this example, the best contact stiffness for both stability and bandwidth is approximately

$$k_c = k_{tr}\frac{J_l}{J_m}. \tag{4.9}$$

This is the stiffness for the cross-over point of the two curves in figure 4.9.b, calculated at the intersection of the curves in equation (4.7). However, this method of selecting the contact stiffness is strictly valid only for small values of N. The error in using this method is apparent from the family of curves in figure 4.9.c, where the bandwidth is plotted versus k_c for high and low values of N compared to N_m. We see that as the

* This is a recurring example used again in chapters 5 and 6.

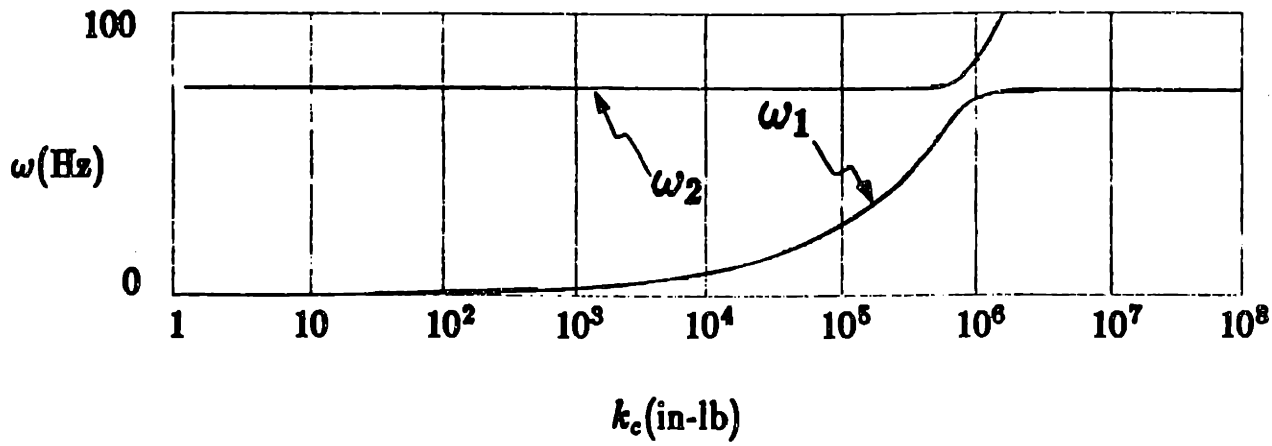

a) *True breakpoint frequencies.*

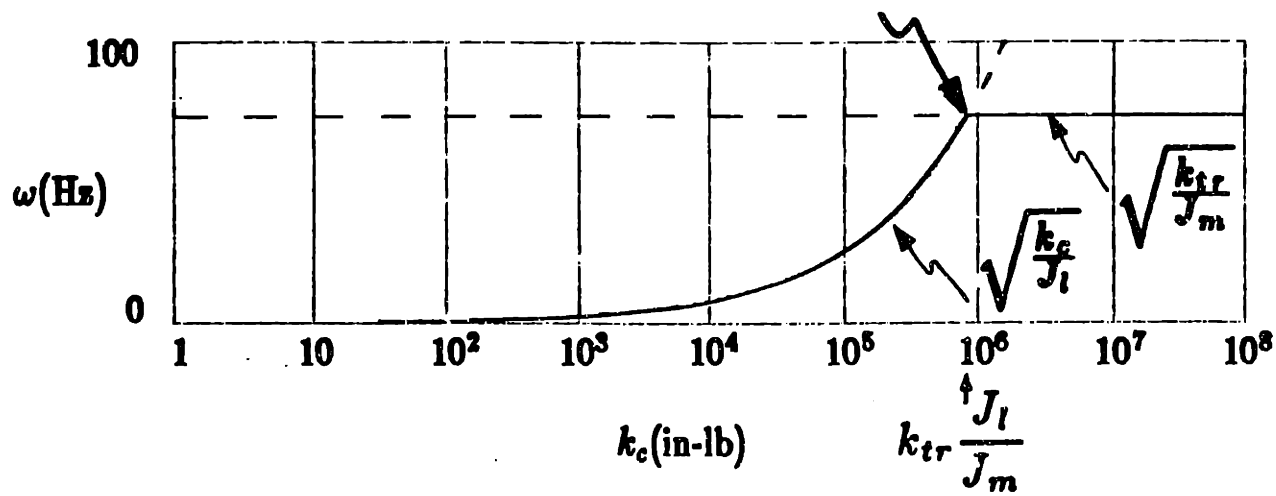

b) *A good approximation for small N.*

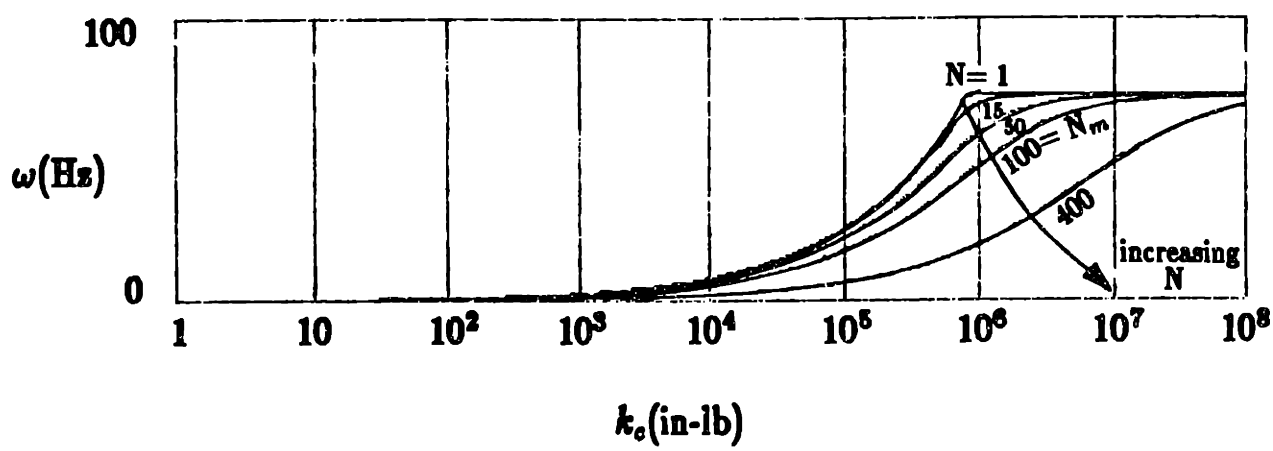

c) *True breakpoint frequencies for several values of N.*

Figure 4.9. *Open-loop force bandwidth versus contact stiffness.*

transmission ratio approaches N_m, the sharp corner at the cross-over point is smoothed, making it more difficult to select the best contact stiffness. In this case, it may be necessary to decide on an acceptable level of bandwidth as a fraction of the asymptote of equation (4.6) and solve, numerically or graphically, from the appropriate curve of figure 4.9.c for the contact stiffness that will allow that fraction of the asymptotic bandwidth.

4.4 Design Implications

We can make several comments now about how to design a transmission to increase open-loop bandwidth. We showed that it is best to locate any speed reduction at the joint rather than the motor for improving the transmission stiffness and therefore the bandwidth of position control; a similar argument leads to the same conclusion for improved force-control bandwidth. We have found that for $N \ll N_m$ the value of the transmission ratio has negligible effect on the open-loop bandwidth of force control but higher values of the ratio degrade bandwidth. For practical force-controlled transmission designs, N is much less than N_m.

If the transmission stiffness and transmission ratio are fixed in a design, but it is possible to adjust the contact stiffness, for example by adding a soft covering; then the best stiffness is that given in equation (4.9) for low N or some fraction of the asymptote, $\sqrt{\frac{k_{tr}}{J_l}}$, for high N.

If the mechanical designer is free to select the transmission stiffness for maximum bandwidth, then the maximum contact stiffness, limited by the environment stiffness, guides the selection. In this case we solve for k_{tr} in equation (4.9) to find the best transmission stiffness,

$$k_{tr} = k_c \frac{J_m}{J_l}. \qquad (4.10).$$

Chapter 5
The Effect of Dry Friction and Compliance

In this chapter, we study the effect of dry friction (both Coulomb friction and stiction) on force control with integral feedback. The force is applied through a compliant transmission by a velocity-controlled motor. Our results show that stiction can cause the contact force to enter a limit cycle. Coulomb friction can extend the system stability bounds but may lead to an input-dependent stability. Under certain conditions Coulomb friction causes an actuator limit cycle even though the contact force approaches the desired steady-state force. Based on the analysis, we give design guidelines for increasing the performance.

5.1 Introduction

5.1.1 The Problem Statement

What are Coulomb friction and stiction, and why should we care about them?

Friction is present in most mechanisms. It may take one of many forms but is commonly modeled as linear-viscous damping, Coulomb friction, stiction, or some combination of these, as shown in figure 5.1. In linear control theory, either it is assumed that the friction is linear viscous or attempts are made to linearize the friction about some operating point in order to make a linear analysis possible. Unfortunately, attempts to neglect or linearize significant Coulomb friction or stiction, both of which are discontinuous at zero velocity (figure 5.1.a and 5.1.b), may lead to erroneous predictions of a system's behavior. We usually rely on linear control theory because it is a powerful, well-developed design tool for predicting the behavior of controlled systems such as force-controlled manipulators; however, it fails to predict limit cycles* or input-dependent instabilities which are commonly found in real hardware. These are the characteristics of inherently nonlinear systems, and nonlinear analysis [Gelb 68, Graham 61] is required in order to predict their behavior.

---

* For a non-conservative system a limit cycle is a closed trajectory of the state vector in state space. In a system with nonlinear elements one or more limit cycles may be present and each may be stable or unstable. Trajectories begun near a stable limit cycle converge to it. Trajectories begun inside an unstable limit cycle diverge to another (stable) limit cycle within it or to a single steady-state value. Trajectories begun outside an unstable limit cycle diverge to another (stable) limit cycle outside it or to infinity.

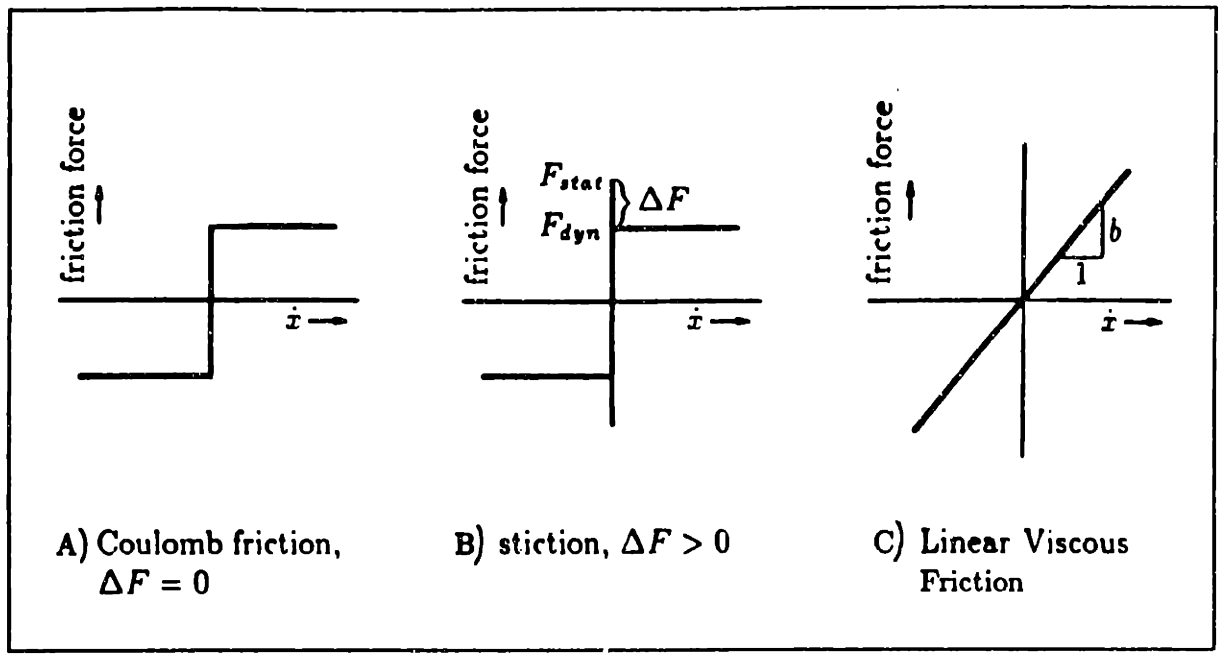

Figure 5.1. *Common models of friction.*

5.1.2 Previous Work by Other Researchers

The magnitude of friction, often neglected in the analysis of manipulator position, velocity, and force control, is significant in today's manipulators. Armstrong [Armstrong 88] has shown that the dry-friction forces in the transmission are over twice the magnitude of the inertial forces in the first joint of the PUMA-560 robot when commanded to maintain a sinusoidal position trajectory 2 radians peak to peak at 0.17 Hz (2.0 radians/sec^2 maximum acceleration). The friction level in this joint is 12 % of the 100-N-m maximum stall torque. Armstrong notes that for higher accelerations the motor quickly saturates, at which point inertial forces disappear, and friction forces dominate completely.

The problems Coulomb friction and stiction are thought to impose have been identified in several force-controlled manipulators. Raibert and Craig [Raibert 81] found limit-cycle oscillations in a hybrid position/force controlled manipulator which they believed to be caused by the interaction of Coulomb friction and integral gain. In designing the Utah/MIT dexterous hand [Jacobsen 86] abandoned the idea of using tendon sheaths in favor of pulleys in order to reduce friction. He identifies the tradeoff between high sheath friction on one hand and complex, volume-expensive tendon routing via low-friction pulleys on the other. Many designers have tried to feed

forward compensation torques to cancel the effect of Coulomb friction. Armstrong [Armstrong 88] uses a sophisticated feedforward technique on the PUMA 560 which focuses particular attention on the exact form of the friction model. Hollars and Cannon [Hollars 85] attempted to feed forward compensation torques for Coulomb friction in the motor, pulleys, and joints of a two-link, compliant-tendon-driven manipulator with some success. However, in any manipulator, torque cannot be input directly to distal pulley, gear, linkage and/or joint friction nodes because of the transmission dynamics. Finally, the force-controlled stability may be input or disturbance dependent, a fact which we have found under certain conditions in the Salisbury three-finger hand.

There are several methods of implementing force control with force feedback [Maples 86]. The actuator is commonly used as a torque source [Salisbury 80, An 86]. However, as explained in section 2.1, stiff inner control loops to servo motor position [Maples 86] and velocity [Whitney 77, Salisbury 84] reduce the effect of brush and motor bearing friction. In our analysis we study the effect of a velocity-controlled motor applying contact force through a compliant transmission; although the analysis applies to position-controlled motors also. Since a proportional gain on force error, used to produce output positions of the actuator pushing against a simple compliant transmission, gives the response of a proportionally controlled system; we prefer to show the output of the controller in figure 5.2 as a position x_m, pushing against a combined transmission-and-compliance, rather than as a velocity to avoid confusion in the use of the terms proportional and integral control. In our system the contact force, F_c, is fed back and subtracted from the commanded desired force, F_{des}, and the difference creates an error signal F_{error}, to be utilized by the control law with G_P (proportional gain), or G_I (integral gain).

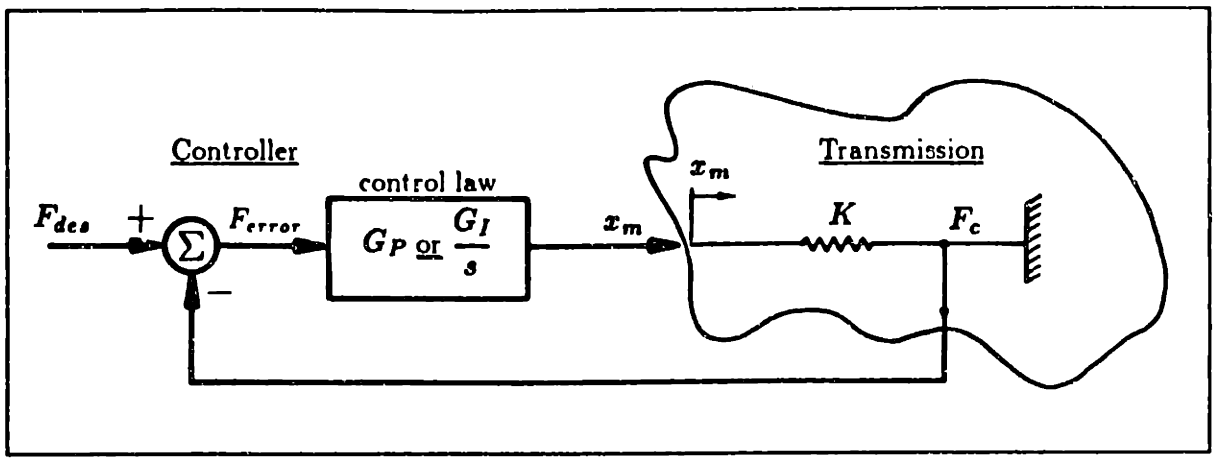

Figure 5.2. *Force control with a simple transmission model.*

5.1.3 Our Analytical Approach

After pausing to state the obvious effect of dry friction as a deadband in systems *without* force feedback, we treat increasingly complex transmission models *with* force feedback. In each case, we examine the response of the contact force to a step in desired force because we consider the step to be a worst-case input when mapping stability bounds for a nonlinear transmission. First we characterize the response of a simple system in which the transmission is modeled as an inertialess, frictionless compliance. Next we add friction to a nearly-inertialess node in the transmission. For simple Coulomb friction at this node, the only effect on the response is a simple time delay. For stiction, the response enters a stable limit cycle of known size. Finally we look at the complex case of an inertial transmission. The complexity of this case precludes most quantitative results although the qualitative results on stability, derived through nonlinear analytic techniques and confirmed with simulations, show why a given system can be sometimes-stable-sometimes-unstable. It is found through analysis and simulation that in the inertial case, as in the nearly-inertialess case, stable limit cycles in F_c occur only when stiction is present. However, for high feedback gains the system may diverge to infinity and never reach a stable limit cycle. With stiction, the system, inertial or inertialess, never settles to F_{des}. For a stable inertial transmission with Coulomb friction we predict a limit cycle in the actuator node even though the error between F_c and F_{des} approaches zero.

5.2 Open-Loop Model

In open-loop (motor-torque based) force control, the effect of dry friction is straightforward. In this case Coulomb friction acts as a pure deadband nonlinearity between the input force, F_m, or F_{des} as it is called in this chapter, and F_c. So the minimum controllable force is limited by the level of friction. In this no-feedback case the system, driven by dynamically stable motors, is itself always dynamically stable.

5.3 Simple Transmission Model with Force Feedback and No Friction

Figure 5.2 illustrates the simplest transmission model for the force-feedback case — a linear, inertialess, frictionless compliance, $1/K$. Control of motor *position* proportional to force error (proportional control) elicits a zero-order response as shown in figure 5.3.a. The contact force reaches its final value infinitely fast with a steady-state error,

$$F_{error} = \frac{F_{des}}{1 + G_P K}. \tag{5.1}$$

This response would require a step change in actuator position, a change which is clearly impossible and only poorly approximated with real motors. The presence of friction would simply increase the steady-state error.

A more realistic control law for step inputs that has zero steady-state error is one which commands motor *velocity* proportional to force error (integral control). The step response in figure 5.3.b is first order with the time constant,

$$\tau = \frac{1}{G_I K}, \tag{5.2}$$

and requires step changes only in actuator velocity, which can be more closely approximated with real motors.

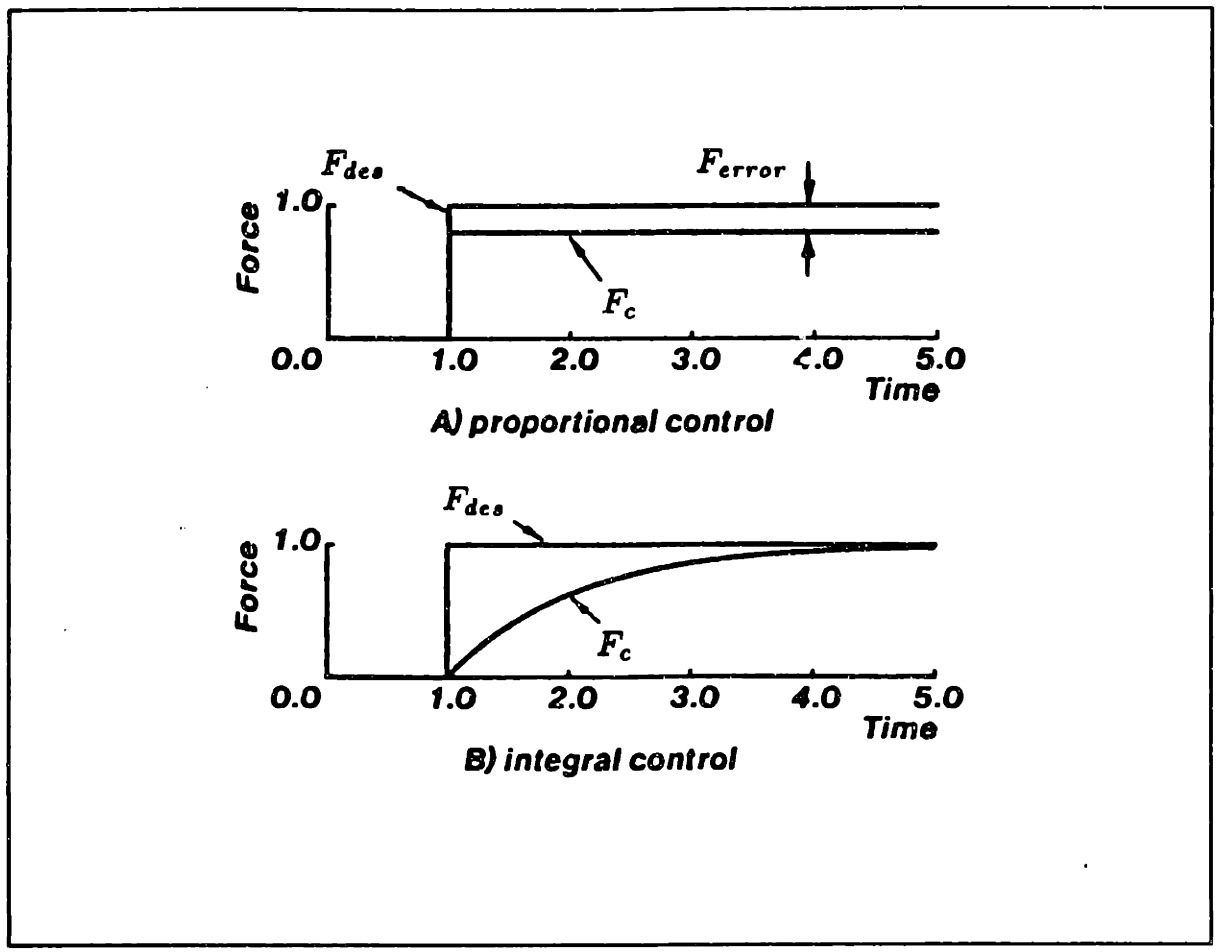

Figure 5.3. *Step response with a simple transmission.*

5.4 Stiction-Induced Limit Cycles and the Nearly-Inertialess Friction Node

We extend the simple transmission model by including certain models of linear and nonlinear friction. We define the nonlinear friction in figure 5.1 as "Coulomb friction" when the static and dynamic friction are equivalent ($F_{friction} = F_{static} = F_{dynamic}$ in figure 5.1.a); otherwise ($F_{static} > F_{dymanic}$ in figure 5.1.b) it is called "stiction." The friction acts on a nearly-inertialess* node located at some point in series with the transmission and contact stiffnesses, k_{tr} and k_c, as shown in figure 5.4. Since we assume the link is inertialess, we may apply a broader, more-useful definition of k_{tr} and k_c for the inertialess case to mean the stiffnesses on either side of a friction node located anywhere in the transmission and not just at the joint. In physical hardware,

* Since $\lim_{J_l \to 0}$ momentum $\neq 0$ in the case of stiction where high velocities of the node occur, we cannot neglect inertia altogether.

this friction may arise for example between a tendon and its sheath [Salisbury 84] or at an intermediate stage of the transmission, as well as at the joint.

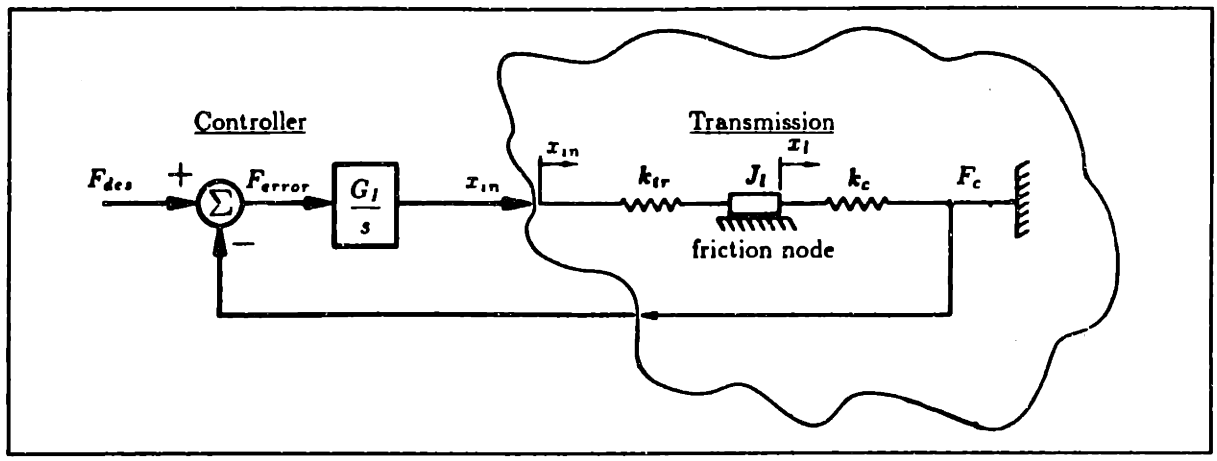

Figure 5.4. *Block diagram of a system with friction.*

If, on one hand, only Coulomb friction is present, then a simple time delay,

$$\tau_{delay} = \frac{F_{friction}}{G_I k_{tr} F_{error}}, \tag{5.3}$$

will precede a close approximation to the normal, first-order step response for the simple frictionless model. The first-order approximation assumes that the friction node dynamics are much faster than the actuator node dynamics, which implies that

$$\frac{G_I k_{tr} k_c}{k_{tr} + k_c} \sqrt{\frac{J_l}{k_{tr} + k_c}} \ll 1.0. \tag{5.4}$$

Equation (5.4) is derived by requiring the natural frequency of the friction node when the actuator position is locked to be much higher than the speed of the actuator response (the inverse of equation (5.2)).

If, on the other hand, stiction is present, then a stable limit cycle appears, as shown in figure 5.5. The response, consisting of two linear modes, stick and slip, is piecewise linear. In the stick mode

$$\dot{x}_m = G_I F_{error}, \tag{5.5}$$

and the friction node is stationary. During the slip mode we again assume that the inertia dynamics are much faster than the actuator dynamics or that $\Delta x_m \ll \Delta x_l$.

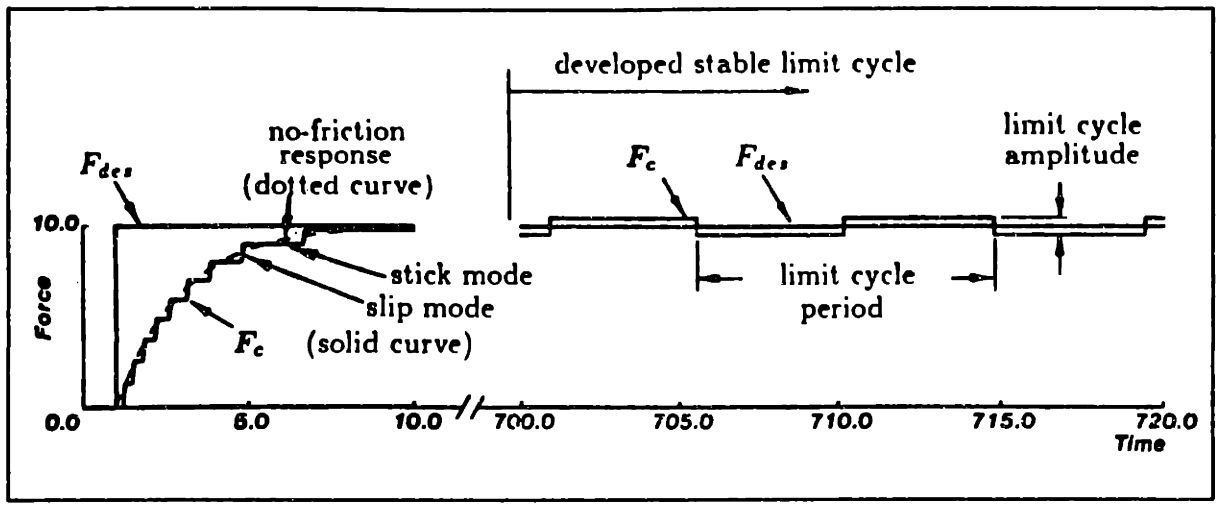

Figure 5.5. *Step response in a nearly-inertialess transmission with stiction.*

Without this assumption the system is third order and we cannot determine the response as a function of the system parameters. With the assumption the equations of motion during slip are only second order which means $F_c(t)$ can be determined in closed form as

$$F_c(t) = F_c(0) + \frac{\Delta F k_c}{k_{tr} + k_c}\left(1 - \cos\left(\sqrt{\frac{k_{tr} + k_c}{J_l}}t\right)\right), \tag{5.6}$$

where

$$\Delta F = F_{static} - F_{dynamic}. \tag{5.7}$$

The piecewise-linear response for the next stick phase is found by applying the initial conditions $\dot{x}_l(0) = 0$ and $\ddot{x}_l(0) = \Delta F / J_l$ and matching initial to end conditions for x_l.

If $\Delta x_m \ll \Delta x_l$ is satisfied, F_c will settle into a limit cycle with

$$\text{amplitude} = \Omega\left(\frac{\Delta F k_c}{k_{tr} + k_c}\right), \text{ and} \tag{5.8}$$

$$\text{period} = \Omega\frac{4}{G_J k_{tr}}\left(\frac{k_{tr} + k_c}{k_c}\right)\left(\frac{2F_{static}}{\Delta F} - 1\right), \tag{5.9}$$

where

$$1 < \Omega \leq 2. \tag{5.10}$$

Ω, which depends on the linear damping, b, equals two in the absence of damping and approaches unity as damping is increased (until the nearly-inertialess assumption no

longer holds). The $\Delta x_m \ll \Delta x_l$ assumption for a limit cycle must be altered slightly from inequality (5.4) to include the effect of damping because, if the damping is higher than the critical damping ratio (i.e., $\zeta > \frac{\sqrt{2}}{2}$), then the actuator motion during the slip phase will be significant. In this case, the assumption becomes

$$\frac{G_I k_{tr} k_c}{k_{tr} + k_c} \frac{\sqrt{\frac{J_l}{k_{tr}+k_c}}}{\sqrt{1-\zeta^2}} \ll 1.0. \tag{5.11}$$

where

$$\zeta = \frac{b}{2\sqrt{(k_{tr} + k_c)J_l}}. \tag{5.12}$$

Dynamic simulations show that limit cycles can occur even if inequality (5.11) is false; adherence to inequality (5.11) simply means that we can predict the amplitude and period of the limit cycle and analytically guarantee its existence.

The limit cycle generally begins asymmetrically (especially with no damping) then evolves into a symmetric limit cycle. During this transition time the period will converge from a large value to the value predicted by equation (5.9). If

$$\frac{\pi G_I F_{error} \sqrt{(k_{tr} + k_c)J_l}}{\Delta F \sqrt{1-\zeta^2}} \ll 1.0, \tag{5.13}$$

so that the friction-node dynamics are much faster than the actuator dynamics, and if F_{error} is greater than the limit-cycle amplitude, then F_c will approach F_{des} in a stepped manner and approximate a first-order response as seen in figure 5.5 with each step equal in height to the eventual limit-cycle amplitude.

5.5 An Inertial-Node Analysis

In the case of an inertial friction node the analysis becomes more complex and our chief results are limited to finding the qualitative description of stability. A heavy robot link with friction at its joint is a physical example of an inertial node. The transfer function for the linear system is

$$\frac{F_c}{F_{des}}(s) = \frac{(G_I + G_P/s)k_{tr}k_c}{s^3 J_l + s^2 b + s(k_{tr} + k_c + G_P k_{tr} k_c) + G_I k_{tr} k_c}. \tag{5.14}$$

It is impossible to factor the third-order characteristic equation symbolically to isolate the effect a certain parameter change has on the step-response quality. Techniques such as the root locus indicate the relative stability and the quality of response as a function of one variable such as G_I only *after* the other system parameters are chosen. The Routh stability test gives

$$\frac{J_l G_I k_{tr} k_c}{(k_{tr} + k_c)b} < 1.0 \tag{5.15}$$

as the condition for stability in the linear system when $G_P = 0$, and this result is conservative for the nonlinear system as we will show in section 5.7.

5.5.1 Describing-Function Analysis

Since the friction problem is highly nonlinear, we use nonlinear techniques to search for instabilities and limit cycles. We begin with the sinusoidal-input-describing-function (SIDF) technique which assumes that the input to the nonlinearity is sinusoidal. First, through block-diagram reduction, we separate the linear and nonlinear elements as shown in figure 5.6. If the linear feedforward block, G(s), has good low-pass filtering characteristics (i.e., the order of the denominator is much greater than that of the numerator), then the input to the nonlinearity will closely approximate a sinusoid. However, in the system we are studying, filtering is inherently poor; and therefore the SIDF results are inaccurate. If a sinusoidal velocity signal is input to Coulomb friction, the output force will have the frequency spectrum of a square wave, i.e., the fundamental frequency equal to that of the input followed by an infinite series of odd harmonics. We can filter this signal analytically, one harmonic at a time, and compare the relative attenuation of the fundamental frequency to each following harmonic. Ideally, we want the output of the filter to consist only of the fundamental frequency, but we find that the

magnitudes of the remaining harmonics are significant. Although the SIDF prediction itself is independent of ΔF, the accuracy of the prediction is worse when stiction is present because the output of this nonlinearity contains a square wave plus two impulses per cycle. Dynamic simulations show that the SIDF predictions for Coulomb friction are qualitatively useful though quantitatively inaccurate. The SIDF predictions for stiction become even qualitatively incorrect.

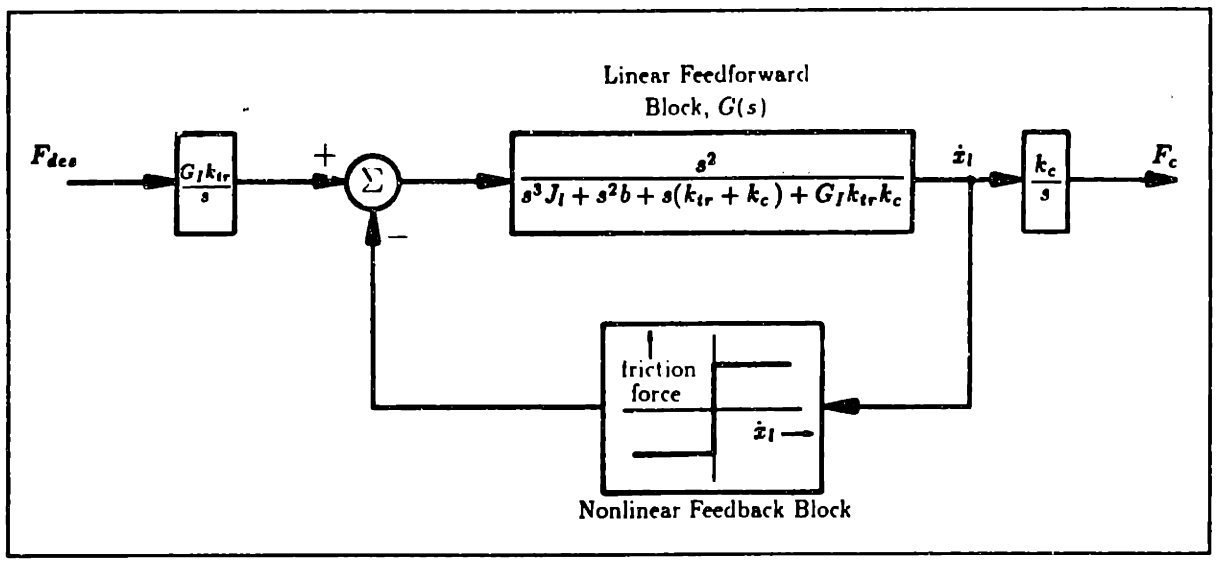

Figure 5.6. *Reduced block diagram of the inertial system with Coulomb friction.*

Candidate limit cycles occur when

$$1 + \mathrm{G}(j\omega)N(\mathrm{A}) = 0 \tag{5.16}$$

where,

G(s) = the linear feedforward block in figure 5.6,

A = the amplitude of the fundamental frequency
of the input to the sinusoidal describing
function of the nonlinearity, N(A), and,

ω = the limit-cycle frequency.

Solutions to equation (5.16) occur at intersections of G($j\omega$) and $-1/N$(A) in figure 5.7. This figure shows G($j\omega$) for unity parameters and two values of G_I. For low G_I, when the system is linearly stable, no intersections occur for finite ω; but for the higher G_I, when the system is linearly unstable, we find a candidate limit cycle. Small perturbations about this intersection indicate that the limit cycle here is unstable; that

is, all trajectories of F_c diverge from this limit cycle and approach either infinity (or some other unmodeled stable limit cycle) or F_{des}. The existence of an unstable limit cycle means that the stability is input dependent. For big step inputs the system trajectory is unstable, and for small step inputs the system is stable. The low and high G_I are examples of domains I and II in figure 5.8.

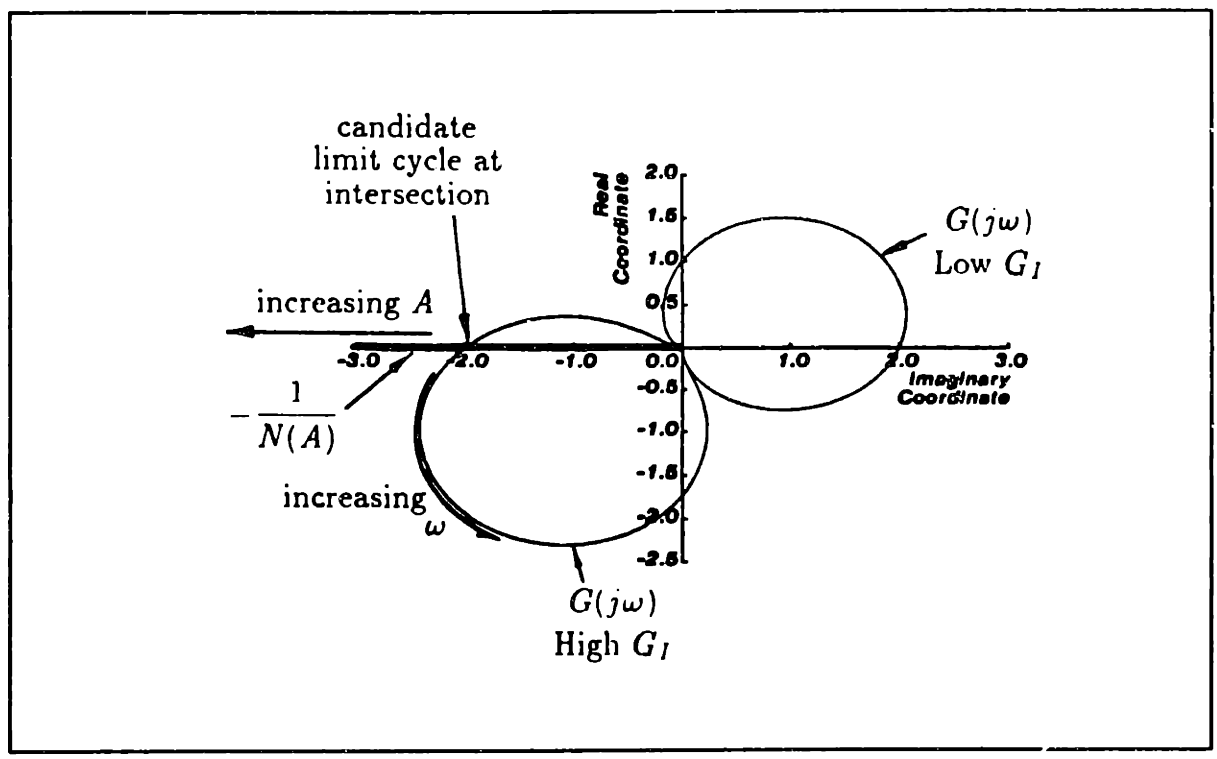

Figure 5.7. *SIDF analysis: complex plot of* $-1/N(\mathrm{A})$ *and* $G(j\omega)$ *for two* G_I.

Figure 5.8 is a mapping of stability for systems with given step-error initial conditions. We simplified the mapping in figure 5.8 by letting $k_{tr}/2 = k_c/2 = K$. The bound for a system with Coulomb friction is determined by J_l, K, and b. We found through simulation and dimensional analysis that the bound stretches to the right if we increase either b or the product J_lK. The bound is always vertical above the dotted line and curved down to point A below it as shown in figure 5.8. This bound is contrasted with the bound at $G_I = b/J_lK$ that the Routh criteria predicts for the linear system. The horizontal axis indicates G_I, and the vertical axis is a normalized measure of the input size.

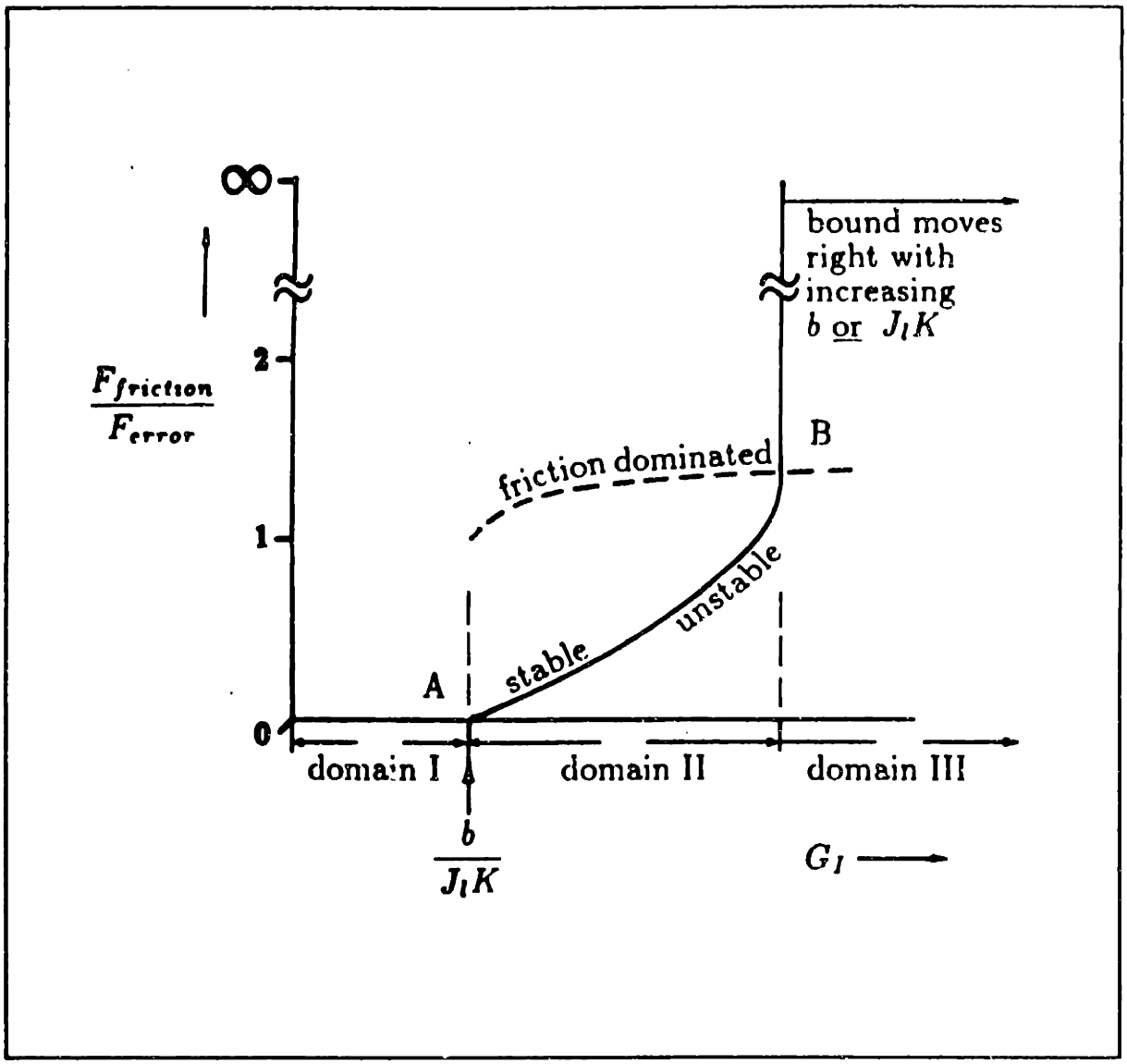

Figure 5.8. *Extended stability region for a system with Coulomb friction.*

5.5.2 Piecewise-Linear Analysis

Piecewise-linear analysis for an inertial node complements the SIDF analysis by predicting domain III which is always unstable. First we define a Coulomb-friction-dominated system as one in which the Coulomb friction exceeds the forces applied to the friction node through the transmission stiffnesses, k_{tr} and k_c, at the end of each half cycle and so causes the node to stick once per half cycle as shown in figure 5.9. If the system is initially Coulomb-friction dominated (the stability bound above point B in figure 5.8), then stability is guaranteed if

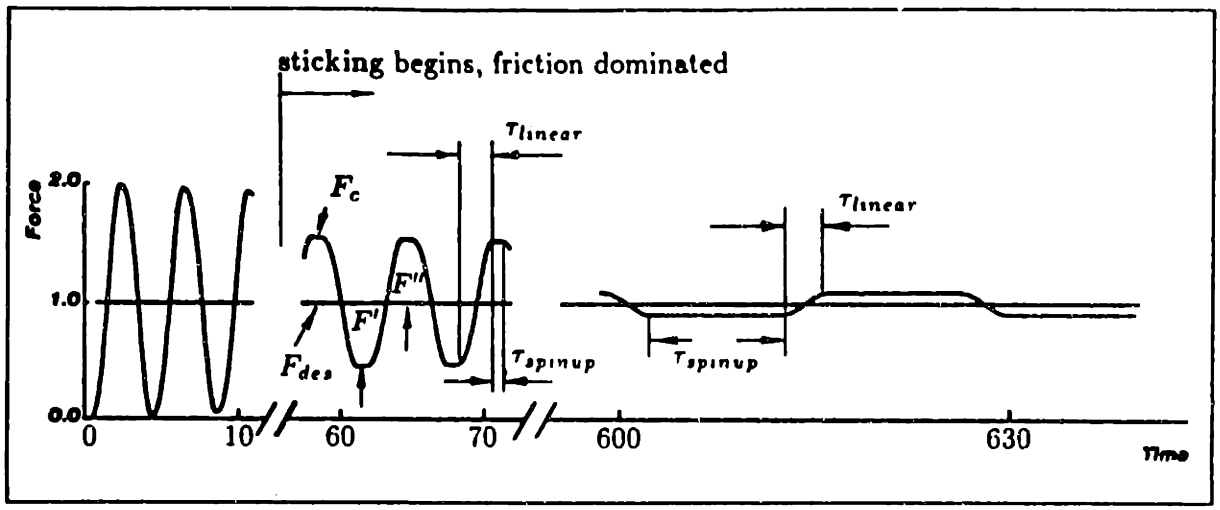

Figure 5.9. *Typical step response of the inertial system with Coulomb friction.*

$$\Psi < 1.0, \tag{5.17}$$

where,

$$\Psi = \frac{F'}{F''}. \tag{5.18}$$

When the friction node begins to slip, the transmission stiffness has already been compressed to an internal force equal to friction, canceling the effect of Coulomb friction until the velocity reverses. The linear transfer function in equation (5.14) gives the response during slip. By calculating time function of equation (5.14) for a step input with fixed J_l, k_{tr}, k_c, b, and G_I, we find that Ψ is constant and independent of F_{error}. Therefore, if $\Psi < 1$, F_{error} of the following half cycles will always decrease (as the system becomes more Coulomb friction dominated); and the system is therefore stable. If $\Psi > 1$, F_{error} will increase by Ψ for the following half cycles until the Coulomb-friction energy dissipation is dominated by viscous energy dissipation. At this point Coulomb friction can truly be neglected, and the Routh criteria correctly predicts instability. If the system is not friction dominated and if, therefore, the inertia node does not stick at the end of the first half cycle, then the SIDF analysis and simulations indicate the curved portion of the stability bound in domain II where the stability is input dependent. Thus our stability mapping for Coulomb friction is complete.

It should be noted that, if the manipulator is found to be unstable for the transmission we have modeled with Coulomb friction, it may still enter a stable limit cycle because of the yet-unmodeled, nonlinear k_c resulting from discontinuous contact with

the environment, as shown in figure 5.10. If the manipulator is stable with Coulomb friction, then continuous manipulator/environment contact is guaranteed because the contact force in figure 5.9 is always positive for positive F_{des} commands.

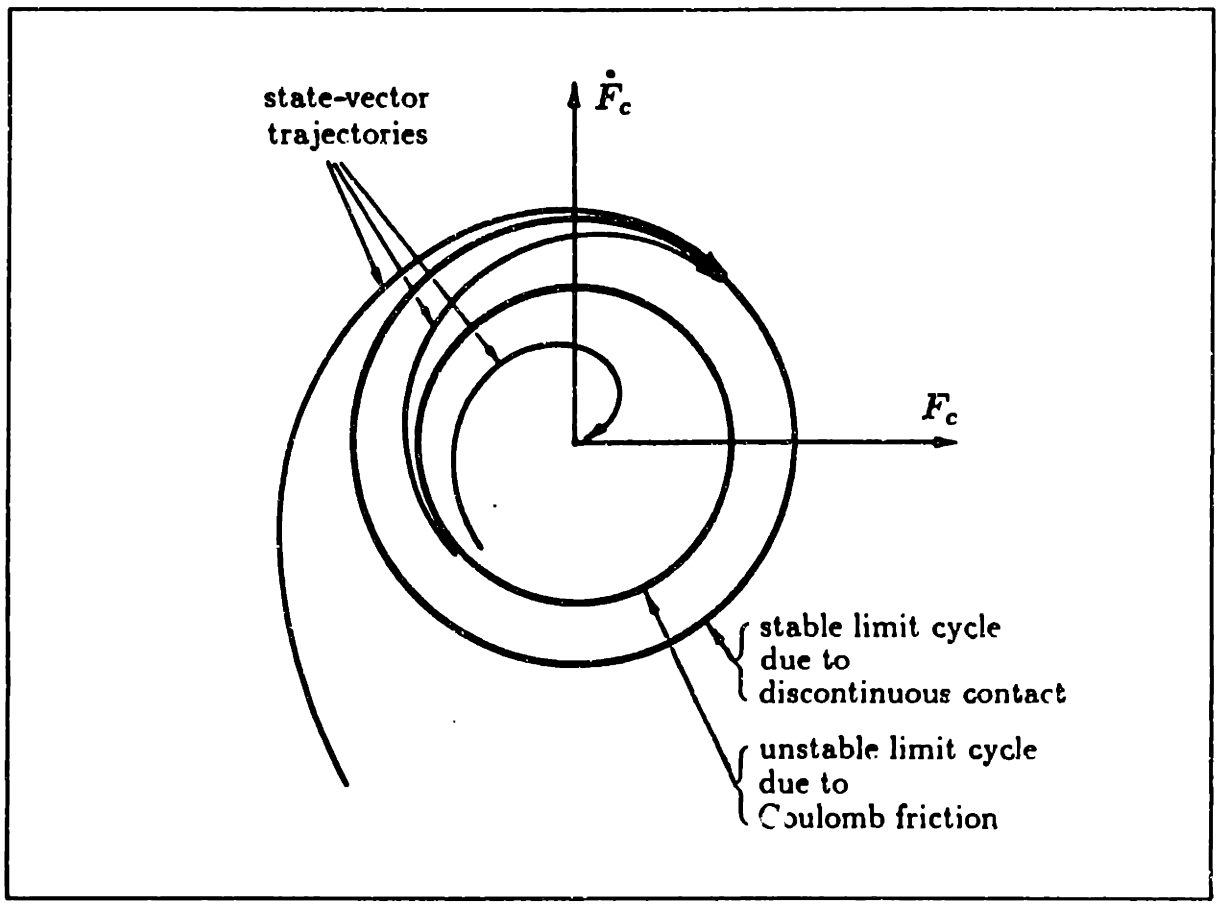

Figure 5.10. *Phase-plane visualization of the unmodeled discontinuous-contact limit cycle.*

5.5.3 Form of the Response

Two comments on the quality of response are necessary. First in the stable system the $\lim_{t\to\infty} F_c = F_{des}$ in figure 5.9; but the envelope of the response does not diminish linearly nor even exponentially, as might be expected, because although the slip-mode duration (τ_{linear}) for each half cycle remains constant, the stick-mode duration, τ_{spinup}, increases as the inverse of F_{error}. Indeed

$$\lim_{t\to\infty} \tau_{spinup} = \infty. \tag{5.19}$$

Second, although there is no limit cycle in F_c, the actuator node (x_m) does enter a limit cycle* with

$$\text{amplitude} = \frac{2F_{friction}}{k_{tr}}, \tag{5.20}$$

as seen in the three-dimensional trajectory of figure 5.11. The work dissipated per half cycle is

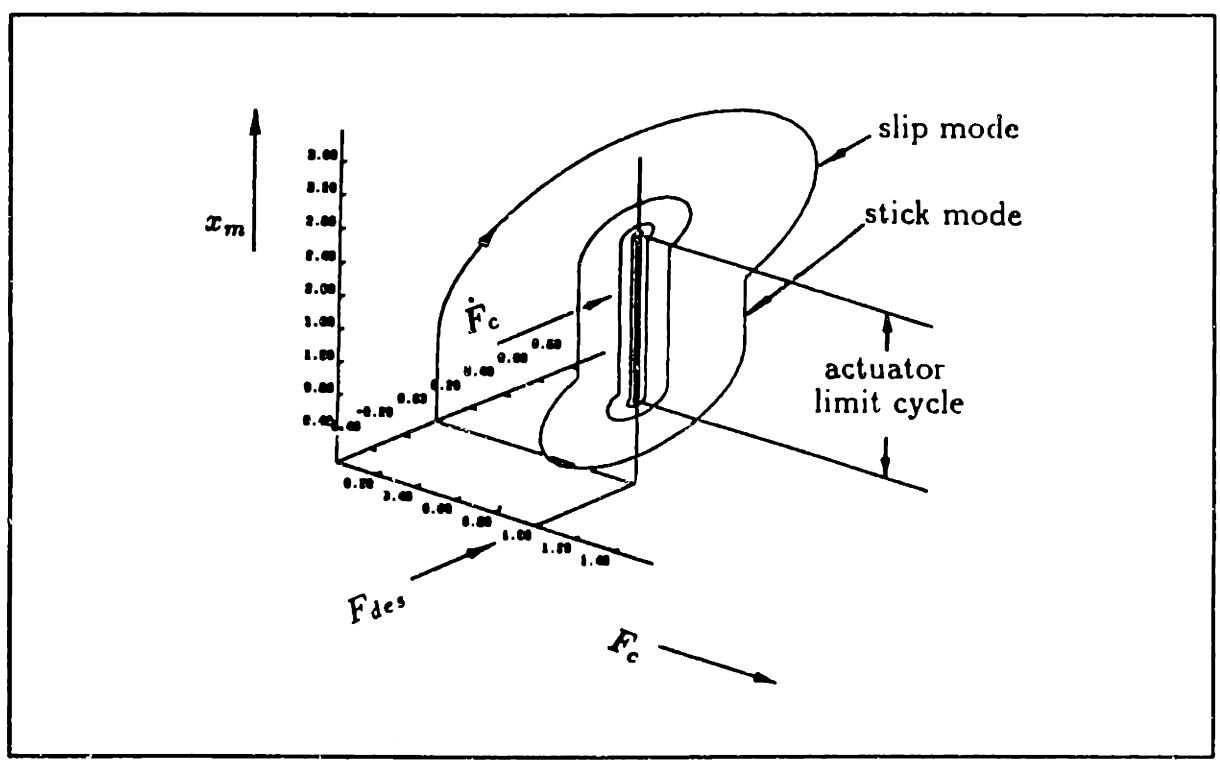

Figure 5.11. *Three-dimensional trajectory illustrating an actuator-only limit cycle.*

* This is not a limit cycle in the strict sense because, although the amplitude is constant, its frequency decreases with time.

$$\mathcal{W} = \frac{F_{friction}^2}{k_{tr}}, \tag{5.21}$$

and the average power dissipated per half cycle is

$$\mathcal{P} = \frac{G_I F_{error} F_{friction}}{4}. \tag{5.22}$$

5.5.4 Stiction in the Extended-Stability Mapping

Now, what if the transmission has stiction rather than Coulomb friction? The form of the stability mapping is the same as for Coulomb friction in figure 5.8 if $F_{friction}$ is replaced with $F_{dynamic}$ on the vertical axis, however the stable region becomes a stable-limit-cycle region and point B moves to the left and below the Coulomb friction dominated line. A strictly stable region no longer exists. A partial explanation for this behavior is found by noting that ΔF adds (linearly) an initial acceleration component, $\Delta F/J_l$, to the simple Coulomb response at the beginning of each slip-mode half cycle. In domain I the trajectory undergoes increasingly larger oscillations until the constant per-cycle energy input by $\Delta F/J_l$ equals the growing per-cycle energy dissipation of inherent viscous damping. In domain II the SIDF analysis still correctly predicts an unstable limit cycle, but the stiction limit-cycle argument for domain I indicates that the SIDF analysis fails to predict the presence of a stable limit cycle within the unstable limit cycle. The previous reasoning for domain III in the Coulomb friction case holds in the stiction case.

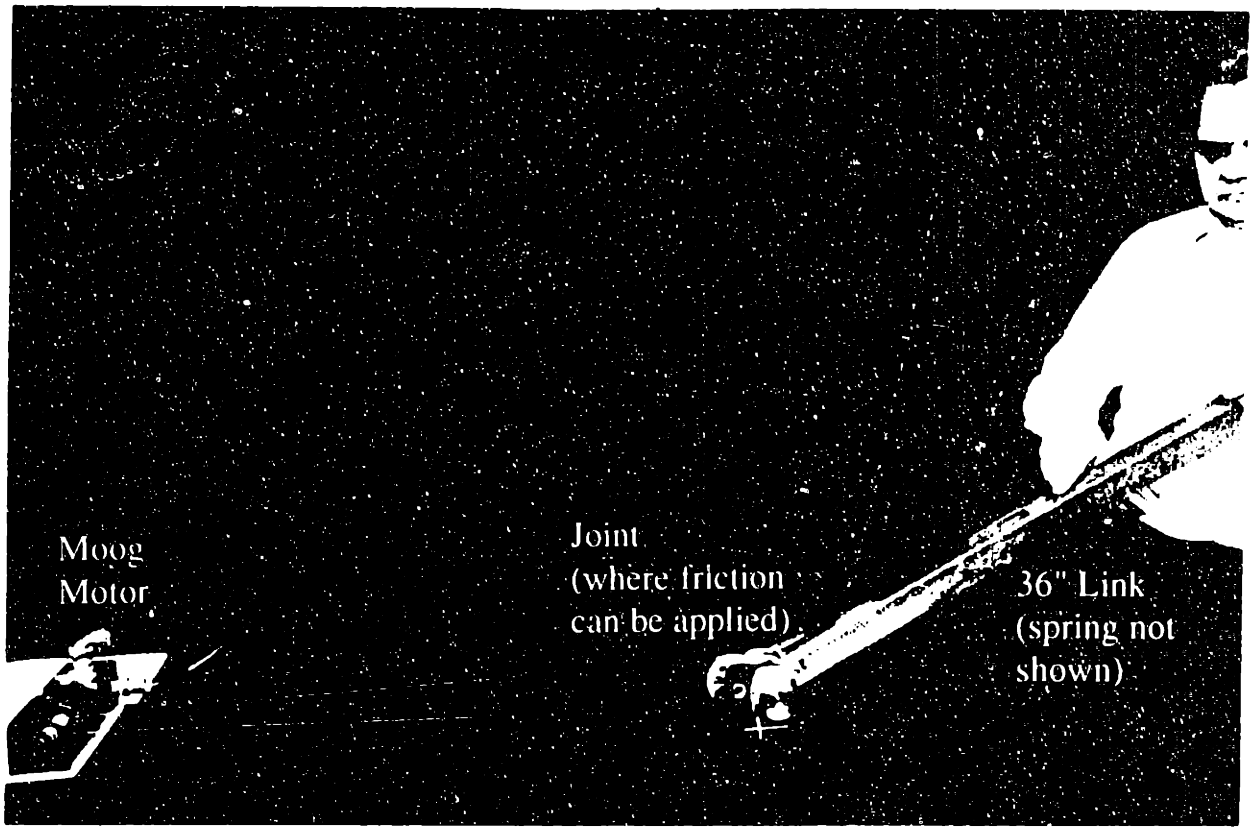

Figure 5.12. *Transmission testbed for verifying stability mapping.*

5.6 Experimental Verification of Stability Predictions

We performed some simple experiments in order to verify qualitatively the stability mapping of figure 5.8 for Coulomb friction. We built a one-degree-of-freedom testbed transmission with the same parameters as the practical example design described in section 4.3.2. The testbed, pictured in figure 5.12, was built to have particularly low dry and viscous friction by using a low-friction Moog DC brushless motor, by employing high-quality bearings in the joint and in the speed reduction, and by following low-friction design suggestions from chapter 6. The apparent friction of the joint was measured to be less than 1 % of peak torque when supporting the link against gravity.

The Moog DC brushless motor was driven in its velocity-servo mode. A spring (not shown in the figure), with stiffness, $k_c = 10$ lb/in, was placed under the tip of the relatively rigid link, supporting the link horizontally. A Hall-effect transducer measured angular joint position so that contact force could be inferred from the measured spring deflection. The control system was implemented on a VAX-750 computer which read joint positions and updated velocity commands to the servo-motor at 50 Hz based on

the force error generated from steps in desired force and force disturbances applied by human contact along the link.

We found the marginally-stable gain empirically by gradually increasing the integral gain until the unperturbed link began to shake violently, indicating instability. Once the marginally-stable gain was established, we reduced the gain 10 % to a stable gain. The arm was commanded to exert a net force of zero, disturbed vigorously, given a step command to apply a 10-lb force against the spring, and disturbed vigorously once again. These commands and disturbances at no time made the arm unstable. As one would expect the linear system remained stable, independent of commanded input and disturbances.

Next we applied Coulomb friction to the transmission, near the joint, by pressing a stationary Teflon rod against the moving transmission cable. Again, the arm was commanded to exert various steps in applied force and disturbed vigorously, but remained stable — adding Coulomb friction did not destabilize the linearly-stable system.

The system was then brought to rest. While still applying Coulomb friction to the joint, we increased the gain beyond the marginally-stable gain of the original low-friction system, to a new, higher marginally-stable gain. Then the gain was reduced by 10 % — which was still well above the marginally-stable gain for the low-friction system. Without disturbances or changes in the commanded force the system was stable. Indeed, for small disturbances and small step changes in commanded force, the system remained stable. So Coulomb friction actually increased the stable gain of the system. However, when either the disturbances or commanded forces were increased even further, the link would begin to shake violently, indicating instability. Clearly, the quality of the stability observed at the higher gain was not robust.

The experimental observations may be explained in reference to the stability mapping of figure 5.8. Apparently, for the lower gain, the system had been operating in domain I of figure 5.8; and so the system was stable for any value of $F_{friction}$ or F_{error}. When the Coulomb friction was applied and we increased the gain above the linearly-stable gain, we moved the operating point into domain II where stability is dependent on the magnitude of F_{error}. For small F_{error} (i.e., when disturbances or commanded forces were small), the operating point remained above the stable-unstable border.

However, when F_{error} was large compared to $F_{friction}$, the operating point fell below the stable-unstable transition line and caused the link to shake violently.

5.7 Design Guidelines

It may seem obvious to the designer that one wants to minimize nonlinear friction, but how does the designer make intelligent cost and design tradeoffs in this regard? E.g., "Should I buy a bearing with half the friction, or should I double the transmission stiffness, k_{tr}, between the actuator and the friction node?" We answer such questions by highlighting from the analysis what effect the form and size of friction, transmission and contact stiffness, damping, and the controller design have on performance.

Coulomb friction is bad because it slows the response time below that of the no-friction case in figure 5.3.b by adding a time delay to the initial response and, in the inertial transmission, increasing the time constant each half cycle, as shown in figure 5.9. Decreasing $F_{friction}$ reduces both τ_{spinup} and τ_{delay} proportionally. It also reduces the actuator limit cycle and the resulting power dissipation proportionally and reduces the work per half cycle by the square of $F_{friction}$. It does increase the region of stability for a limited step in F_{error}. Unfortunately, the increased region of stability may lead to disaster. If G_I is set low enough that the manipulator is linearly stable and operates somewhere in domain I, then the stability will be independent of the normalized step size in F_{error}. If G_I is set in domain III, then the system will always be unstable. However, if G_I is set empirically to domain II and found to be stable for some step size in F_{error}, there will always be some large-enough step in F_{error} which will destabilize the system. It is therefore recommended either that G_I be limited by the Routh criteria (domain I) or that F_{error} be limited in software with a saturation applied to F_{error} to a known stable point (domain II) to prevent large commands, disturbances, or noise from destabilizing the manipulator.

Stiction is always bad. In an inertial transmission it reduces the region of stability below that for Coulomb friction and transforms the region of stability into a region of limit cycles. In a nearly-inertialess transmission it always causes limit cycles. Decreasing ΔF in this case reduces the limit-cycle amplitude proportionally.

To combat friction directly one can use good material selection and/or lubricants [Rabinowicz 59]. Some materials such as teflon can eliminate stiction. Clean metals tend to have extremely high stiction levels ($\Delta F/F_{dynamic}$), especially in ultra-

clean environments such as outer space where many robots of the future will operate. Lubricants introduced between otherwise dry sliding surfaces can reduce the level of Coulomb friction; but, unless all solid-solid contact is eliminated, some component of Coulomb friction remains. Frequently utilized journal bearings can eliminate solid-solid contact for some minimum journal velocity, but force control by its nature often requires zero velocities.

In addition to altering the level or type of friction, the designer may improve performance by altering other design parameters. When a friction node divides the transmission between k_{tr} and k_c, as in figure 5.4, k_{tr} should be maximized and then k_c adjusted so that the response is stable. When stiction is present, increasing k_{tr} decreases the limit-cycle amplitude (according to equation (5.8) in the nearly-inertialess case). When the friction is Coulomb, increasing k_{tr} decreases τ_{spinup} and τ_{delay} proportionally. Increasing k_{tr} also reduces the inertial-transmission actuator-limit-cycle amplitude and the work per half cycle but has no effect on the power consumed.

The analysis shows no clear gain or loss in performance as the inertia is increased or decreased; although, if the manipulator were also designed for fast position control, the inertia would already have been minimized. Some inherent passive mechanical damping at least is important. It is absolutely necessary for stability; and, in the stiction case, it cuts the limit-cycle amplitude nearly in half by reducing Ω.

Finally, the designer must implement the controller in analog circuitry or software. We have already mentioned increasing G_I in the nearly-inertialess case. With Coulomb friction this reduces τ_{spinup} and τ_{delay} proportionally, but in the inertial transmission it increases the power consumption proportionally. Of course, as is the case with a purely linear transmission, increasing G_I decreases the margin of stability in figure 5.8. For power considerations and to eliminate limit cycles in F_c, the designer may want to add a deadband nonlinearity to the system at the input of G_I large enough to stop the stiction-induced limit cycle of equation (5.8) or the Coulomb-friction-induced actuator limit cycle of equation (5.20). Since the limitations imposed by stiction affect the exertion of small forces, they directly effect the dynamic range (ratio of largest to smallest controllable force) of force control. Also, the designer may want to adjust any unavoidable limit cycle so that its frequency (the inverse of equation (5.9)) is not near any system resonance. Finally, if we operate in domain II of a transmission with Coulomb friction, we must limit the size of F_{error} with a saturation block preceding

G_I.

We have neglected the role of proportional force control until now. Although proportional control will ask the actuator to perform impossible step changes in position in response to step changes in F_{des}, its tendency, according to our simple frictionless model, is to increase the speed of response. It also tends to increase system stability for a given G_I and physical parameters for the linear inertial system by adding effectively an adjustable compliance term, G_P, to the Routh stability criterion:

$$\frac{J_l G_I}{b}\left(\frac{1}{\frac{1}{k_{tr}}+\frac{1}{k_c}+G_P}\right) < 1.0. \tag{5.23}$$

5.8 Conclusion

This chapter has characterized the effect of Coulomb friction and stiction on force control with integral feedback. Our results show that stiction can cause the contact force to enter a limit cycle. Coulomb friction can extend the system stability bounds but may lead to an input-dependent stability. Under certain conditions Coulomb friction causes an actuator limit cycle even though the contact force approaches the desired steady-state force. The results of this chapter extend to tendon-tension control, robot-finger-contact force control, heavy-manipulator force control, biological systems, and the dynamics of sliding finger contact.

Chapter 6
The Efficiency Limit of Tension-Element Drives

This chapter discusses the performance limitations of tension-element drives. The analysis reveals that compliant belt and cable drives cannot approach perfect efficiency. Some friction loss in the form of tension-element/pulley slippage must be present. Thermodynamic principles may be applied to a simple control volume drawn around a belt or cable drive to show that there is a *limit* on efficiency. This maximum efficiency applies to all belt and cable drives. Chain/sprocket drives, though similar to belt and cable drives, may not be limited to this efficiency. Consequences of the analysis relevant to belt and cable transmission design are that:

1) multiple transmission stages degrade the total efficiency, and
2) it is best to maximize the cable or belt speed and stiffness per unit length for a given power transmitted.

Near the end of this chapter we discuss other sources of performance limitations in cable drives which decrease the efficiency below its theoretical *limit* and introduce torque ripples. The magnitudes of these other sources are proportional to pretension in the cable.

6.1 History of Tension-Element Drives

Early in recorded history cables were used for power transmission [Homer] in boring tools. Power was transmitted to a wooden boring shaft via a cable wrapped around it. The ends of the cable were pulled alternately to spin the boring shaft. Before the industrial revolution the need for cables and belts to transmit power was slight. Power plants, e.g., oxen, horses, and humans, were small and portable and so had no need for a cable or belt transmission because their power could be applied directly to a single load. Hydro and wind plants were not portable, but each plant's power output was small enough that in general it consumed its power locally on a single load and transmitted power to its load through either a single shaft or a gear train.

The development of large-power-output heat engines during the Industrial Revolution created the need for power transmission from a single heat engine to several end-use machines in factories and sped the development of mechanical transmissions. From the 1830's to the 1930's leather belts were used increasingly as power transmissions because of their high power-to-weight characteristic over distances of several meters relative to contemporary transmissions such as gear trains. During this time a large volume of literature was published on the empirical study of leather belt transmissions [Swift 28]. Much of this literature was specific to leather belts, and some of it has wrongly been generalized into rules of thumb for today's belts and cables.

One exceptionally insightful publication, however, by Osborne Reynolds [Reynolds 1874] in 1874 looked at belt power transmission from a more analytical and general viewpoint. In order for belts to transmit torque the belt begins and ends pulley contact with different tensions. Reynolds realized that, because the cable is subjected to different tensions, it must have different velocities due to cable stretch before and after contact with the pulley. This change in velocity implies that the cable must slip relative to the pulley at some point. He correctly acknowledged that there exists a power loss proportional to this slipping. However, it does not appear that his contemporaries appreciated the importance of his paper because parasitic losses, such as bearing friction, were far greater than the slip losses.

During the 1930's and 1940's the electric generator-motor set was quickly replacing the leather-belt power transmission. Since that time, belt and cable transmissions with a drive and driven pulley and a circulating cable or belt have been used relatively

infrequently,* and have therefore prompted only few additional studies of cable and belt transmissions. Recently, however, the application of cables [Salisbury 84, Bejczy 80, Vertut 86] and belts [Jacobsen 86] in teleoperator and robot transmissions has become more frequent. Pretensioned cable transmissions have no backlash. Also, in teleoperators, the low mass of cable transmissions makes its inertia low compared to other transmissions. In robots cable transmissions can permit relatively heavy electric or hydraulic motors to be located remotely from the joints they drive. In these applications, especially where force control is important, friction must be minimized in the pulley bearings and other moving parts of the transmission in order to reduce transmission losses and to avoid stability problems [Townsend 87]. A few of the recent studies on cables have focused on the complex details of cable mechanics [Phillips 85] whereas the main thrust of our analysis is a simple control-volume approach.

6.2 Control-Volume Analysis of a Tension-Element Transmission

In this chapter, we show that for a given tension difference and stiffness per unit length of the cable there is a maximum transmission efficiency.* Employing the principles of thermodynamics, our analysis focuses on the simple interactions across a control-volume surface rather than with the details of the complex mechanical interactions within the control volume.

---

* Although we do not treat other types of cabled transmissions such as those used for chairlifts, elevators, and cranes their analyses are similar to the one presented in this chapter.

* This analysis is equally valid for belt/pulley transmissions, but we will use the word cable to imply cable, belt, or any similar type of transmission.

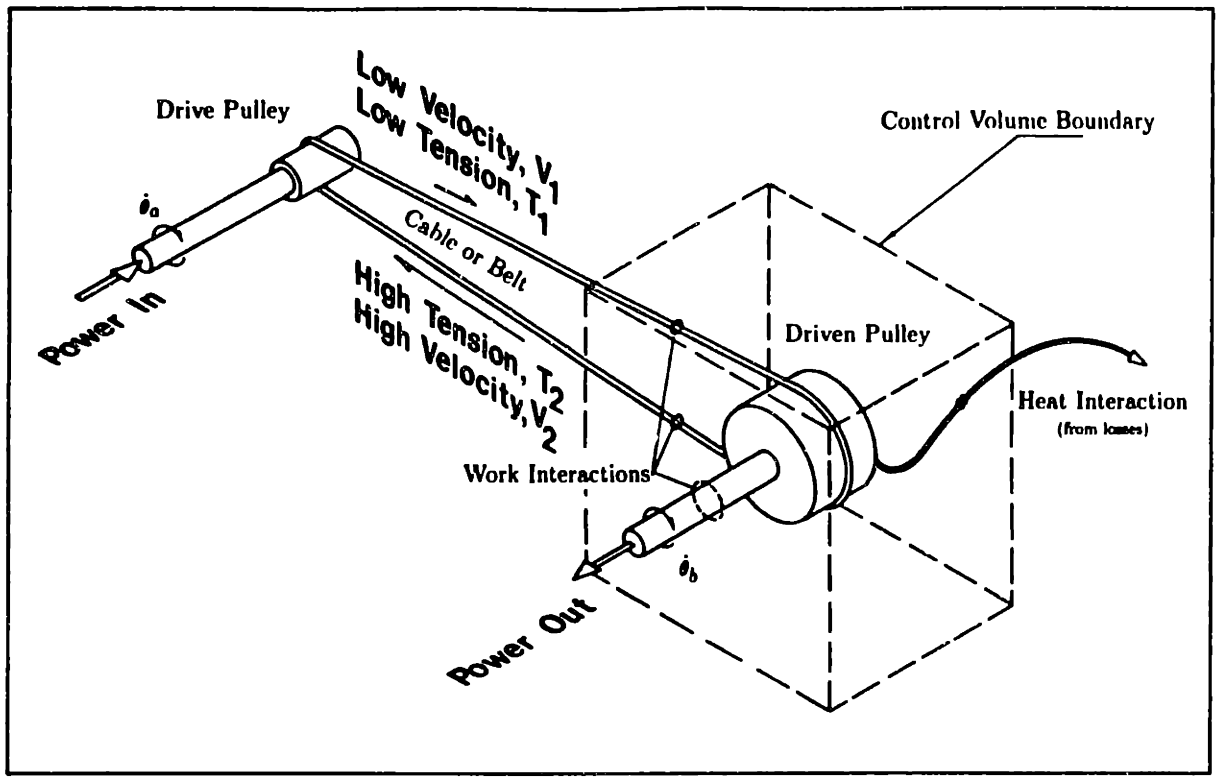

Figure 6.1. *Tension-element (e.g., cable, belt, etc.) drive.*

6.2.1 Assumptions

Figure 6.1 illustrates a cable/pulley transmission. r_a and r_b are the drive and driven pulley radii. $\dot{\theta}_a$ and $\dot{\theta}_b$ are the drive and driven angular velocities. The subscripts a and b represent the drive and driven pulleys respectively. The cable has an effective modulus of elasticity E and cross-sectional area A. The magnitude of torque transmitted through each pulley is the difference in tension between the high-tension, T_2, and low-tension, T_1, halves of the cable times the pulley radius. The control volume, drawn for the driven pulley in figure 6.1, is represented by straight dashed lines; and power and heat-flux energy interactions across its surface are circled with dashed lines.

Our assumptions about the system are that:

1) the cable begins and ends pulley contact at the same radius, e.g., r_a or r_b,
2) there is no slip at at least one point on the pulley including either the initial or the final point of pulley/cable contact,
3) the system is in steady state,
4) the cable material is linearly elastic,

5) the power flows due to the kinetic energy convected across the control-volume surface are negligible, and

6) potential-energy differences due to changes in cable height in a gravity field are negligible.

As long as these assumptions hold, the following analysis is valid for cables, belts, chains, or any similar type of transmission. The first two of these assumptions will be explained in greater detail. The remaining four of these assumptions hold for common materials such as steel and Kevlar over common operating conditions.

6.2.2 Dissimilar Cable Speeds

The first step in the analysis is to realize that the high- and low-tension halves of the cable (figure 6.1) must travel at dissimilar velocities [Reynolds 1874]. Solid objects elongate when subjected to tension. If the solid is linearly elastic, e.g., steel, with elastic modulus E, then the elongation is determined by Hooke's law,

$$\epsilon = \frac{\sigma}{E} \tag{6.1}$$

where ϵ is the strain and σ is the normal stress. The normal stress is simply the tension, T, divided by the cross-sectional area, A, so that

$$\epsilon_1 = \frac{T_1}{EA} \tag{6.2.a}$$

and

$$\epsilon_2 = \frac{T_2}{EA} \tag{6.2.b}$$

where the subscripts 1 and 2 refer to the low- and high-tension sections of the cable respectively. Since the mass of the control volume of figure 6.1 is conserved, the mass entering and leaving the control volume per unit time are equal. But identical masses of cable have different lengths when subjected to different tensions and so must have different velocities. The ratio of the large velocity, V_2, to the small velocity, V_1, is

$$\frac{V_2}{V_1} = \frac{1 + \frac{T_2}{EA}}{1 + \frac{T_1}{EA}}. \tag{6.3}$$

If $\epsilon \ll 1$, we can expand equation (6.3) in a Taylor series and eliminate higher-order terms to obtain

$$\frac{V_2}{V_1} = 1 + \frac{T_2 - T_1}{EA}. \tag{6.4}$$

Therefore, if we transmit torque, then $T_1 \neq T_2$; and subsequently $V_1 \neq V_2$.

6.2.3 Application of First Law

The next step in the control-volume analysis is to equate the sum of the energy flows out of the control volume to zero according to the first law of thermodynamics. The interactions across a control volume, drawn around either the driven or drive pulley, are similar; so we will derive the results for the driven pulley and state the results for the other. The power transmitted by the driven pulley shaft is $\tau_b\dot{\theta}_b$ where τ_b is the torque applied to the output shaft opposite to the direction of rotation. The power transmitted by the cable has four components:

1) a tension-times-velocity term, TV,

2) a convected strain-energy term, $\frac{1}{2}\frac{T^2V}{EA}$,

3) a convected kinetic-energy term, $\frac{1}{2}\rho AV^3$, and

4) a convected gravity-potential term, $\rho AVgz$,

where ρ is the cable density, g is the gravitational constant, and z is the height, measured from a fixed reference in a gravitational field, of the cable crossing the control-volume surface.

Finally the heat flux out of the control volume, which is equal to the power loss, we will name P_{Lb}. In steady state then

$$P_{Lb} = -\tau_b\dot{\theta}_b + (V_2T_2 - V_1T_1) + \frac{1}{2EA}(T_1^2V_1 - T_2^2V_2) + \frac{1}{2}\rho AV_2(V_1^2 - V_2^2) + \rho AV_2g(z_1 - z_2) \tag{6.5}$$

where ρ is the density of the cable on the high-tension side which, for $\epsilon \ll 1$, is equivalent to the cable density in the unstressed condition. Further, we drop the last two terms in equation (6.5) according to the original assumptions that,

1) the convected kinetic-energy term is negligible which requires

$$\frac{\rho AV^2}{T_2 - T_1} \ll 1 \tag{6.6}$$

and

2) the gravity potential-energy term is negligible which requires that

$$\frac{4\rho gEA^2r_b}{(T_2 - T_1)^2} \ll 1. \tag{6.7}$$

$T_2 - T_1$ is the characteristic tension difference and V ($\approx V_1 \approx V_2$ for $\epsilon \ll 1$) is the characteristic velocity. These assumptions are valid for any common cable transmission with low enough characteristic velocity, small enough pulleys, and a characteristic tension difference on the order of the cable breaking strength. Suppose, for example, we built a steel-cable transmission with a 170-lb minimum-breaking-strength cable, measured effective elastic modulus times cross-sectional area, EA, of 9,500 lb, and density per unit cable length of $3 \cdot 10^{-4}$ lb_m/in. Characteristic velocities would have to approach 10^4 in/sec before inequality (6.6) would be invalid, and a pulley whose axis is perpendicular to the gravity field would have a 275-in radius before inequality (6.7) would be invalid.

6.2.4 Two No-Slip Assumptions and Application of Second Law

In order to relate the pulley velocity to the cable velocity, we consider two possibilities:

1) the region of no-slip includes the initial point of contact between the pulley and cable so that

$$\dot{\theta}_b = V_1/r_b, \tag{6.8}$$

or

2) the region of no-slip includes the last point of contact between the pulley and cable so that

$$\dot{\theta}_b = V_2/r_b. \tag{6.9}$$

We can substitute either equation (6.8) or (6.9), and equation (6.4) into equation (6.5), expand, and eliminate higher order terms by assuming $\epsilon \ll 1$ to obtain an expression of P_{Lb} for each no-slip possibility. The resulting power losses for the two possibilities are

$$P_{Lb} = \frac{\dot{\theta}_b r_b}{EA}(T_2 - T_1)\left[T_2 - \frac{1}{2}(T_2 + T_1) - \frac{T_2^2}{2EA}\right] \tag{6.10.a}$$

and

$$P_{Lb} = \frac{\dot{\theta}_b r_b}{EA}(T_2 - T_1)\left[T_1 - \frac{1}{2}(T_2 + T_1) - \frac{T_1^2}{2EA}\right] \tag{6.10.b}$$

respectively.

A consequence of the second law of thermodynamics is that the power loss, P_{Lb}, cannot be negative. Since equation (6.10.a) is always positive and equation (6.10.b) is

always negative, we must choose equation (6.10.a) as the only valid expression for P_{Lb}. Since $\epsilon \ll 1$, the last term in equation (6.10.a) is negligible, and since $\tau_b = (T_2 - T_1)r_b$, equation (6.10.a) may be rewritten as

$$P_{Lb} = \dot{\theta}_b \tau_b \left[\frac{T_2 - T_1}{2EA} \right]; \tag{6.11}$$

and the no-slip condition holds for initial cable/pulley contact. If we repeat the preceding analysis for a control volume drawn around the drive pulley, we find

$$P_{La} = \dot{\theta}_a \tau_a \left[\frac{T_2 - T_1}{2EA} \right]; \tag{6.12}$$

and again the no-slip condition holds for initial cable/pulley contact. Note that $\dot{\theta}_a \tau_a$ and $\dot{\theta}_b \tau_b$ are the shaft-power flows to each pulley. The expression for the output power of the driven pulley as a function of the input power of the drive pulley is

$$P_{out} = P_{in} \left[1 - \frac{T_2 - T_1}{EA} \right]. \tag{6.13}$$

An upper-bound power efficiency, η, may be defined then as the ratio of the output power to the input power for the entire transmission so that

$$\eta = 1 - \frac{T_2 - T_1}{EA}. \tag{6.14}$$

If n multiple stages are used in series and designed so that each stage has equal cable stress, then the new overall efficiency based on any stage of the transmission decreases to

$$\eta = \left[1 - \frac{T_2 - T_1}{EA} \right]^{\mathrm{n}}. \tag{6.15}$$

6.2.5 Possible Mechanisms of Energy Dissipation

By its nature the thermodynamic, control-volume approach predicts only that the efficiency is limited; it does not predict the mechanism which causes this limit. However, we know that, if no cable stretch occurred, the efficiency, η, in equation (6.14) would be unity. Therefore, the dissipation mechanism is related to cable stretching and shrinking between its high- and low-tension states.

The actual dissipation mechanism may take several forms. We will give two examples. First, the mechanism may be slip between the pulley and cable when Coulomb friction is present. This relative slip has been known about for over one hundred years [Reynolds 1874] and is commonly quoted in modern design handbooks [Shigley 83]. If we assume that this is the dominant dissipation mechanism, the arc angle, β, over which slip occurs [Cotterill 1892] is

$$\beta = \frac{\ln(T_2/T_1))}{\mu}^{*}, \tag{6.16}$$

where μ is the coefficient of friction between the pulley and cable.

Second, the mechanism may be viscous dissipation. If we assume that the cable has heavy internal viscous damping so that for the operating speed of the pulley the cable elongates mainly after it has left the pulley but mainly before it leaves the control volume, then the power-dissipation mechanism will be viscous dissipation. These two mechanisms are directly related to cable stretch and so do not reduce the efficiency below η.

However, one can imagine other types of power dissipation, such as pulley bearing friction or the rubbing of cable strands as the cable bends and then straightens about the radius of the pulley, in which the dissipation mechanism is unrelated to the cable stretching and shrinking. These parasitic losses lower the transmission efficiency below that defined by equation (6.14).

We performed a simple qualitative experiment to check the slip-location results of equations (6.11) and (6.12). A rubber band was stretched over two pulleys, and

---

* Actually many texts [Shigley 83] modify this equation by including the effect of centrifugal force of the cable, but this effect is more important when relatively heavy leather belts are used.

then a load was applied to the driven pulley while the drive pulley was turned. On both pulleys the rubber band never slipped at the initial band/pulley contact unless the band slipped at all points on the pulley. On the driven pulley the band slipped forward relative to the pulley rotation as it wound off the pulley. On the drive pulley the band slipped backward relative to the pulley rotation as it wound off the pulley. The arc angle, β, over which the slip occurred, increased as the transmitted torque increased. All of these observations are consistent with and support the results of the control-volume analysis.

6.3 Interpretation of Results

6.3.1 Velocity Loss

In steady state there is a power loss when we attempt to transmit power from one pulley to another in a cable or belt transmission. According to equation (6.4) the driven pulley rotates more slowly than the ratio of pulley radii would predict, although the transmitted torque remains a function of the ratio of pulley radii. The velocity loss between the cable and pulley is proportional to the torque transmitted by either pulley and accounts for the power loss, P_L, for each pulley.

In fact we can integrate this velocity loss to determine a position error. That is, without the velocity loss we would have expected that

$$\theta_b = \frac{r_a}{r_b}\theta_a. \tag{6.17}$$

However, the velocity loss adds a position error, θ_{berror}, to equation (6.17) so that

$$\theta_b = \frac{r_a}{r_b}\theta_a + \theta_{berror}. \tag{6.18}$$

We combine equations (6.4), (6.8), and (6.9) and calculate the integral along a contour, C, to obtain

$$\theta_{berror} = \int_C \mathrm{sgn}(\tau_b)\left[\frac{T_2 - T_1}{EA}\frac{r_a}{r_b}\right]d\theta_a. \tag{6.19}$$

C is defined by points in a plane with the coordinates θ_a and the integrand of equation (6.19). If, in addition, the load torque, τ_b, on the drive pulley is non-zero and constant, then

$$|\theta_{berror}| > 0 \tag{6.20}$$

always. For example, if the drive pulley is rotated in one direction one radian and then back again while a constant torque is applied to the driven pulley, the driven pulley will move in the direction of the applied torque the amount $\theta_{b_{error}}$ from its initial position.

6.3.2 Paradox for Chain and Toothed-Belt Drives

We stated above that the analysis for a cable transmission extends to belt and chain transmissions; however, the fact that pulleys which transmit power at the same radii rotate at different velocities presents a paradox for the chain/sprocket transmission because the sprocket teeth guarantee that two sprockets with equal numbers of teeth rotate at the same velocity. We hypothesize that the assumption that the chain begins and ends contact with the sprocket at the same radius is violated for chain/sprocket transmissions or any transmission where the ratio of radii and the ratio of number of sprocket teeth are equal. One can imagine the roller on a roller chain climbing up toward the tip of the sprocket tooth as the link elongates under higher tension thus increasing the effective sprocket radius as shown in figure 6.2. In this manner a toothed sprocket may effectively have a radius which varies between r_I and r_{II} and allows a higher maximum efficiency than that predicted for a fixed-radius sprocket. Unfortunately, chain/sprocket transmissions have other problems such as backlash; and they may introduce torque and velocity ripples by the same variable-radius mechanism of figure 6.2.

6.4 Application of Results to Transmission Design

6.4.1 Reduction of Tension-Difference by Using High-Speed Elements

The results of our analysis indicate how to improve high-performance belt and cable transmissions. For instance, we can alter the limiting belt or cable efficiency by increasing its stiffness per unit length, EA, or by reducing the tension difference, $T_2 - T_1$. For a given transmitted power, the tension difference can only be reduced by a proportional increase in cable velocity. This suggests using a high-speed rather than a high-tension transmission. The high-speed transmission has the added benefit of increased overall transmission stiffness and strength for a given EA but may require either a large pulley or multi-stage reduction at the load.

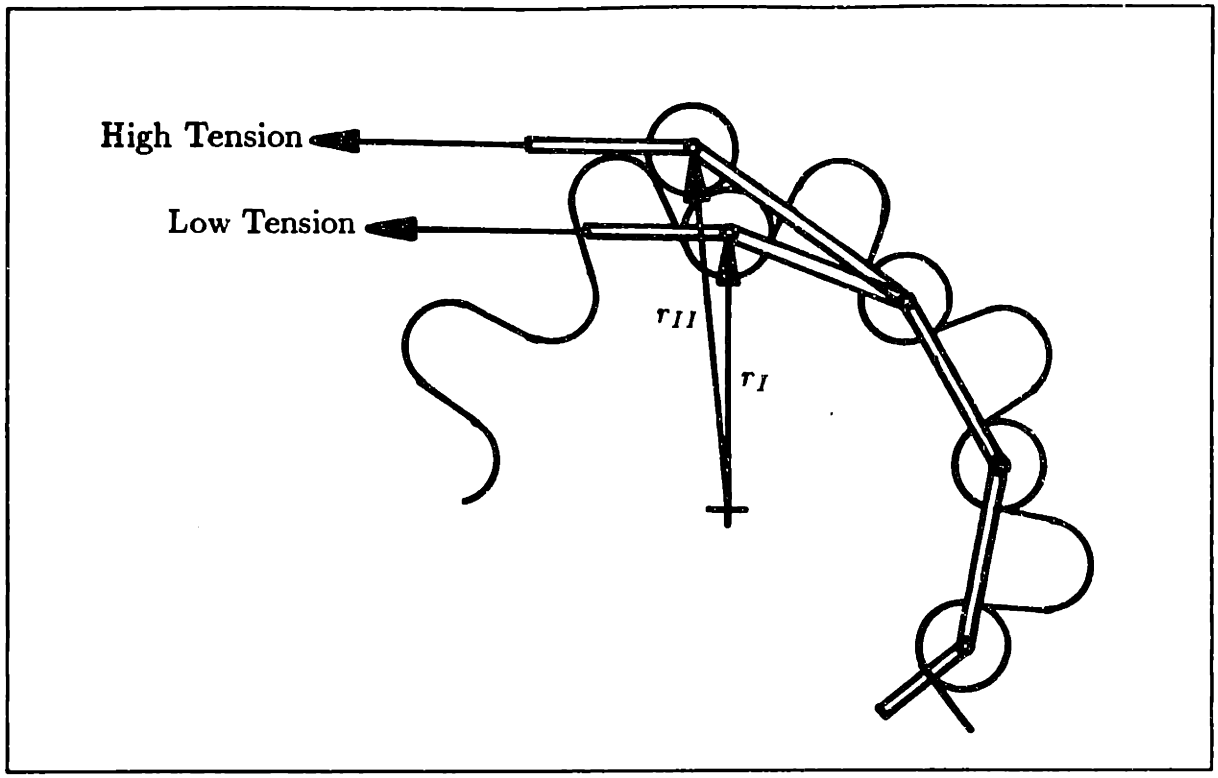

Figure 6.2. *The variable radius of chain/sprocket drives.*

6.4.2 Minimization of Number of Transmission Stages

As an implication of the n-powered function of equation (6.15) it is best to avoid multiple stages. For example, instead of using multiple stages to guide cables around a complex geometry, use idler pulleys to guide a single cable or belt from the power source to the load. Of course, if one must employ a certain number of stages, equation (6.15) increases the importance — by the n^{th} power — of using stiff cables and minimizing the tension difference.

6.4.3 Position and Velocity Estimators To Improve Accuracy

In control systems, open-loop position and velocity control will be inaccurate if we estimate the position and velocity by the transmission ratio. Equation (6.19) can improve the estimate significantly but does not account for second-order effects. In robotic applications, where the total travel of the output pulley is mechanically restricted, it may be worth terminating the cables on both pulleys. Although doing so will limit maximum position error, it may require the cable to be wrapped many times before termination.

6.4.4 Coulomb-Like Friction

Also the transmission may appear to have torque-dependent Coulomb-like friction when operating under pure torque control thereby making torque control difficult [Townsend 87]. We can rearrange equation (6.12) to the following:

$$P_{L_a} = \dot{\theta}_a \left[\frac{\tau_a^2}{2 r_a E A} \right]. \tag{6.22}$$

The bracketed term now represents a Coulomb-like friction torque which has a torque dependency analogous in some respects to the normal-force dependency of true Coulomb friction. For example, if we specify an input torque, as is commonly done in force-controlled robots, instead of position or velocity, then the bracketed term is a squared function of that specified input torque and is independent of position or velocity.

6.4.5 An Example Transmission Design

The authors designed the prototype, two-stage transmission shown in figure 6.3 to control the velocity and torque at the joint of the one-link manipulator of figure 5.12. A single-cable transmission spans the 1-m distance between a DC brushless motor and the joint. The 7x49, stranded-construction, 0.044-in diameter, steel cable has a 170-lb minimum breaking strength and circulates between a 0.75-in drive pulley and a 2.9-in driven pulley. Its stiffness per unit length, EA, has been found empirically to be 9,500 lb. A second stage with multiple parallel cables and the same pulley diameters as the first stage is located at the joint and increases the total torque transmission ratio to 14:1. The maximum efficiency attainable under the peak motor torque of 60 in-lb is 0.966 according to equation (6.15). We could have improved the limiting efficiency to 0.983 had we used only a single-stage transmission, but the joint pulley would have had a 11.2-in diameter instead of the existing 2.9-in diameter which more closely matches the 2-in manipulator width. The improved aspect ratio of the link (with joint) seems to justify the decrease in efficiency.

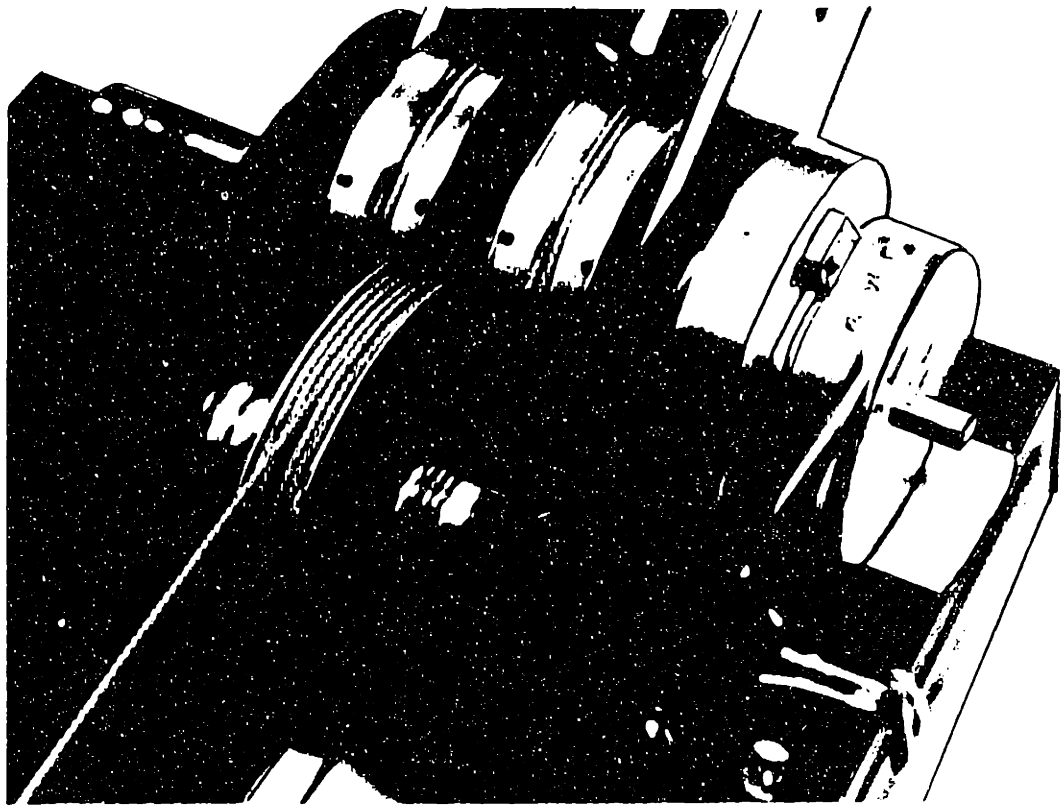

Figure 6.3. *Close-up view of two-stage cabled reduction mechanism.*

6.5 Other Sources of Performance Limitations

The preceding analysis discovers a Coulomb-like friction which must be present regardless of the coefficient of friction at the pulley surface. However, other disturbances also affect the transmission of forces via cables. This section notes two sources of dry friction and one source of torque ripple.

Recent experiments, performed by the author while at JPL/NASA, on cable/pulley friction caused by lateral cable compliance, show that this friction is stiction-like and *proportional* to cable tension. However, the proportionality does not hold for very-low cable tensions, where the resistance goes to some small positive value rather than zero. It has been predicted and shown experimentally [Reynolds 1876] that small-scale slipping between materials which are compliant in the direction normal to their mutual contact surface is the source of rolling resistance. Pulley/cable friction may arise from this small-scale slipping which occurs in a limited region near where the cable wraps onto and unwraps from the pulley.

The other source of friction is bearing friction. It is well known [Mark's Hand-

book] that ball and roller bearings which support the pulleys have stiction-like friction that is *proportional* to bearing load and therefore, to a large extent, on the cable pretension.

Torque ripple originating in the transmission can also degrade the performance of force control. Beyond the motor-induced torque ripple, large torque ripples in cable transmissions can be caused by a small pulley eccentricity, ϵ. These ripples originate from the drive, driven, or idler pulleys and are all *proportional* to the pretension in the cable circuit. The torque-ripple magnitude, τ_{ripple}, caused by the changing effective radius is

$$\tau_{ripple} = 2\epsilon T \sin\theta, \tag{6.23}$$

where θ is the pulley angular position, and T is the cable pretension. For example, a cable pretensioned to 50 lb and with a 0.010-in eccentricity would introduce a sinusoidally varying torque of 2 in-lb.

For these *other* sources of disturbance, it is important to reduce the cable pretension in order to reduce the resulting torque ripple and dry friction and thereby increase the dynamic range of force control. The designer should reduce the maximum cable-tension difference to reduce the necessity for high pretension. Also, when the cost of extra actuators is justified, the designer may wish to control the pretension actively so that for delicate tasks requiring small forces the pretension is low and for tasks requiring the application of large forces, the pretension is high. Without active pretension, the cable pretension must be set to one half of the full-torque tension so that neither cable will become slack.

6.6 Conclusion

This chapter has described a simple, thermodynamic, control-volume analysis for tension-element drives to derive a limiting efficiency. This efficiency follows a definite law and is due to belt/pulley or cable/pulley slip. The limit may be improved by increasing the per-unit-length cable or belt stiffness, by reducing the tension difference, or by minimizing the number of transmission stages.

Also, torque ripple and other sources of dry friction are found in cable drives which are proportional to pretension.

Chapter 7
Conclusions

This chapter reviews the important points of the thesis and introduces a manipulator design which illustrates many of these points. Concluding remarks on the future suggest that high-performance force control through improved mechanical design may improve the richness of tasks that force control can achieve.

7.1 Review

We have shown that it may be naive to purchase a manipulator off-the-shelf, add a force sensor, and expect the control algorithm to enable high-performance force control. Many mechanical-design issues not considered or poorly considered in today's manipulators, such as geometry, proper distribution of compliance and friction, and speed-reducer location, must be considered simultaneously.

This thesis has shown that proper design will increase dynamic range of force control, robustness, bandwidth, aspect ratio, efficiency, and backdrivability. Details such as minimizing the number of transmission stages and decreasing the tension difference to improve efficiency are given for cabled transmissions. For all types of transmissions with outer-loop force feedback and inner-loop position or velocity feedback, we suggest boosting the stiffness, k_{tr}, between the major source of friction and the actuator to diminish the amplitude of stiction-induced limit cycles that degrade the dynamic range of force control. In this feedback scheme, often employed to reduce the effects of Coulomb friction in the actuator, we have shown that Coulomb friction in the transmission extends the stability bounds, but we warn that setting stable gains empirically may result in poor stability robustness.

Our study of bandwidth suggests placing the speed reducer at the joint instead of at the motor. Also we introduced a method for selecting the best combination of transmission and contact stiffnesses.

Finally we discussed the importance of the external geometry — that it be free

of protrusions which could snag on the environment and that it have long and slender links which enable the manipulator to interact with the environment via large portions of its surface and not just via one point.

7.2 MIT/WAM Manipulator

The MIT/WAM manipulator was designed and built by the author* to exemplify some of the design strategies discussed in this thesis. At the writing of this thesis the MIT/WAM manipulator has only recently been assembled, and performance testing to determine inertias, stiffnesses, bandwidth, etc. is expected to take several months. However, even a description of the design is instructive.

7.2.1 Kinematics and Geometry

The concept of whole-arm manipulation is new and requires a reexamination of manipulation kinematics [Salisbury 87]. We use four joints because they:

1) enable redundant degrees of freedom for positioning any point along the outer link and
2) allow the controller to manipulate the outer link as a line, rather than just as a point, which is one of the promising techniques in whole-arm manipulation [Salisbury 88].

The coordinate frames, Denavit-Hartenberg parameters, kinematic and actuator transformations, and Jacobian matrices needed for trajectory and force control are included in the appendix. All degrees of freedom are revolute and built as a serial chain. The two links of nonzero length, referred to as the inner and outer links in figure 7.1, have lengths of 22 and 16 inches. Both of these links were designed to be easily replaced with shorter or longer links since choosing the best lengths is still an open topic.

Figure 7.1 also shows the locations of the joint axes, which are labeled θ_1, θ_2, θ_3, and θ_4. The first three joint axes intersect at the base of the inner link. The θ_1 axis is vertical and has a range of 350°. The θ_2 axis intersects the θ_1 axis at right angles

---

* This design would never have been possible without the tremendous assistance by the authors advisor and colleagues at MIT and Woods Hole, friends, family, and a spirited machine shop.

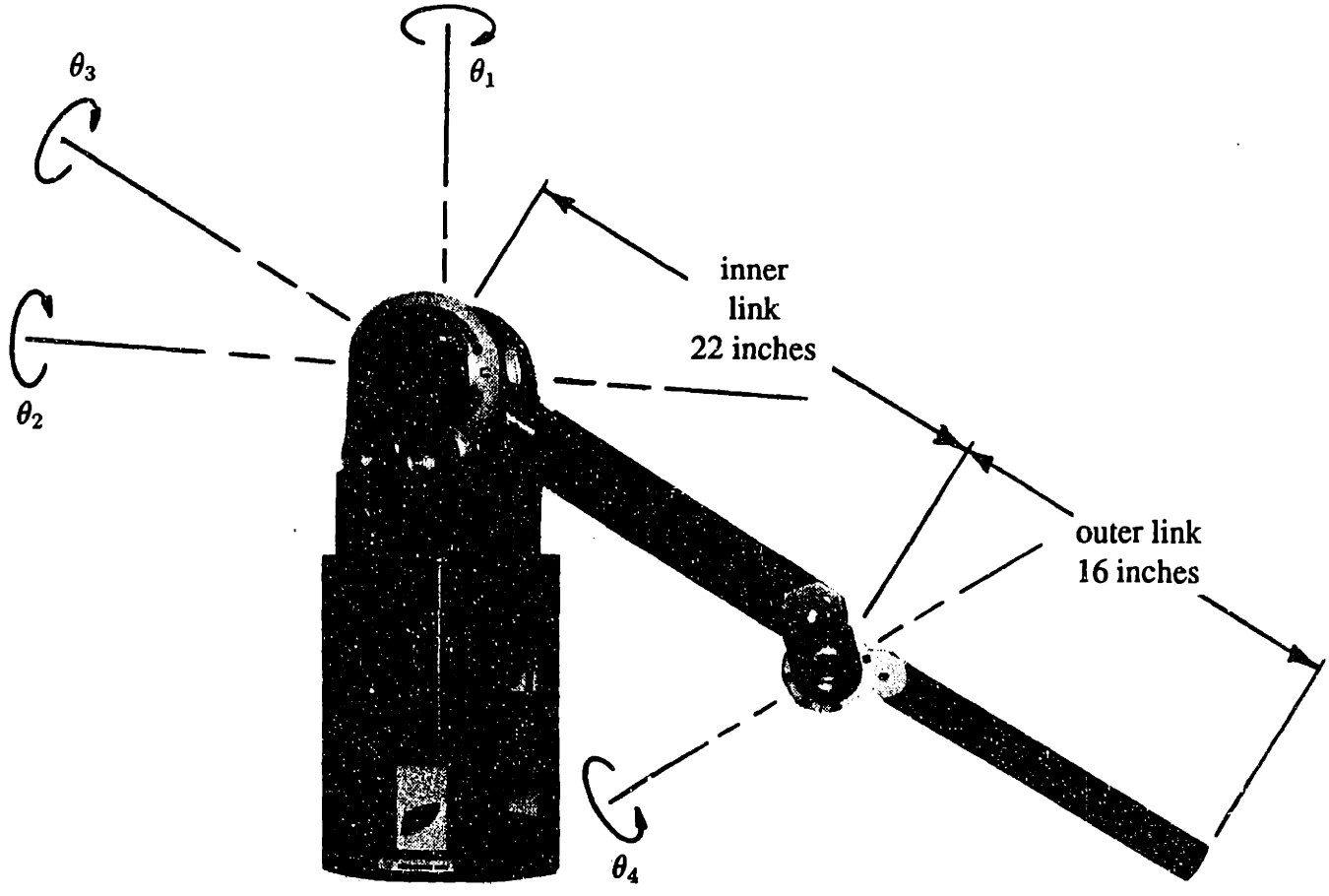

Figure 7.1. *Location of links and joints.*

and has a range of 270°. The θ_3 axis intersects the θ_2 axis at right angles and has a range of 300°.

The last joint axis, θ_4, is located away from the base and is perpendicular to the θ_3 axis although it is an offset joint and so does not intersect the θ_3 axis. The offset joint is included to allow the links to close flatly against one another at one extreme of the θ_4 joint travel as shown in figure 7.2. This distal joint requires a transmission to span 22 inches in order to remove the actuator bulk from the inner link, thereby maximizing aspect ratio and easing the structural and actuator requirements of the inner link and first three joints.

The aspect ratio of the inner link, which includes the maximum width dimension of the θ_4 joint mechanism is 5. The aspect ratio is calculated by divided the link length, 22 inches, by the smallest diameter hole that the θ_4 joint mechanism would fit through, 4.4 inches. The aspect ratio of the outer link is 9, which is calculated by dividing its length, 18 inches, by its diameter, 2 inches.

These high aspect ratios allow a large fraction of the link length to be available for manipulation according to equation (3.2) and as seen in figure 7.3 where the manipulator explores the soft surfaces of a foam box. Figure 7.4 shows the manipulator grasping an object between adjacent links. Its ability to grasp is enhanced by its long, slender links and high-friction, foam-rubber covering as indicated by equation (3.3).

Note in figures 7.1 through 7.4 that the surfaces of the manipulator are smooth and free of protrusions which might snag on the environment. The joint mechanism for θ_4 uses as few separate parts as possible in order to minimize the need for fasteners which add weight to the mechanism and often disrupt the exterior smoothness. The transmission mechanism is enclosed by the cylindrical link structure to protect it from damage and to prevent it from snagging on the environment.

7.2.2 Cabled Transmissions and Actuators

The MIT/WAM design uses pretensioned cabled transmissions to drive all joints. It was decided not to use active pretension which would require at least 5 (instead of 4) motors, thus increasing cost and complexity beyond the financial and design resources of this project. Mechanical counterbalancing of the links was excluded from the design in favor of greater joint mobility and lower overall weight. Furthermore, the backdriven inertia was not made isotropic [Asada 84a]; to do so would have

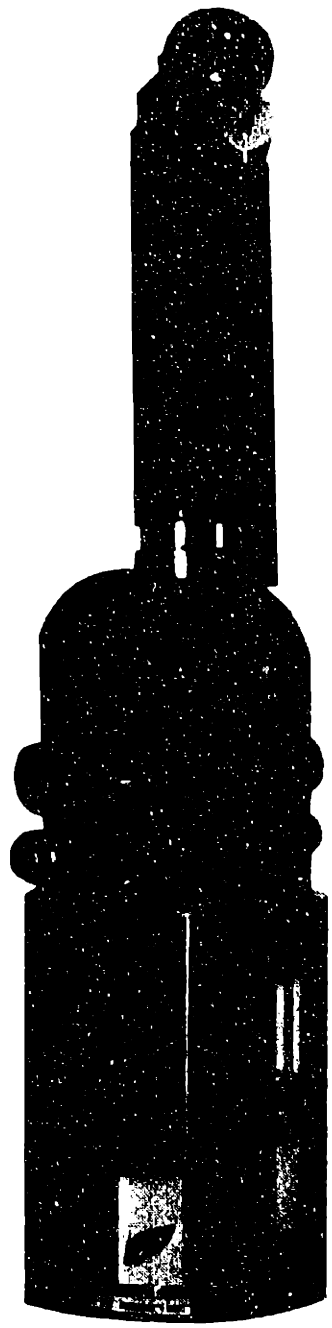

Figure 7.2. *Offset joint allows links to close flatly.*

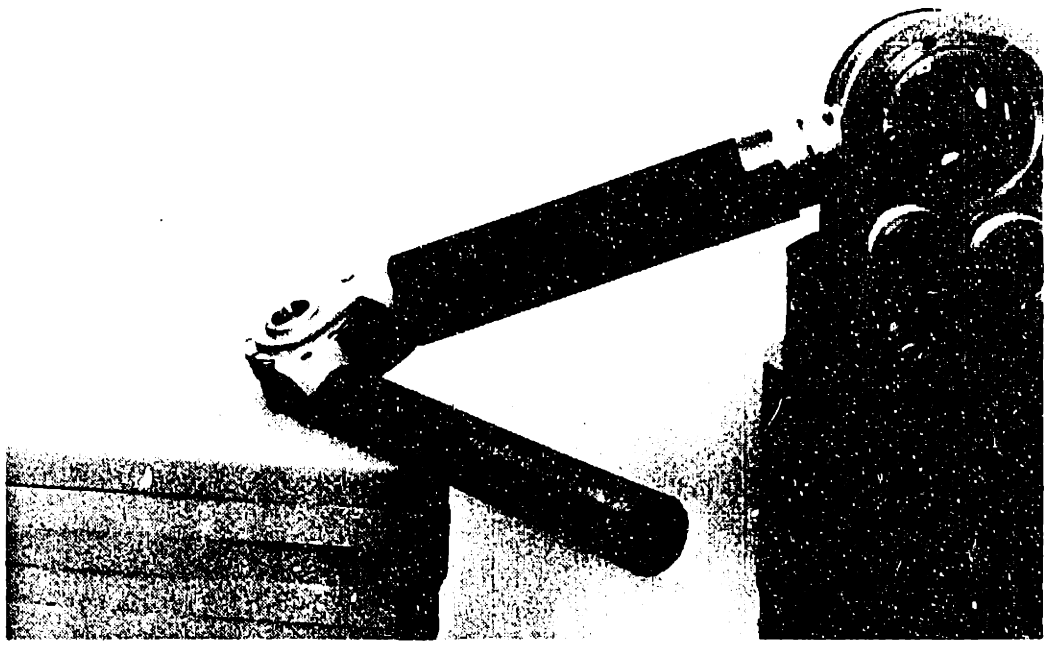

Figure 7.3. *Manipulator explores a foam box.*

required making the outer link several times more massive. Low inertia was considered more important than isotropic inertia.

Each of these transmissions is actuated by one DC brushless motor. For modularity, we selected identical motors – the Moog 300-003. This high-performance motor has 8 Samarium-Cobalt poles and a 3-phase, Y-connected winding. Its rotary inertia and framed weight, including resolver, are only 0.00036 lb-in-sec^2 and 3.5 lb; but it is capable of producing 15 in-lb steady state and 43 in-lb peak torque under stall conditions. Its torque output enables the manipulator to apply a steady contact force of 10 lb at any point along its link surfaces while in any configuration.

By using these high-performance motors in conjunction with high-performance transmissions we can reduce greatly the reliance on explicit-force feedback and thereby reduce dynamic-stability problems associated with feedback. Without feedback, significant dry friction in the transmission has a direct effect on dynamic range by limiting the lowest controllable force. The highest measured no-load joint friction in this design is 1.4 % of peak torque in the base joint. The other axes have measured friction levels below 1 %. Part of the measured friction is actually motor cogging, which is difficult to

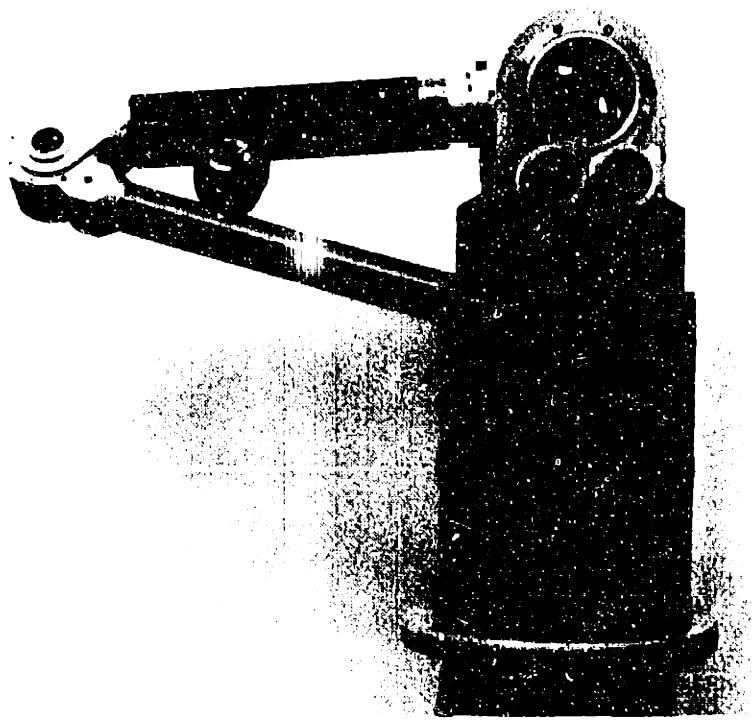

Figure 7.4. *Grasping an object between adjacent links.*

distinguish from motor friction in these joint-friction measurements. The major source of this friction (and cogging) is at each motor where feedforward compensation can successfully counter its effect. Since explicit-force feedback control may be used in the future to increase the dynamic range, the transmission adheres to the design strategies for the feedback case introduced in chapter 5 by maximizing the transmission stiffness between the motor and the next largest source of friction (at the joint).

Each transmission includes a two-stage 30:1 reduction (20:1 in the fourth joint) located at the joint it drives. A two-stage transmission greatly improves the aspect ratio possible over a single-stage transmission while maintaining the efficiency limit calculated from equation (6.16) under full torque load to better than 96 %.* The magnitude of the ratios were selected so that with an endtip payload of 2 kg the contribution to

* Actually, the number of stages for the θ_2 and θ_3 joints is three because of the

backdriven inertia of the reflected inertia of the motors would be relatively small over most of the workspace.

The 7x49-construction, stainless-steel cables are scaled in size and number so that the cables of each stage experience the same stress. The length of free cable in each high-tension second stage is kept very close to zero to maximize stiffness in this stage (see equation (4.1)); and the output-pulley diameter is maximized for high stiffness until it just begins to reduce the aspect ratio for the adjacent links.

The θ_1 transmission drives its joint directly. To implement the kinematics described above we drive θ_2 and θ_3 through the cabled differential* of figure 7.5. This differential is designed to have very high stiffness by making the input and output pulleys as large as possible and using particularly heavy cable with $EA = 51,500$ lb. Also the *free* length of cable between pulleys in the differential is zero. Although some of the cable wrapped around the pulleys becomes active when tensioned, thereby giving the differential some compliance, this compliance is negligible compared to the cable drives between the actuators and the differential. Cables are used in place of bevel gears to produce a clean (i.e. no surface lubricant) differential with no backlash, low friction, high stiffness, low torque ripple, and low cost.

The differential serves two purposes. The first purpose is to drive two intersecting, perpendicular degrees of freedom, neither of which is burdened with accelerating the housing mass of either input actuator. The second purpose is to minimize the backdriven inertia while delivering high torque. The two motors being used in parallel or anti-parallel double the effective motor rotor length. This increases the total rotor inertia less than would selecting a single motor for each degree of freedom with a larger diameter to obtain the same torque. The transformation between the differential inputs and outputs, given in the appendix, is constant and always invertible.

The motor bulk for the distal fourth joint is located at the base to improve aspect ratio and reduce the mass which must otherwise be accelerated by the first three joints. A single high-speed, low-tension cable circuit spans the 22-inch length of the inner link. Its speed is reduced at the joint with the light-weight, compact speed

---

use of a cabled differential.

* MIT has applied for patent protection of the concept on which the design of this cabled differential is based.

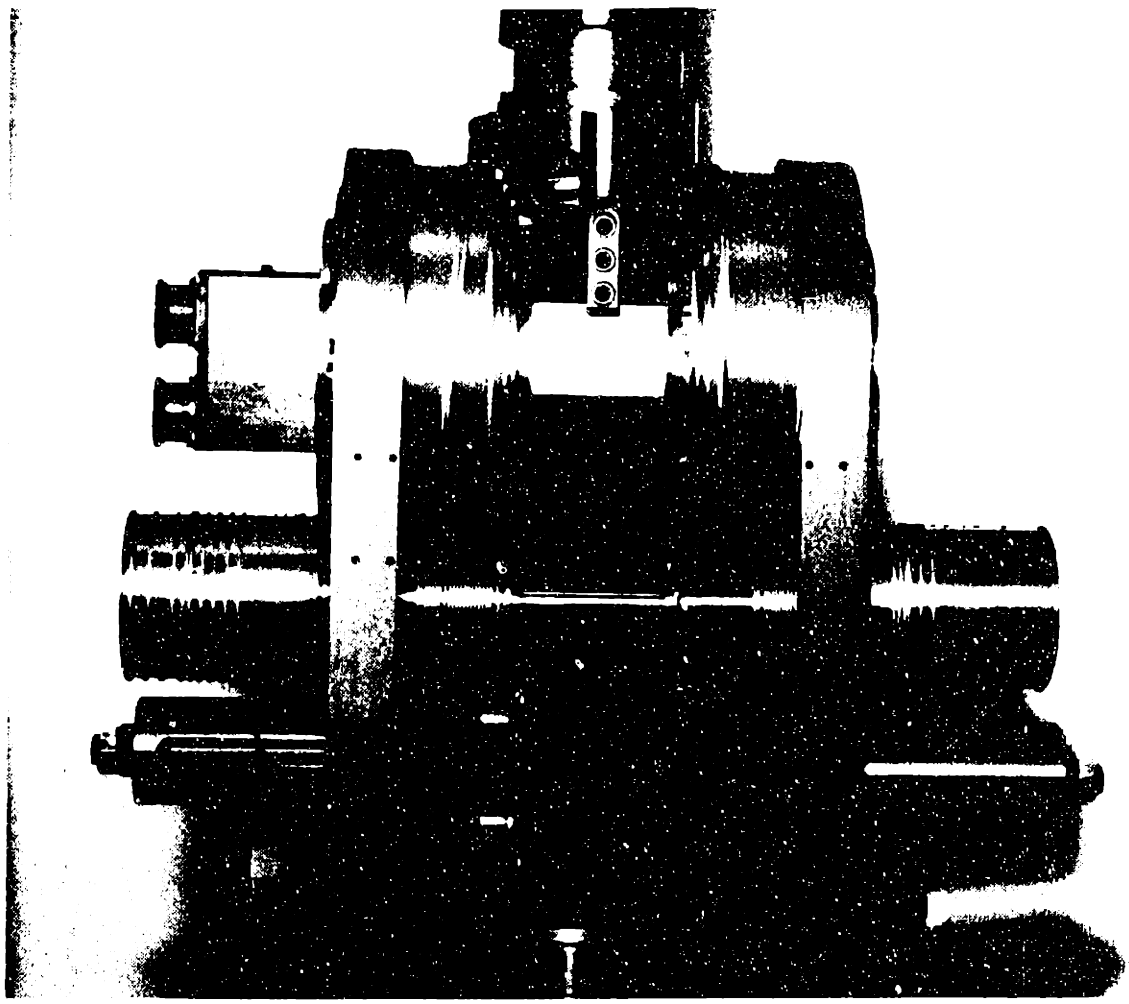

Figure 7.5. *Cabled differential.*

reducer shown in figure 7.6. The cable circuit is guided down the center of and is separated from the environment by the cylindrical, structural shell of the inner link. The torsional flexibility of cables allows this circuit to be twisted nearly $\pm 180°$ as θ_3 is rotated without fatiguing, mistracking, or scrubbing the θ_4 cable. The small changes in θ_4 pretension during θ_3 rotation do not appear to affect performance.

In all of the cable circuits, the pretensioning for both stages is done at a single point, the motor pinion, as shown in figure 7.7. The motor pinion is split allowing the two halves to be counter-rotated and impose pretension. A nut then locks the two halves. This method of pretensioning does not reduce the stiffness of the transmission as do other techniques which use relatively compliant springs at the cable terminations to maintain pretension. Stainless-steel cables can maintain pretension for years after an initial stretch because of their low creep rates. The pretension is propagated to the

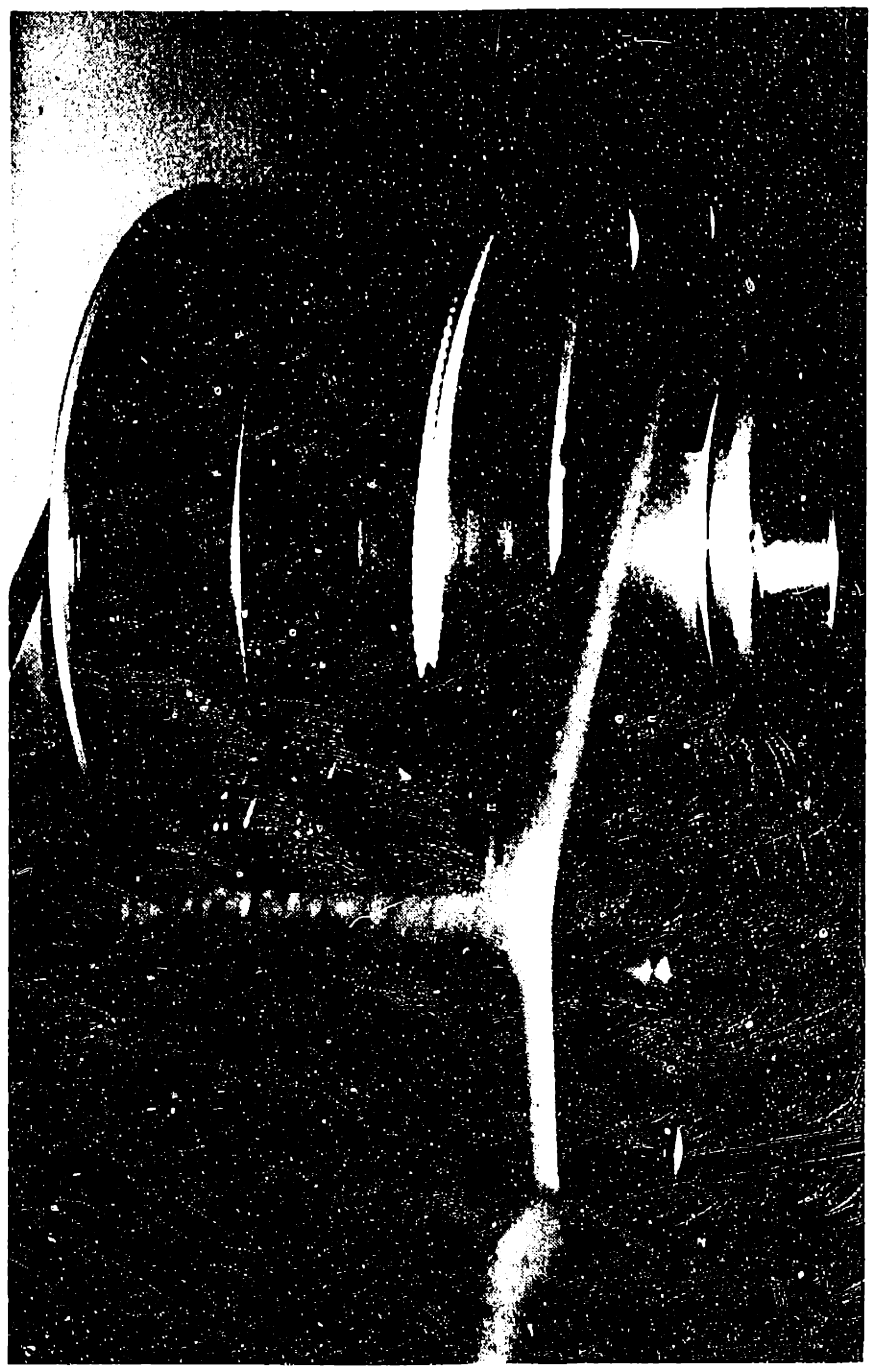

Figure 7.6. *Joint 4; light-weight, compact speed reducer.*

second stage by using two separate pulley/pinions between stages as shown in figure 7.8 for the leaving and return cable. Each half of the differential uses a separate but similar scheme for pretensioning. In each second stage, where dual parallel cable circuits must be used to transmit the larger tension, a loop-back scheme is employed to guarantee that the cables share the load equally. The cabling scheme for the entire arm is shown in figure 7.9.

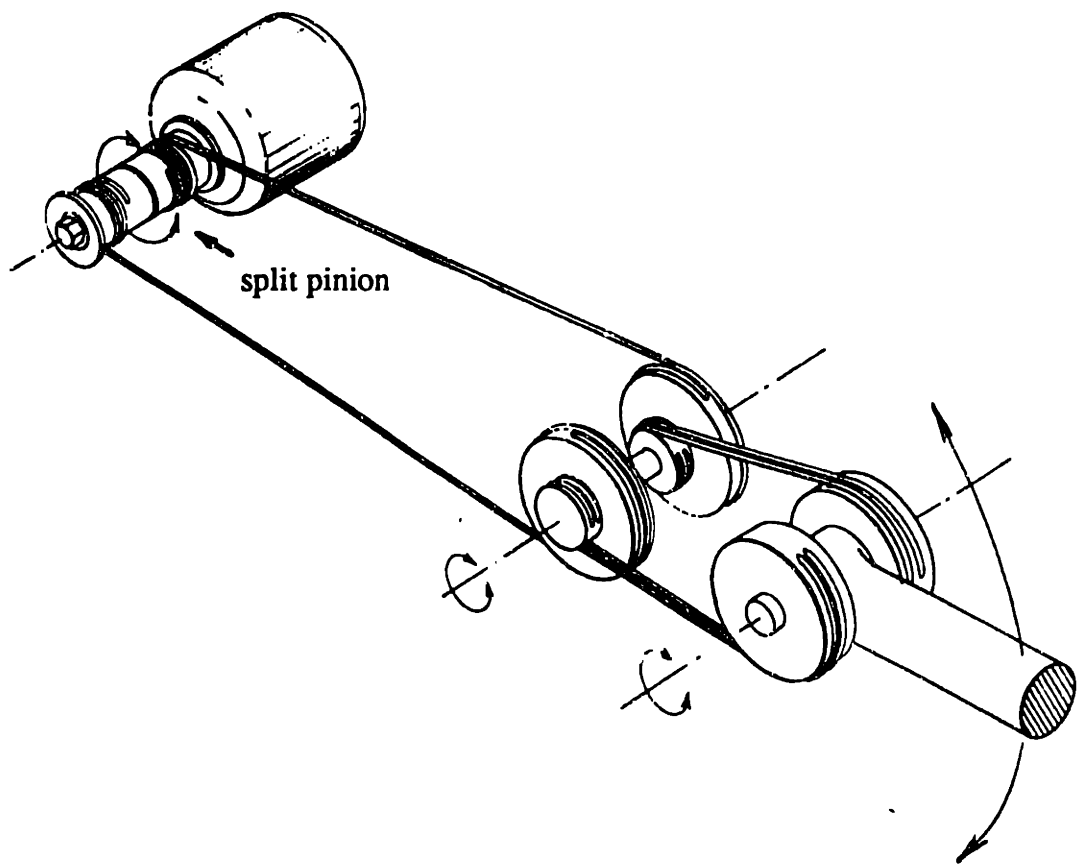

Figure 7.7. *Split motor pinion with pretension propagation.*

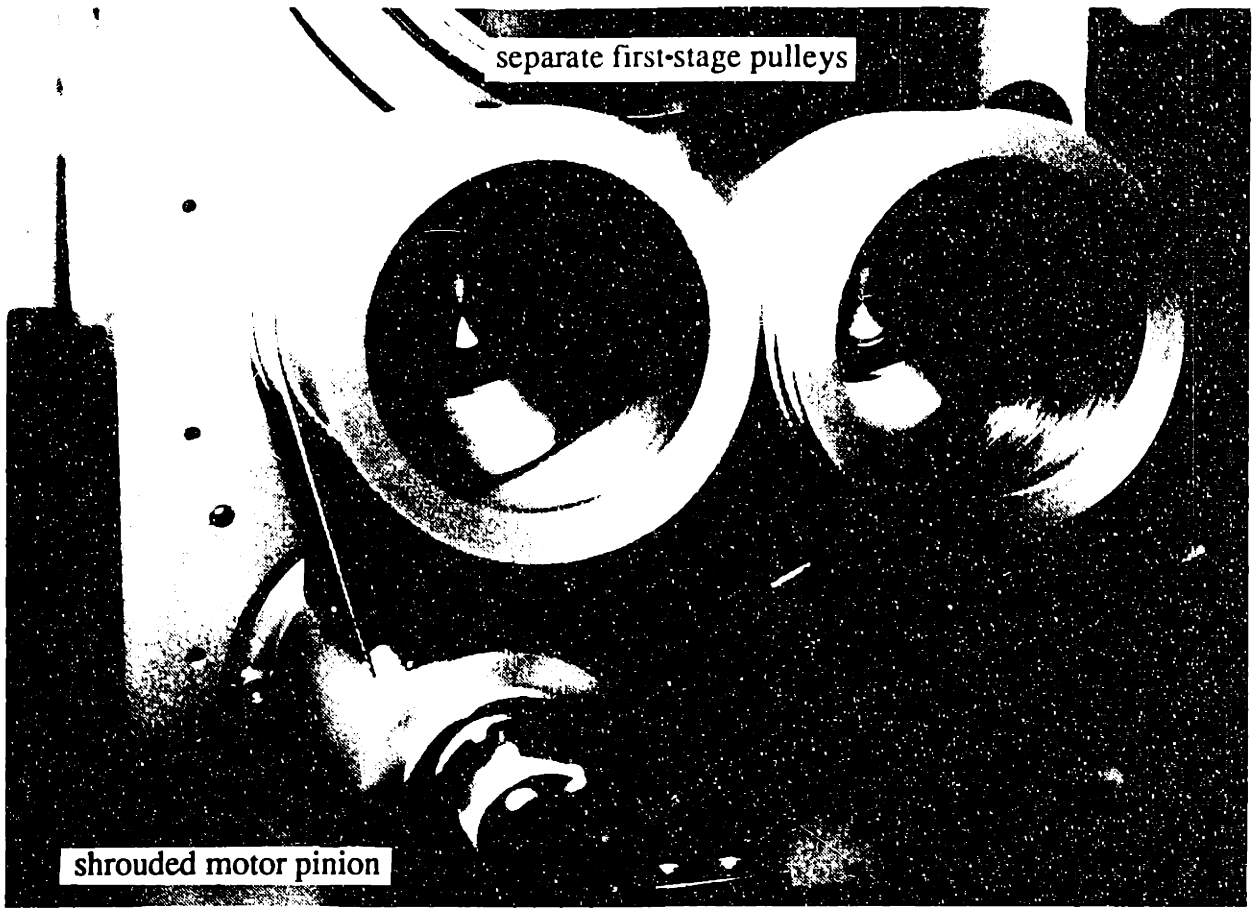

Figure 7.8. *Propagated-pretension implementation.*

7.3 The Future

This work was originally motivated by the author attempting to understand what caused the Salisbury Hand occasionally to exhibit contact-force limit cycles and to be sometimes-stable-sometimes-unstable. A literature survey indicated that these behaviors had been observed in other manipulators as well and impose severe limitations on the real usefulness of force control. It became clear that the mechanical attributes of the transmission such as dry friction and compliance play important roles in causing these behaviors and that appropriate design strategies would improve performance.

Now that we have developed mechanical-design strategies to improve the hardware performance, it is time to pause and consider the implications of a high-performance transmission. For instance, higher performance increases the need for actuators with lower levels of torque ripple, cogging, friction, and controller deadband. This has been anticipated in recent work on brushless motors [Paul 87] with the improvement

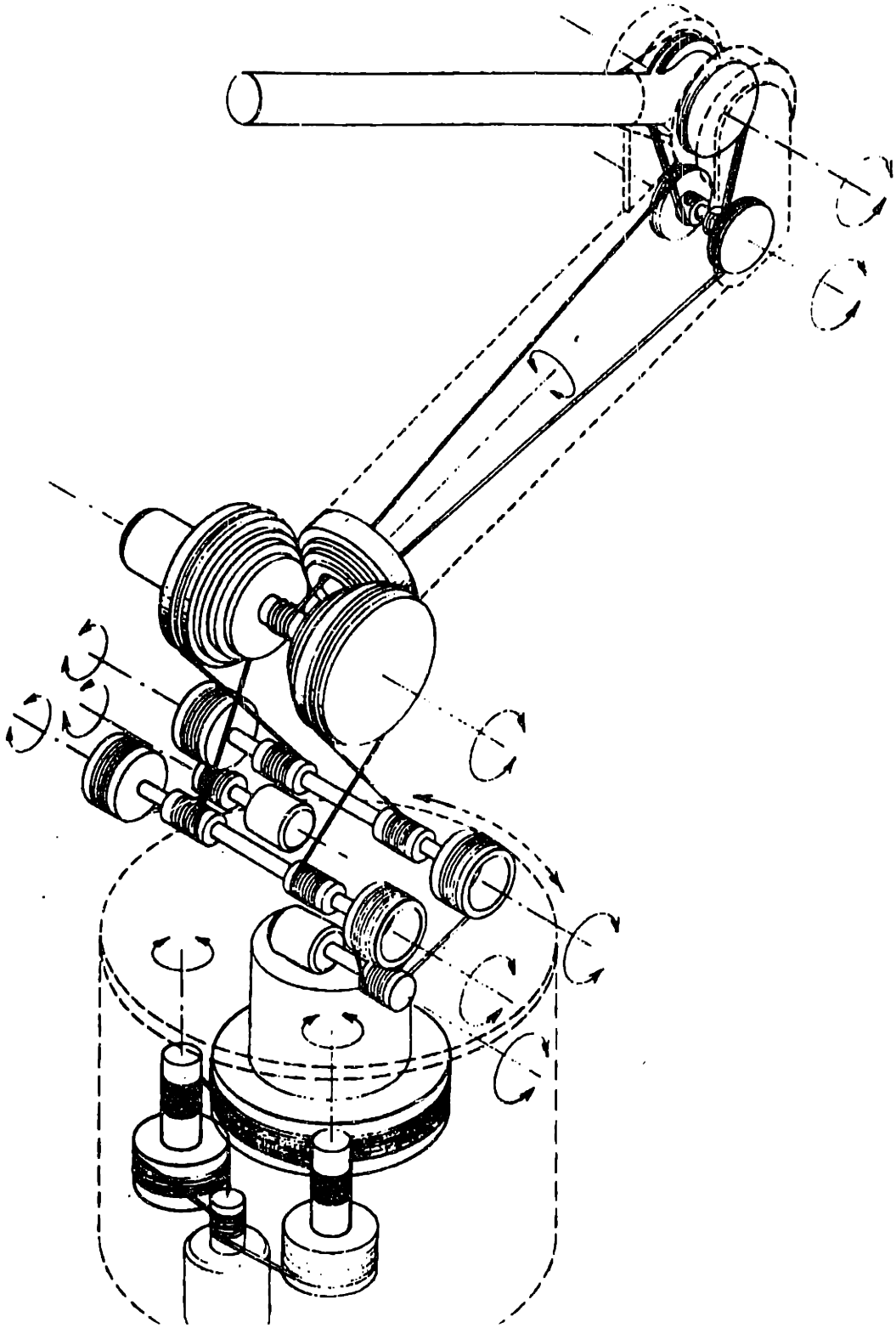

Figure 7.9. *Cabling scheme for entire arm.*

of electronic-commutation schemes for better feedforward DC brushless motor control.

Research is needed to explore the new possibilities for intelligent manipulation. Since high-performance transmissions, driven by actuators of comparable quality, reduce the reliance on endtip-force feedback, high-level force-control schemes based on a vector of joint torques become practical. New strategies such as controlling large forces near the base of a link and controlling small-but-accurate forces near the tip of a link should be considered. Similar strategies could be employed to vary the effective contact impedance passively by choosing the point of contact along a link.

Appropriate kinematics must be considered to maximize the observability and controllability of forces for exploring uncertain environments and for performing a variety of manipulation tasks such as grasping between adjacent links and controlling line contacts. There are many human tasks which involve capabilities only now becoming achievable in robot hardware. In soccer, the ball is guided by a line contact between it and the side of the player's foot. A person gathers a scattered collection of objects between her arms. The Olympic-style wrestler controls forces with tremendous speed and agility along many parts of his body simultaneously. Without vision, the edges of a box are explored quickly by groping with arms and hands. The capabilities which enable these human tasks will also enable tasks more appropriate for robotic hardware. As researchers and designers, we must expand our expectations for force control and begin to explore these entirely new horizons in machine/environment interaction.

APPENDIX A

Coordinate Frames and Transformations for MIT/WAM

Figure A.1 shows the coordinate frames for performing cartesian/joint transformations by using Craig's [Craig 86] conventions. In this figure, the two cylinders represent the inner and outer links. x, y, and z are general cartesian coordinates. The subscript, 0, identifies the coordinate frame attached to ground and the subscript, 5, represents a (tool) coordinate frame attached to the end of the outer link. *

Hartenberg-Denavit parameters are listed in the following table:

coordinate frame number, i	link twist (radians), α_{i-1}	link length, a_{i-1}	link offset, d_i	joint angle, θ
1	0	0	0	θ_1
2	$\pi/2$	0	0	θ_2
3	$-\pi/2$	0	L_3	θ_3
4	$\pi/2$	0	0	θ_4
5	0	L_4	0	0

L_3 and L_4 are the inner and outer link lengths, 22 inches and 16 inches.

$$\begin{pmatrix} \theta_1 \\ \theta_2 \\ \theta_3 \\ \theta_4 \end{pmatrix} = \begin{pmatrix} 0 \\ 0 \\ 0 \\ 0 \end{pmatrix} \tag{A.1}$$

* Note that the cylindrical structure of the inner link in the physical MIT/WAM manipulator is offset latterally by 1.6 inches (0.0726 radians) at the outer-most joint. Therefore, this cylinder does not align exactly with the cyliner of figure A.1 representing the inner link.

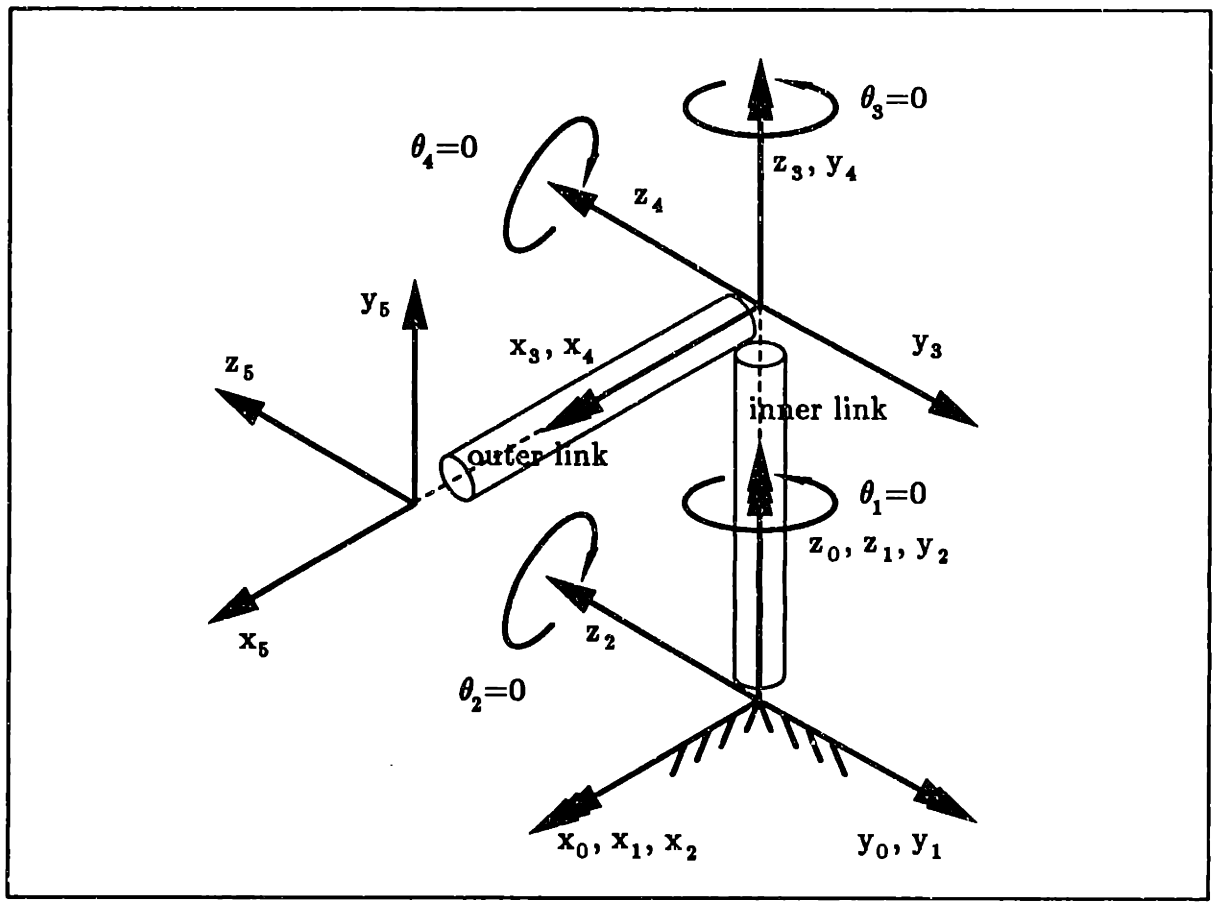

Figure A.1. *Definition of coordinate frames for MIT/WAM.*

when the arm is in the configuration of figure A.1.

$$\begin{pmatrix} \theta_1 \\ \theta_2 \\ \theta_3 \\ \theta_4 \end{pmatrix} = \begin{pmatrix} 0 \\ -\pi/4 \text{ radians} \\ 0 \\ 0 \end{pmatrix} \tag{A.2}$$

when the arm is in the configuration of figure A.2 when the manipulator tip is in the "middle" of its workspace, far from kinematic singularities.

$$\begin{pmatrix} \theta_1 \\ \theta_2 \\ \theta_3 \\ \theta_4 \end{pmatrix} = \begin{pmatrix} 0 \\ -\pi/4 \text{ radians} \\ 0 \\ 0 \end{pmatrix} \tag{A.3}$$

when the two links are stretched out horizontally.

The following equation gives the transformations, ${}^{i-1}_{i}\mathbf{T}$, to transform the $i-1$

coordinate frame into the i coordinate frame.

$$ {}^{i-1}_{i}\mathbf{T} = \begin{pmatrix} \cos\theta_i & -\sin\theta_i & 0 & a_{i-1} \\ \sin\theta_i \cos\alpha_{i-1} & \cos\theta_i \cos\alpha_{i-1} & -\sin\alpha_{i-1} & -\sin\alpha_{i-1} d_i \\ \sin\theta_i \sin\alpha_{i-1} & \cos\theta_i \sin\alpha_{i-1} & \cos\alpha_{i-1} & \cos\alpha_{i-1} d_i \\ 0 & 0 & 0 & 1 \end{pmatrix}. \qquad \text{(A.4)} $$

The following equation gives the transformation between motor and joint space.

$$ \begin{pmatrix} \theta_1 \\ \theta_2 \\ \theta_3 \\ \theta_4 \end{pmatrix} = \begin{pmatrix} \frac{1}{N_1} & 0 & 0 & 0 \\ 0 & \frac{-1}{2N_2} & \frac{1}{2N_2} & 0 \\ 0 & \frac{-1}{N_2} & \frac{-1}{N_2} & 0 \\ 0 & 0 & 0 & \frac{1}{N_4} \end{pmatrix} \begin{pmatrix} \theta_{m_1} \\ \theta_{m_2} \\ \theta_{m_3} \\ \theta_{m_4} \end{pmatrix} \qquad \text{(A.5)} $$

where θ_{m_i} are the motor positions and

$$ (\mathrm{N_1} \quad \mathrm{N_2} \quad \mathrm{N_3} \quad \mathrm{N_4}) = (29.97 \quad 30.40 \quad 30.40_2 \quad 19.15). \qquad \text{(A.6)} $$

The following is the Jacobian transpose, $\mathbf{J^T}$,in hand coordinates. s_i and c_i are shorthand for the trigonometric functions $\sin\theta_i$ and $\cos\theta_i$.

$$ \mathbf{J^T} = \begin{pmatrix} -L_3 s_2 s_3 c_4 & L_3 s_2 s_3 s_4 + L_4 s_2 s_3 & L_4 s_2 c_3 s_4 - L_4 c_2 c_4 + L_3 s_2 c_3 \\ -L_3 c_3 c_4 & L_3 c_3 s_4 + L_4 s_3 & -L_4 s_3 s_4 - L_3 s_3 \\ 0 & 0 & -L_4 c_4 \\ 0 & L_4 & 0 \end{pmatrix}. \qquad \text{(A.7)} $$

Figures A.2 through A.5 show assembly drawings of the MIT/WAM manipulator. Figure A.2 is an early conceptual drawing which illustrates the cable-drive locations in the final design. This sketch does not show the method for propagating pretension through the transmission stages which was included later in the design process. Figure A.3 is a later conceptual sketch which shows several views and the range of motion of the fourth joint. Figure A.4 shows a cut-away and corresponding side view of the differential with its motors and drives as well as the location of the fourth-joint motor. Figure A.5 is an assembly drawing of the base which is supported through a single, four-point, Gothic-arch bearing and first-joint drive.

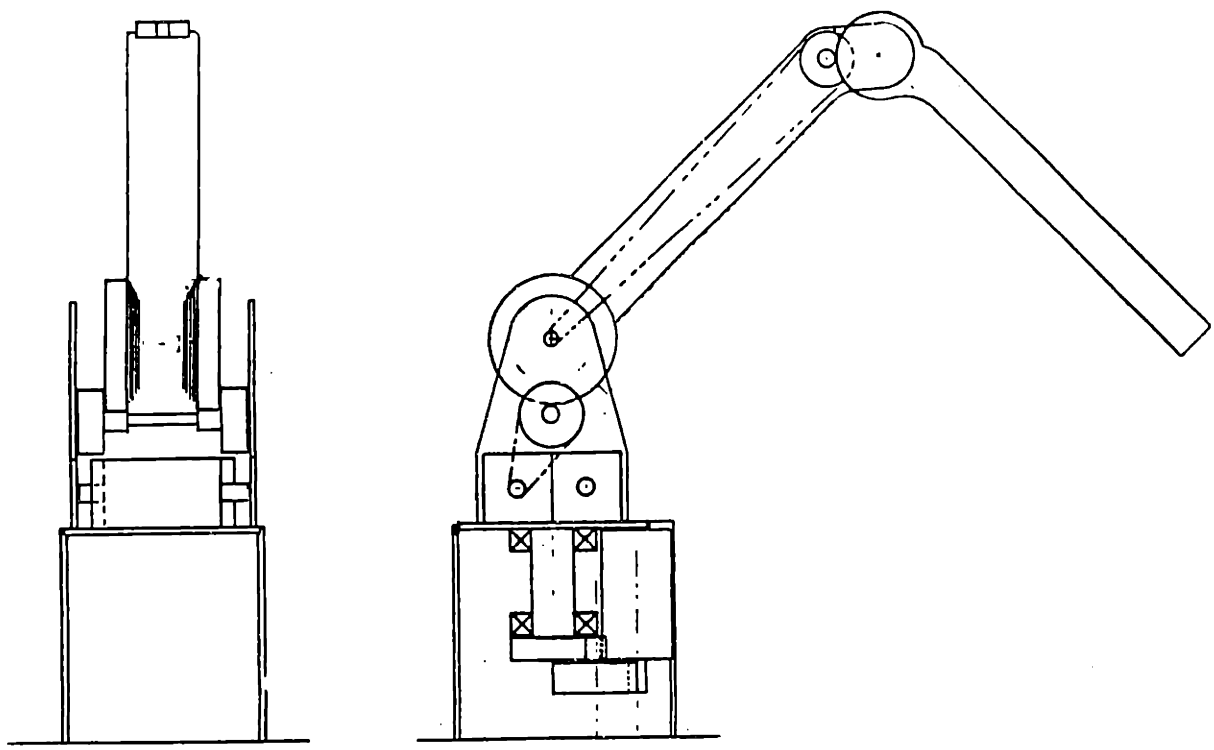

Figure A.2. *Sketches indicating drive locations.*

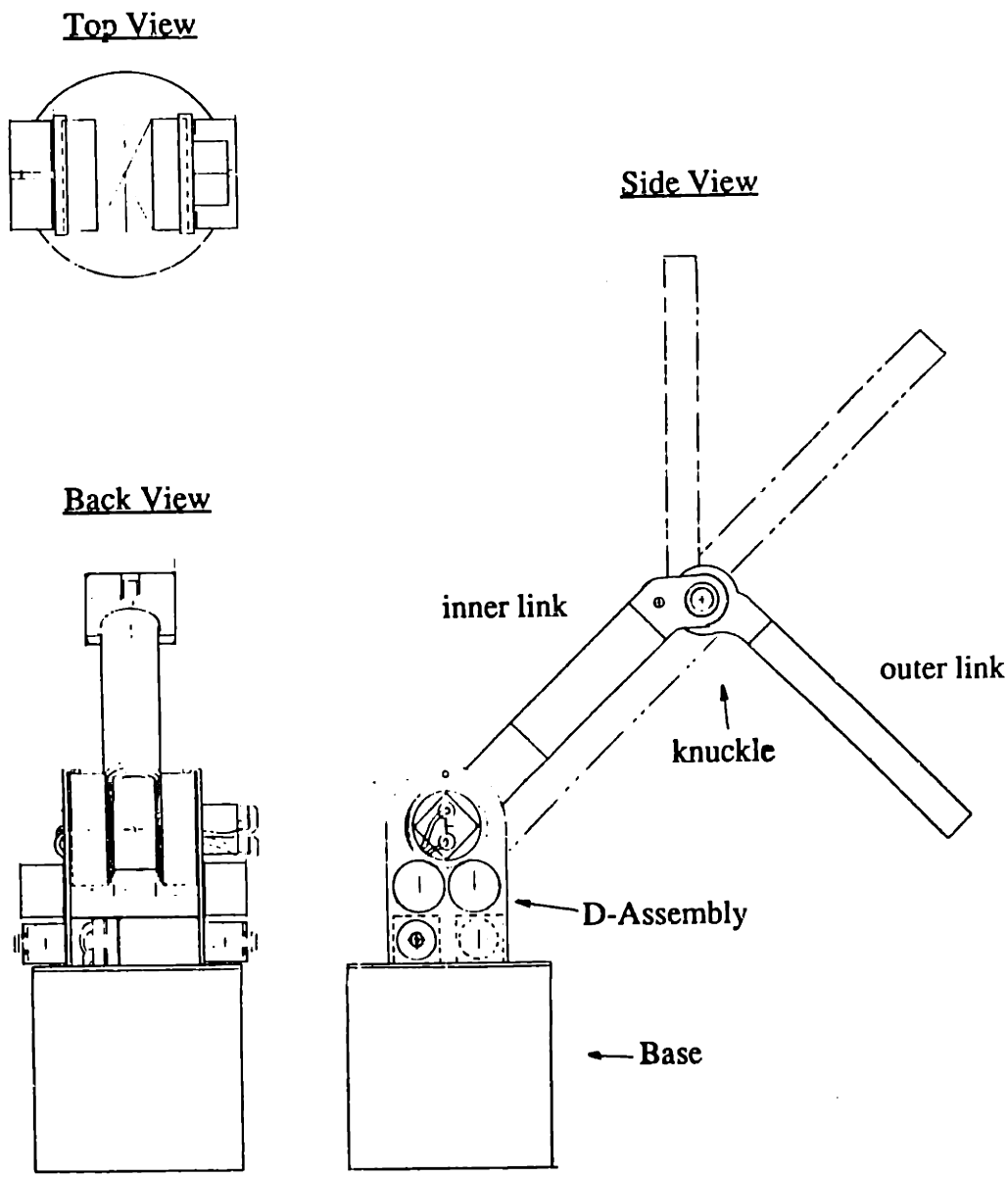

Figure A.3. *Full assembly views.*

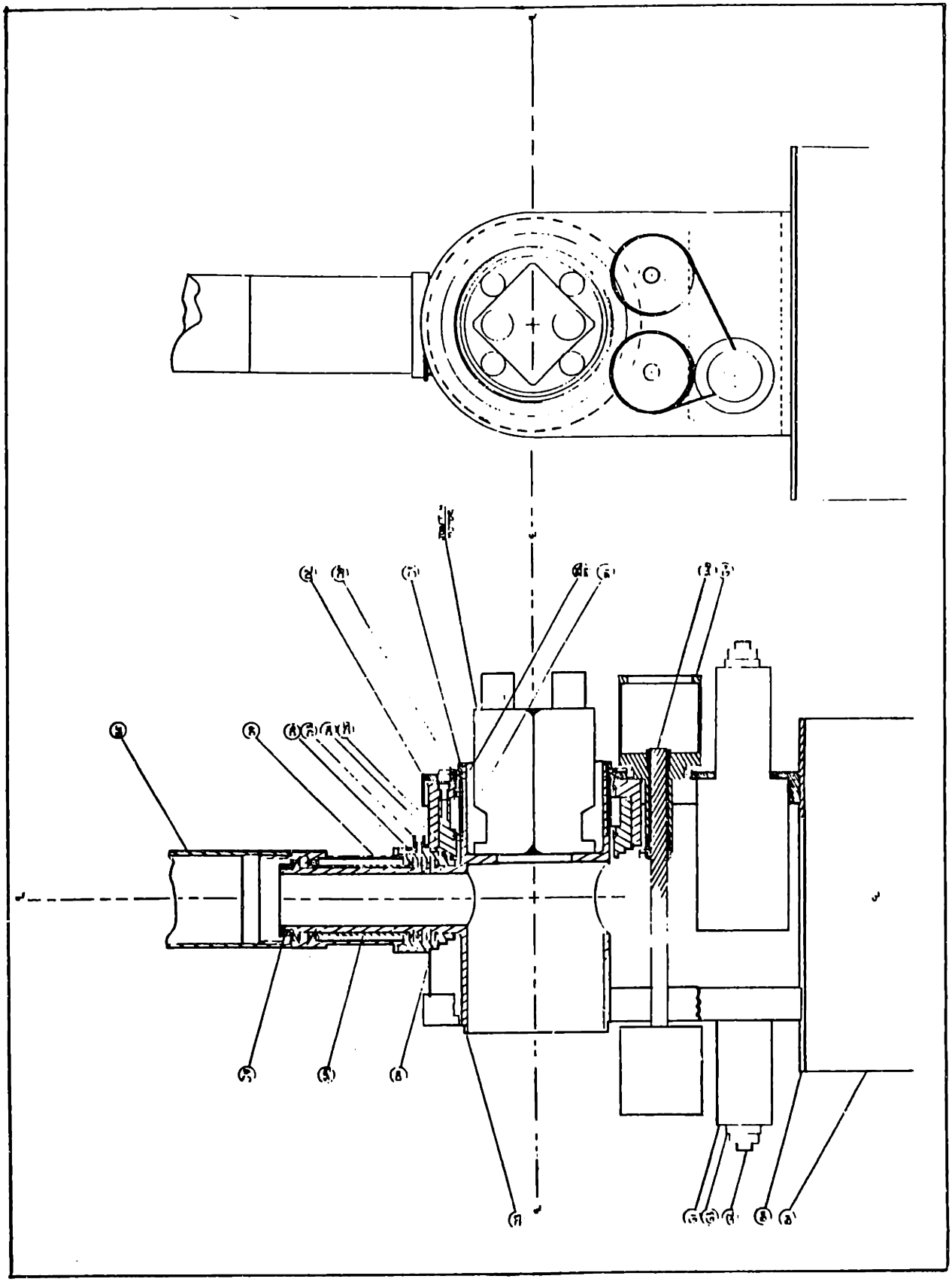

Figure A.4. *Assembly drawing of the differential.*

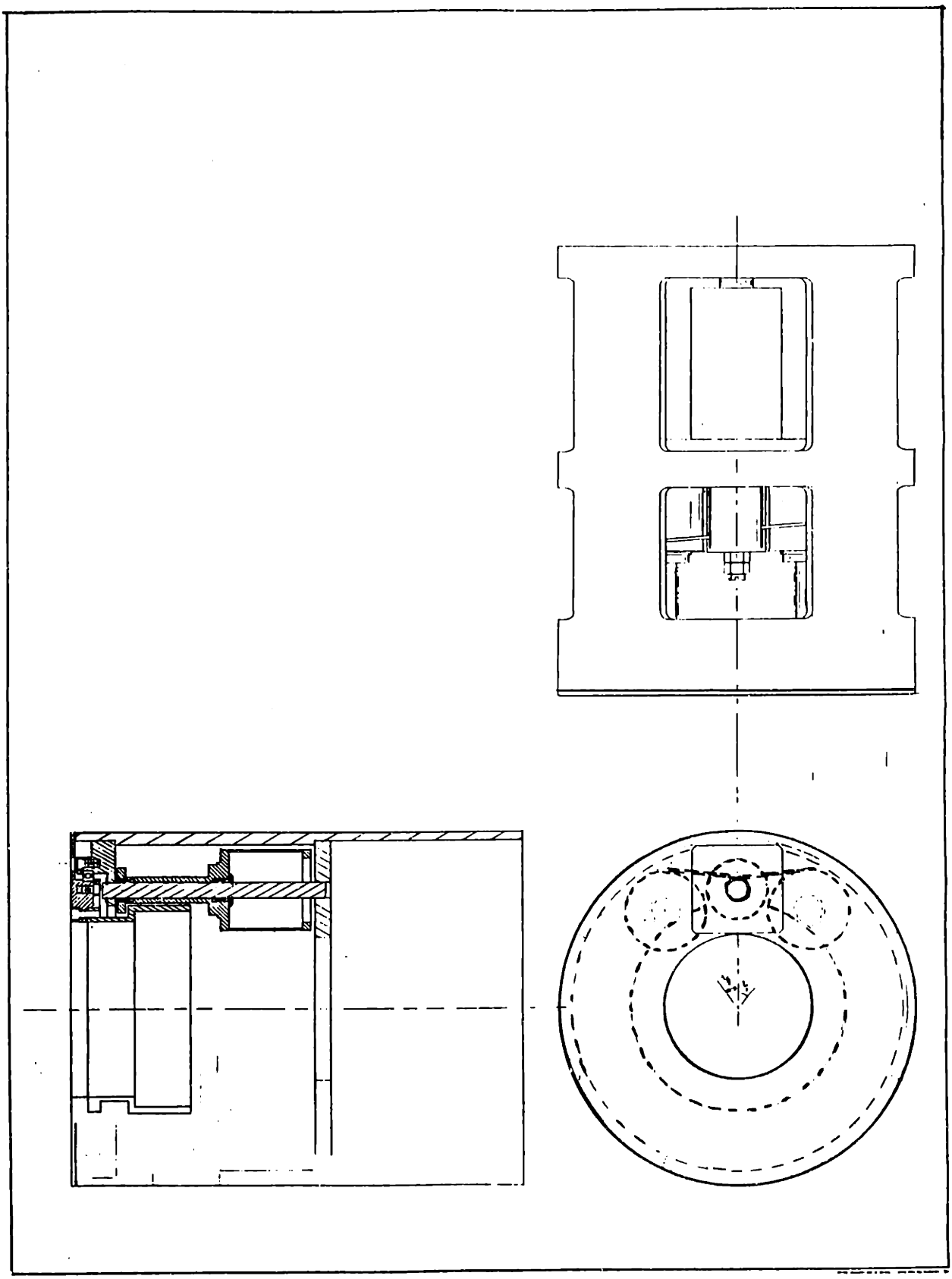

Figure A.5. *Assembly drawing of the base.*

REFERENCES

An, C.H., "Trajectory and Force Control of a Direct Drive Arm," MIT AI Technical Report AI-TR-912, MIT Artificial Intelligence Lab, Cambridge, MA, 1986.

Andeen, G.B., Kornbluh, R., "Design of Compliance in Robotics," *proc. 1988 IEEE International Conference on Robotics and Automation,* Philadelphia, PA, April 1988.

Armstrong, B., "Dynamics for Robot Control: Friction Modeling and Ensuring Excitation during Parameter Identification," Ph.D thesis, Department of Electrical Engineering, Stanford University, Stanford, CA, June 1988.

Asada, H., and Kanade, T., "Design of Direct-Drive Mechanical Arms," *Journal of Vibrations, Acoustics, Stress, and Reliability, Transactions of the ASME,* vol. 105, no. 3, July 1983, pp. 312–316.

Asada, H., "Dynamic Analysis and Design of Robot Manipulators Using Inertia Ellipsoids," *proc. First International Conference on Robotics,* Atlanta, GA, March 1984a.

Asada, H., Youcef-Toumi, K., and Lim, S.K., "Joint Torque Measurement of a Direct-Drive Arm," *23d IEEE Conference on Decision and Control,* December 1984b, pp. 1332–1337.

Bejczy, A.K., and Salisbury, J.K., "Kinesthetic Coupling Between Operator and Remote Manipulator," *Advances in Computer Technology,* ASME, vol. 1, August 1980, pp. 197–211.

Book, W.J., "Modeling, Design and Control of Flexible Manipulator Arms," Ph.D. thesis, Department of Mechanical Engineering, Massachusetts Institute of Technology, Cambridge, MA, April 1974.

Brock, D. L., "Enhancing the Dexterity of a Robot Using Controlled Slip," Report AI-TR-992, Artificial Intelligence Laboratory, Massachusetts Institute of Technology, Cambridge, MA, October 1987.

Colgate, J.E., Hogan, N., "Robust Control of Dynamically Interacting Systems," accepted in July 1987 to the *International Journal of Control.*

Cotterill, J.H., *Applied Mechanics,* 3rd ed. rev.; London, England: Macmillan and Co., 1892, pp. 250–253.

Craig, J.J., *Introduction to Robotics, Mechanics, and Control,* Addison-Wesley Publishing Company, Reading, MA, 1986.

Dalgetty, B.L., "Joint Torque Sensor for a Direct-Drive Arm," Master's thesis, Department of Mechanical Engineering, Massachusetts Institute of Technology, Cambridge, MA, 1984.

Eppinger, S.D., and Seering, W.P., "On Dynamic Models of Robot Force Control," *proc. 1986 IEEE International Conference on Robotics and Automation,* San Francisco,

CA, April 1986.

Eppinger, S.D., and Seering, W.P., "Understanding Bandwidth Limitations in Robot Force Control," *proc. 1987 IEEE International Conference on Robotics and Automation,* Raleigh, N.C., April 1987.

Gelb, A., and Vander Velde, W.E. *Multiple-Input Describing Functions and Nonlinear System Design,* McGraw-Hill, New York, 1968.

Graham, D., and McRuer,D. *Analysis of Nonlinear Control Systems,* John Wiley & Sons, New York, 1961.

Hogan, N., "Stable Execution of Contact Tasks Using Impedance Control," *proc. 1987 IEEE International Conference on Robotics and Automation,* Raleigh, NC, April 1987.

Hollars, M.G., and Cannon, R.H. Jr., "Initial Experiments on the End-Point Control of a Two-Link Manipulator with Flexible Tendons," *ASME Winter Annual Meeting,* Miami Beach, Fla., November 1985.

Hollerbach, J.M., "Optimum Kinematic Design for a Seven Degree of Freedom Manipulator," *Robotics Research: The Second International Symposium,* ed. H. Hanafusa and H. Inoue, MIT Press, Cambridge, MA, 1985.

Homer, *Odyssey,* book IX, lines 384–387

Jacobsen, S.C., Iversen, E.K., Knutti, D.F., Johnson, R.T., and Biggers, K.B., "Design of the Utah/MIT Dexterous Hand," *proc. 1986 IEEE International Conference on Robotics and Automation,* San Francisco, CA, April 1986.

Khatib, O., "The Operational Space Formulation in the Analysis, Design, and Control of Robot Manipulators," *Robotics Research: The Third International Symposium,* ed. O. Faugeras and G. Giralt, MIT Press, Cambridge, MA, 1986.

Lim, S.K., "Measurement and Control of Joint Torque for a Direct-Drive Arm," Master's thesis, Department of Mechanical Engineering, Massachusetts Institute of Technology, Cambridge, MA, 1985.

Luh, J.Y.S., Fisher, W.D., and Paul, R.P., "Joint Torque Control by a Direct Feedback for Industrial Robots," *IEEE Transactions on Automatic Control,* AC-28, 1983, pp. 153–160.

Maples, J.A., and Becker, J.J., "Experiments in Force Control of Robotic Manipulators," *proc. 1986 IEEE International Conference on Robotics and Automation,* San Francisco, CA, April 1986, pp. 695–702.

Marks' Standard Handbook for Mechanical Engineers, 8th ed., edited by T. Banmeister, McGraw-Hill, New York, NY, 1978, pp. 8–140.

Mason, M.T., and Salisbury, J.K., *Robot Hands and the Mechanics of Manipulation,* MIT Press, Cambridge, MA, 1985.

Nevins, J.L., and Whitney, D.E., "The Force Vector Assembler Concept," *proc. of the*

First CISM-IFToMM Symposium, Udine, Italy, September 5–8, 1973, pp. 273–288.

Paul, B.J., "A Systems Approach to the Torque Control of a Permanent Magnet Brushless Motor," Master's thesis, Department of Mechanical Engineering, Massachusetts Institute of Technology, Cambridge, MA, August 1987.

Paul, R.P., and Shimano. B., "Compliance and Control," *proc. of the Joint Automatic Control Conference*, 1970, pp. 694–699.

Phillips, J.W., and Costello, G.A. "Analysis of Wire Ropes With Internal-Wire-Rope Cores," *Journal of Applied Mechanics*, Transactions of the ASME, vol. 52, September 1985.

Rabinowicz, E. "A Study of the Stick-Slip Process," published in *Friction and Wear*, Ed. by Robert Davies, Elsevier Pub. Co., New York, 1959.

Raibert, M.H., and Craig, J.J. "Hybrid Position/Force Control of Manipulators," *Journal of Dynamic Systems, Measurement, and Control*, ASME, vol. 103, no. 2, June 1981, pp. 126–133.

Reynolds, O., "On the Efficiency of Belts or Straps as Communicators of Work," *The Engineer*, vol. 38, 1874, p. 396.

Reynolds, O., "On Rolling-Friction," *Philosophical Transactions of the Royal Society of London*, vol. 166, Part I, London, England, 1876.

Roberts, R.K., Paul, R.P., and Hillberry, B.M., "The Effect of Wrist Sensor Stiffness on the Control of Robot Manipulators," *proc. 1985 IEEE International Conference on Robotics and Automation*, St. Louis, MO, March 1985, pp. 269–274.

Roth, B., "Performance Evaluation of of Manipulators from a Kinematic Viewpoint," *NBS Special Publication: Performance Evaluation of Programmable Robots and Manipulators*, 1975, pp. 39–61.

Salisbury, J.K. "Active Stiffness Control of a Manipulator in Cartesian Coordinates," *19th IEEE Conference on Decision and Control*, Albuquerque, NM, December 1980.

Salisbury, J.K., "Design and Control of an Articulated Hand," *International Symposium on Design and Synthesis*, Tokyo, Japan, July 1984a.

Salisbury, J.K., "Interpretation of Contact Geometries from Force Measurements," *proc. 1st International Symposium on Robotics Research*, Bretton Woods, NH, September 1984b, published by the MIT Press, Cambridge MA.

Salisbury, J.K., "Teleoperator Hand Design Issues," *proc. 1986 IEEE International Conference on Robotics and Automation*, San Francisco, April 1986.

Salisbury, J.K. "Whole-Arm Manipulation," Proceedings of the 4th Internatinal Symposium of Robotics Research, Santa Cruz, CA, August 1987. Published by the MIT Press, Cambridge MA.

Salisbury, J.K., Townsend, W.T., Eberman, B.S., DiPietro, D., "Preliminary Design

of a Whole-Arm Manipulation System (WAMS)," *proc. 1988 IEEE International Conference on Robotics and Automation,* Philadelphia, PA, April 1988.

Shigley, E.S., and Mitchell, L.D., *Mechanical Engineering Design,* 4th ed.; New York, NY: McGraw-Hill, Inc., 1983, pp. 758–761.

Slotine, J.J., "Sliding Controller Design for Nonlinear Systems," *International Journal of Control,* vol. 40, no. 2, 1984.

Swift, H.W., "Power Transmission by Belts: An Investigation of Fundamentals," *The Institution of Mechanical Engineers,* vol. 1, 1928.

Takase, K., Inoue, H., Sato, K., Hagihara, S., "The Design of an Articulated Manipulator with Torque Control Ability," proc. ISIR4, Tokyo, Japan, 1974.

Townsend, W.T., and Salisbury, J.K., "The Efficiency Limit of Belt and Cable Drives," submitted on 17 March 1987 and subsequently accepted for publication in the ASME *Journal of Mechanisms, Transmissions, and Automation in Design.*

Townsend, W.T., and Salisbury, J.K., "The Effect of Coulomb Friction and Stiction on Force Control," *proc. 1987 IEEE International Conference on Robotics and Automation,* Raleigh, NC, April 1987, pp. 883–889.

Vertut, J., Charles, J., Coiffet, P., Petit, M., "Advance of the New MA 23 Force Reflecting Manipulator System," *porc. CISM-IFToMM Symposium,* Warsaw, Poland, September 1976.

Vertut, J., and Liegeois, A., "General Design Criteria for Manipulators," *Journal of Mechanism and Machine Theory,* vol. 16, 1981, pp. 65–70.

Vertut, J., and Coiffet, P., *Teleoperations and Robotics: Evolution and Development,* "Robot Technology," vol. 3A; Englewood Cliffs, N.J.: Prentice-Hall, Inc., 1986, pp. 191–194.

West, H., "Kinematic Analysis fo the Design and Control of Braced Manipulators," Ph.D. thesis, Department of Mechanical Engineering, Massachusetts Institute of Technology, Cambridge, MA, June 1987.

Whitney, D.E. "Force Feedback Control of Fine Manipulator Motions," *Journal of Dynamic Systems, Measurement, and Control,* vol. 99, no. 2, June 1977, pp. 91–97.

Whitney, D.E., "Historical Perspective and State of the Art in Robot Force Control," *proc. 1985 IEEE International Conference on Robotics and Automation,* St. Louis, MO, March 1985, pp. 883–889.

Wu, C.H., and Paul, R.P., "Manipulator Compliance Based on Joint Torque Control," *19th IEEE Conference on Decision Control,* December 1980, pp. 88–94.